LONGWAVE RADIATION OVER LAKE ONTARIO

LONGWAVE RADIATION EXCHANGES

OVER

LAKE ONTARIO

By

PETER JOHN ROBINSON, B.Sc., M.Phil.

A Thesis

Submitted to the Faculty of Graduate Studies

in Partial Fulfilment of the Requirements

for the Degree

Doctor of Philosophy

McMaster University

May 1972

DOCTOR OF PHILOSOPHY (1972)
(Geography)

McMASTER UNIVERSITY
Hamilton, Ontario.

TITLE: Longwave Radiation Exchanges over Lake Ontario

AUTHOR: Peter John Robinson, B.Sc. (London University)
M.Phil. (London University)

SUPERVISOR: Professor J.A. Davies

NUMBER OF PAGES: x, 181

SCOPE AND CONTENTS: The components of the radiation balance were measured over Lake Ontario for an 18 week period. Surface temperature and emissivity measurements were also made. Emissivity is constant, and outgoing longwave radiation can be determined from surface temperature alone. Water temperature changes appear to be greatly influenced by non-radiative processes. The presence of flux divergence in the surface layer is demonstrated. Incoming longwave radiation varies rapidly in cloudless conditions. In addition, it is greatly influenced by low and medium cloud. The relationship between net shortwave radiation and net radiation is analysed for varying time periods, and reasons for the variable relationship are advanced. Several empirical methods for predicting net radiation or its components were tested, with variable results.

ACKNOWLEDGEMENTS

Grateful thanks are due to Dr. J.A. Davies, for interest, encouragement and invaluable comments throughout this work. The shortwave radiation data were furnished by Mr. M. Nunez, whose assistance throughout the work is also acknowledged. The sucessful field program was made possible by the co-operation of Messrs. R. and L. Martin, the owners of the farm building used as a recording centre, and Mr. J. Hawkins, assistant during the field program. My thanks also go to the staff of the Upper Air Section, Meteorological Branch, Department of Transport, for assistance with the radiosonde equipment and ascents, and to Mr. J.R. Latimer for the radiometer calibrations. The Canada Centre for Inland Waters provided considerable assistance in erecting the tower and analysing water samples. Dr. T. Timusk provided the equipment, and many helpful comments, for the laboratory determination of emissivity.

This work was supported by a contract from the Government of Canada, Department of Energy, Mines and Resources, Canada Centre for Inland Waters, Great Lakes Division, Burlington, Ontario, through purchase order HO 81276.

TABLE OF CONTENTS

LIST OF FIGURES

LIST OF TABLES

CHAPTER 1

INTRODUCTION

A knowledge of the radiation[1] balance R_n of a surface is vital for studies of surface energy exchange, since R_n is usually the main energy input into a surface, and hence controls the energy balance. This energy balance determines heat transfer into the underlying body and the overlying air. Although water is the largest single surface type on earth, there have been few investigations of the radiation balance of water surfaces. Hence energy transfers within, and vertical transfers over, water can only be estimated within wide limits, and the energy exchanges between ocean and atmosphere, which are important for studies of the general circulation of the atmosphere, cannot be adequately specified. On the local scale the energy balance of water bodies such as the Great Lakes, which differs from the balances of the surrounding land areas, can greatly influence the climate of these areas. The manner in which it does so is imprecisely known.

The surface radiation balance, or net radiation, consists of both shortwave and longwave radiation fluxes, such that

---

[1] Throughout the thesis the term 'radiation' is used in the sense of an energy flux.

$$R_n = Q_n + L_n \quad , \tag{1}$$

or

$$R_n = Q_i - Q_o + L_i - L_o \quad , \tag{2}$$

where Q = shortwave (solar) radiation (wavelengths 0.3 - 3.0μ), and L = longwave (terrestrial) radiation (wavelengths >3.0μ). Subscripts i, o, and n refer to incoming, outgoing and net fluxes[1]. Positive values are assigned to fluxes directed towards the surface. The importance of surface type on the radiation balance can be demonstrated by expanding equation 2 to

$$R_n = (1 - \alpha)Q_i + L_i - [(1 - \varepsilon)L_i + \varepsilon\sigma T_s^4], \tag{3}$$

where α = surface albedo,

ε = surface emissivity,

σ = Stefan-Boltzmann constant,

and T_s = surface temperature.

Hence an understanding of R_n depends on understanding both the component fluxes and the role of the surface. For a study of the influence of surface on net radiation, water, in one important respect, is a more suitable experimental surface than land. In most conditions the exact position of the air-water interface can be defined, and the surface temperature determined (Marlatt 1967). For land surfaces,

---

[1]A complete list of symbols is given in the Appendix.

however, surface temperature cannot be determined adequately (Robinson 1950) since the position of the air-earth interface cannot be precisely defined. If surface temperature and emissivity are known the outgoing longwave radiation can be determined almost independently of radiation measurement results. Additionally, since radiometric determinations must be made some distance from the surface, and T_s and ε refer to the surface, estimates of radiative flux divergence are possible.

Although a pioneer study of radiative fluxes over water surfaces was undertaken by Anderson (1954), few measurements have been made since, and none have used simultaneous surface temperature measurements to assess results. One of the major problems for such studies has been the design of suitable instruments and the development of means of instrument mounting. With the advent of more modern sensors (Funk 1959) and experience with the installation of micrometeorological instruments over water, radiation flux measurements over water surfaces are feasible.

An experimental study of the radiation balance and its components was undertaken from July 1st to November 18th 1969 over Lake Ontario. It attempted to define the nature and causes of temporal variations in radiation fluxes for a water surface by considering the influence of both the surface and the overlying atmosphere. The experiment was designed to provide continuous measurements of R_n, its component fluxes, and surface temperature, with observations of

atmospheric water vapour content and cloud conditions, and sample studies of surface emissivity. This study considers the magnitude and causes of variations in the longwave fluxes and the influence of these fluxes on net radiation. The shortwave fluxes are discussed separately by Nunez (1971), and are only considered here as influences on the variation of net radiation. Using the experimental data, the study aims:

(1) to examine the influence of surface temperature and emissivity on outgoing longwave radiation;

(2) to investigate the degree of control exerted on surface temperature by net radiation;

(3) to ascertain if divergence of outgoing longwave radiation occurs in the lowest atmospheric layer above a water surface;

(4) to investigate causes of variations in incoming longwave radiation in cloudy and cloudless conditions;

(5) to determine the relative influence of the shortwave and longwave flux variations on net radiation variations;

(6) to test simple empirical estimation techniques for incoming longwave and net radiation determinations at remote locations.

CHAPTER 2

THEORETICAL BACKGROUND

In this chapter relevant aspects of the theory of radiation exchange of incoming, outgoing and net longwave radiation will be presented, together with some methods of estimating these fluxes. Attention will also be given to the influence of these fluxes on net radiation, and to the relationship between net radiation and surface heating.

A. INCOMING LONGWAVE RADIATION

The amount of incoming longwave radiation received at the surface depends on radiative exchange processes in the atmosphere where water vapour, clouds and carbon dioxide are of major importance, since they strongly absorb and emit longwave radiation. The relation between the amount and distribution of these gases and radiation is complex. A brief review of the theory will be given to isolate the important factors and also to indicate applications of the theory to radiation modelling.

General solutions of the radiative transfer equations in the atmosphere for cloudless conditions have been presented by Chandrasekhar (1950), Goody (1964) and Kondrat'yev (1965). Solutions are not yet available for conditions with cloud.

The monochromatic flux from a black body (a body that emits the maximum possible radiation) at surface temperature T and wavelength λ, is given by the Planck function,

$$F_\lambda (T) = \pi(c_2/\lambda^5)(e^{c_3/\lambda T}-1)^{-1}, \qquad (4)$$

where c_2 and c_3 are constants. No natural body corresponds exactly to a black body at all wavelengths. Departures from the black-body state can be accommodated by introducing the monochromatic emissivity,

$$\varepsilon_\lambda = F_\lambda'(T)/F_\lambda(T), \qquad (5)$$

in which $F_\lambda'(T)$ is the monochromatic flux from the body.

In the atmosphere, ε_λ varies greatly with amount and partial pressure of water vapour and carbon dioxide, so that a single value cannot be used for each wavelength. Consequently the atmosphere must be divided into layers, and an emissivity coefficient, $\varepsilon_\lambda(u)$, determined for each layer. Here u is the optical depth, or path length, of gas in the layer, corrected for the partial pressure of the gas. The monochromatic flux from the layer is then

$$F_\lambda'(T) = \varepsilon_\lambda(u)\ F_\lambda(T), \qquad (6)$$

where T now represents the average temperature of the layer.

The general radiative transfer equation for a given gas is obtained by integrating equation 6 over all layers and all wavelengths,

$$F_l = \int_0^\infty \int_0^{u_t} F_\lambda(T)\varepsilon_\lambda(u)\ du\ d\lambda, \qquad (7)$$

where u_t is the total corrected optical depth of the gas in the atmosphere.

Since $\varepsilon_\lambda(u)$ varies with λ, and T varies along the emission path, no analytic solution of equation 7 is possible. Several numerical solutions, using various simplifying assumptions have been proposed. From these, radiation charts have been produced which allow L_i to be computed when vertical distributions of water vapour and carbon dioxide are known. These chart methods provide one approach to L_i modelling. A simpler approach can be made using near-surface measurements only. Most of the incoming radiation to a surface originates at low levels, since the flux from any layer depends on the amount and temperature of the radiating gas, and normal atmospheric distributions are such that maximum gas amounts and temperatures occur close to the surface. It has been shown that approximately 60 percent of L_i originates in the lowest 100 m (Sellers 1965), and 37 percent in the lowest 10 m (Moller 1951) of the atmosphere. Hence empirical relationships between L_i and standard observations from meteorological

stations can be established. The two approaches are treated separately below.

1: Chart Methods

Numerical solutions of equation 7 that have appeared in the literature include those of Elsasser (1942), Deacon (1950), Robinson (1950), Shekter (1950), Brooks (1952), Yamamoto (1952) and Elsasser and Culbertson (1960). In each case, non-linear scales of temperature and water vapour or carbon dioxide amounts are used to correspond to linear, orthogonal scales of $F_\lambda(T)$ and $\varepsilon_\lambda(u)$ or equivalent transformations (Goody 1964). The radiation flux can be calculated from charts which incorporate these scales and which use pressure, temperature and humidity data obtained from atmospheric soundings as inputs.

The major difference between the various proposed charts lies in the form used for $\varepsilon_\lambda(u)$ (Kondrat'yev 1965). Godson (1953) used idealised two- and three-layer atmospheric models with general assumptions about $\varepsilon_\lambda(u)$ to compare the assumptions made in chart models. He found that the charts of Deacon (1950) and Yamamoto (1952) gave the best results. Other charts showed differences in L_i of about five percent from these two charts, but generally agreed among themselves.

The Yamamoto and Elsasser charts were chosen for use in the present study. The former was selected since Godson (1953) found it to be the most accurate, and the latter was used since it has been most commonly employed in North America.

Yamamoto (1952) found that his chart gave L_i values from two to eleven percent greater than Elsasser's at corrected optical depths less than 2.5 cm, which is approaching the normal upper limit found in the North American atmosphere. There was good agreement at larger depths. There have been few comparisons of L_i measurements with chart predictions, but Robinson (1950) found that the Elsasser chart gave values from 6 to 14 percent greater than his measurements. Abraham (1960) used two types of radiometer (Gier and Dunkle 1951, Suomi et al 1954) and the charts of Robinson and Elsasser for intercomparison, and concluded that L_i cannot be determined more precisely than to about 5 to 10 percent.

Equation 7 applies to cloudless conditions only, and chart methods based on it are not well suited to other conditions. With complete cloud cover, however, it is possible to assume that the cloud acts as a black-body at the cloud base temperature, although it has been noted (Zdunkowski and Choronenko 1969) that at some wavelengths clouds may have an emissivity as low as 0.5. With blackness assumed, the cloud base can be taken to be the upper boundary of the atmosphere,

and charts can be used without modification. This principle can be extended to obtain some estimate of L_i in partly cloudy conditions, $L_{i(n)}$, using

$$L_{i(n)} = nL_{i(t)} + (1 - n)L_{i(c)}, \tag{8}$$

where n is cloud amount and subscripts c and t refer to cloudless and overcast conditions.

2: Empirical Formulae

Empirical formulae for predicting L_i are based on statistical relationships with easily measured surface parameters. Since only surface data are needed, they are more readily applied than chart methods. Being statistical, the formulae are generally best suited for prediction of averages of L_i for periods of at least a week.

Several relationships between screen level temperature T_a and vapour pressure e and L_i in cloudless conditions ($L_{i(c)}$), have been proposed. Vapour pressure is used as a surrogate variable for total optical depth of water vapour in the atmosphere u_t. The most frequently used formulae are:

$$L_{i(c)} = \sigma T_a^4 [a_a + b_a \exp(-\gamma e)], \qquad (\text{Ångström 1916}); \tag{9}$$

$$L_{i(c)} = \sigma T_a^{\,4}(a_b + b_b\sqrt{e}), \qquad \text{(Brunt 1932);} \qquad (10)$$

and

$$L_{i(c)} = T_a\,(a_e + b_e \log e), \qquad \text{(Elsasser 1942);} \qquad (11)$$

where a_a, a_b, a_e, b_a, b_b, b_e, and γ are constants. The ratio $L_{i(c)} / T_a^{\,4}$ is termed the effective emissivity of the atmosphere, ε_f, and is analogous to $\int_0^\infty \varepsilon_\lambda(u)\,d\lambda$ in equation 7.

These three formulae imply that ε_f is independent of temperature, and hence give reasonable results only because u_t is normally correlated with T_a (Swinbank 1963). It seems likely that differences in the $u_t : T_a$ relationship have resulted in variations of the constants with locality. Swinbank therefore suggested that L_i could be directly related to T_a, since, close to the surface, there will always be sufficient vapour for $\varepsilon_\lambda(u)$ to be a maximum and constant value. From measurements over several surfaces, including water, Swinbank found that two relationships of equal accuracy,

$$L_{i(c)} = a_s + b_s \sigma T_a^{\,4}; \qquad (12)$$

and

$$L_{i(c)} = A_s\, T_a^{\,B_s}, \qquad (13)$$

where a_s, b_s, A_s and B_s are constants, gave good results.

Deacon (1970) linked the humidity-based equations and equation 13 by using data of Yamamoto (1952) to show that equation 13 could be drived from equation 11 when the u_t : T_a relationship was included. Since equation 13 is not dependent on the u_t : T_a relation, which has a spatial variation, the constants should not be dependent on locality. Hence a single set of constants should be universally applicable, except for observations at high altitude, where there may be insufficient moisture above the site for constant $\varepsilon_\lambda(u)$ to be assumed.

Idso and Jackson (1969) found that the Swinbank formula gave incorrect results at temperatures outside the normal atmospheric range. They therefore proposed a relationship between $L_{i(c)}$ and T_a assuming that the relation between e and T_a was similar to that between the saturation vapour pressure and T_a. Since the indicated relations gave values for L_i greater than σT_a^4 for high T_a, the relationship was arbitrarily modified to

$$L_{i(c)} = \sigma T_a^4 \{1 - a_j \exp[-b_j(273-T_a)^2]\}, \qquad (14)$$

where a_j and b_j are constants. This form gave good results for data with a wide T_a range.

The effect of cloud on L_i has been treated by Phillips (1940), Elsasser (1942) and Möller (1954). Their empirical formulae are

variants of the form

$$L_{i(n)} = L_{i(c)}(1+cn) , \tag{15}$$

where c is a constant. Gal'perin (1949) argued that since cloud is highly variable in type, a bulk parameter, such as cn in equation 15, is not adequate. He therefore replaced it by

$$cn = c_L n_L + c_M n_M + c_H n_H, \tag{16}$$

where subscripts L, M, and H refer to low, medium and high cloud, in an attempt to specify the influence of cloud and cloud type on incoming longwave radiation.

Bolz (1949) used the form

$$L_{i(n)} = L_{i(c)}(1 + kn^2) , \tag{17}$$

where k is a constant, varying from 0.04 for high cloud to 0.25 for low cloud. Morgan et al (1971) have shown that this formula gives results close to measured values.

B. OUTGOING LONGWAVE RADIATION

Since the surface of the earth is approximately a grey body, $\varepsilon_\lambda = \varepsilon$ = constant. The flux emitted from the surface can therefore be obtained by integration of equation 4. Inclusion of an additional

term to account for surface reflection of incoming longwave radiation gives the outgoing flux from the surface,

$$L_o = \varepsilon\sigma T_s^4 + (1-\varepsilon)\ L_i . \tag{18}$$

If L_i is unknown, equation 18 must be simplified to

$$L_o = \varepsilon\sigma T_s^4 . \tag{19}$$

This usually results in little loss of accuracy, since $\varepsilon \to 1$, and therefore $(1 - \varepsilon)$ is small. Further, if $\varepsilon \to 1$, simplification to

$$L_o = \sigma T_s^4 , \tag{20}$$

is possible with little loss in accuracy.

The components of the right hand side of equation 18 refer to the actual surface. Radiometric determinations of L_o must be made some distance above the surface. Since radiative transfer upwards through the atmosphere can be treated in the same way as downward transfer, radiation will be both emitted and absorbed by the intervening air layer. Consequently there is likely to be a difference in flux between the two measurement levels. For an air layer close to a water surface, where large amounts of water vapour are usually present, the emissivity of the air layer, $\int_0^\infty \varepsilon_\lambda(u)d\lambda$, will be large (Hettner 1918), and may be of the same order of magnitude as the

surface emissivity ε. Hence the major cause of flux divergence will be the temperature difference between the surface and the measurement level, provided that the layer approaches saturation (Malevskiy-Malevich 1963). Divergence can be determined if the components of both sides of equation 18 are know. L_o, L_i and T_s can be directly measured or calculated.

Emissivity is dependent on wavelength, and it also varies with angle of emission. However, McSwain and Bernstein (1960) have shown that it varies little for water for emission angles between 0^o and 45^o. Values near normal will be considered here.

It is possible to determine the spectral emissivity ε_λ of a sample by laboratory methods, using an infra-red spectrophotometer with a reflection attachment (Bell 1957, Kislovskii 1959) to compare sample spectral reflectivity $S_{\lambda(s)}$ with that of a known standard $S_{\lambda(c)}$. This procedure is easier than working with absolutes. For a given wavelength λ, $S_{\lambda(c)}$ is given by

$$S_{\lambda(c)} = KA_\lambda , \tag{21}$$

where K is a constant and A_λ is the spectrophotometer response, in arbitrary units. For a sample

$$S_{\lambda(s)} = KB_\lambda , \tag{22}$$

where B_λ is the new spectrophotometer response. Hence, in the absence of transmission through the sample,

$$\varepsilon_\lambda = 1 - S_{\lambda(s)} = 1 - S_{\lambda(c)}(B_\lambda/A_\lambda), \tag{23}$$

where ε_λ is the sample spectral emissivity. Thus, the emissivity for any desired wavelength interval, λ_1 to λ_2, is

$$\varepsilon = \int_{\lambda_1}^{\lambda_2} [1 - S_{\lambda(c)}(B_\lambda/A_\lambda)]d\lambda \ . \tag{24}$$

Field methods for the determination of ε for a range of wavelengths have been given by Buettner and Kern (1965), Fuchs and Tanner (1968) and Lorenz (1966). Although each used different field techniques, the underlying theory was approximately the same. The flux from a surface exposed to the atmosphere received at a sensor is

$$F_1 = \omega \int_{\lambda_1}^{\lambda_2} \phi_\lambda \varepsilon_\lambda \pi^{-1} F_\lambda(T_s)\, d\lambda \ + \ \omega \int_{\lambda_1}^{\lambda_2} \phi_\lambda (1-\varepsilon) L_i \, d\lambda \ , \tag{25}$$

where ϕ_λ is the spectral sensitivity of the sensor and ω is the solid angle of sight of the sensor. F_1 can be equated to the flux received at the sensor from a black-body at temperature T_r. Hence

$$F_1 = \omega \int_{\lambda_1}^{\lambda_2} \phi_\lambda F_\lambda(T_r)\pi^{-1} \, d\lambda \ . \tag{26}$$

For the wavelength range of most remote temperature sensing devices (8μ to 12μ), ϕ_λ and ε_λ can be assumed constant (Lorenz 1966). The

atmospheric flux, the second term on the right hand side of equation 25, can be replaced by the Planck function for a suitably chosen temperature, the atmospheric radiation temperature T_u. The constant of integration of the Planck function for the range λ_1 to λ_2 can be assumed constant with temperature at atmospheric temperatures. Hence, combining, rearranging and integrating equations 25 and 26,

$$\varepsilon = (T_r^4 - T_u^4)/(T_s^4 - T_u^4). \qquad (27)$$

The emissivity can thus be determined in the field from a set of three temperature measurements with a remote temperature sensing device.

C. NET LONGWAVE RADIATION

Since the net longwave radiation is simply the difference between the incoming and outgoing fluxes, its behaviour can be understood only in terms of these separate fluxes. However, direct prediction equations for L_n can be obtained if the outgoing flux is approximated by σT_a^4 and ε_f is determined by one of the equations 9 to 11. Thus

$$L_n = \sigma T_a^4 (\varepsilon_f - 1). \qquad (28)$$

Sellers (1965) accounts for the difference between net longwave radiation at the surface, L_{ns}, and that at measurement level, L_n, by the expression

$$L_n - L_{ns} = \sigma(T_s^4 - T_a^4). \tag{29}$$

Using this refinement, and introducing the surface emissivity, equation 28 becomes

$$L_n = \varepsilon\sigma[T_a^4(\varepsilon_f - 1) - (T_s^4 - T_a^4)]. \tag{30}$$

Kondrat'yev (1965) has argued the sound theoretical base for this formula.

D. NET RADIATION

Since net radiation varies with any one of its components, the relative importance of the shortwave and longwave flux variations on R_n variations can be determined by obtaining the rate of change of L_n with Q_n. This rate of change can be defined, following Gay (1971), as

$$dL_n/dQ_n = \lambda_n. \tag{31}$$

If $\lambda_n = 0$, L_n changes are small with respect to those of Q_n, and the latter are dominant in producing R_n changes. As $|\lambda_n|$ increases the influence of L_n on R_n increases, and L_n and Q_n have equal influence when $|\lambda_n| = 1.0$. L_n is dominant when $|\lambda_n| > 1.0$. Also, $\lambda_n > 1.0$ indicates that L_n and Q_n are acting in the same direction to produce R_n changes. Further, since

$$\lambda_n = \lambda_i - \lambda_o \tag{32}$$

where λ_i and λ_o refer to the rate of change of L_i and L_o with Q_n, the relative importance of the two longwave fluxes can also be considered.

Net radiation can be determined if the four components of the radiation balance (equation 2) are known, but errors in the measurement or prediction of these terms are accumulated in R_n. Consequently, in the absence of measurements of R_n, a simple, direct method of estimation is preferable to a determination of the component fluxes.

Since R_n is considerably easier to measure for a land surface than for water, it would be convenient to convert land data to apply for nearby water surfaces. Although differences between R_n over land and water have been noted (Kondrat'yev 1965) there has been no previous attempt to determine suitable conversion factors.

Daytime net radiation can be determined accurately from measurements of incoming or net solar radiation, which can be relatively easily obtained over water. Close correlation between R_n and Q_i or Q_n has often been demonstrated (Ekern 1965, Fritschen 1967). The close correlation arises because: temporal variations in L_i are usually small and depend mainly on cloud amount; L_o is dependent on surface heating and thus usually follows the course of solar radiation

with some hysteresis lag; and the reflected component of solar radiation is directly dependent on the incoming component.

Relationships of the form

$$R_n = a + bQi \tag{33}$$

and

$$R_n = a' + b'Qn, \tag{34}$$

where a, a', b and b' are constants, have been proposed. Since good correlation between R_n and Q_i or Q_n depends to a great extent on the constancy of L_i, cloudless days, when L_i is most nearly constant, are best suited to this type of analysis. High correlations, however, have been obtained on days with cloud (Stanhill et al 1966, Davies 1967).

Since equation 34 can be rewritten as

$$L_n = a' + (b'-1)Q_n, \tag{35}$$

a' must be governed by L_n, and b' by the variation of L_n with Q_n.

For daily regressions using half-hourly data the constants a and a' give some indication of R_n at sunrise and sunset. Since it is not possible to obtain measurements at $Q_i = Q_n = 0$, such values

depend on extrapolations. Consequently it is unlikely that a and a' are identical.

From equations 33 and 34,

$$dRn/dQi = b, \quad dRn/dQn = b'. \tag{36}$$

If L_i and L_o are constant for the period used to determine the regression coefficient,

$$dRn/dQn = 1, \quad b' = 1. \tag{37}$$

Any departure from this value indicates that the longwave fluxes are not constant. For example, if L_n shows a midday minimum, as usually occurs because of surface heating, $b' < 1$. However, the correct b' value for any given data set with known L_n variations is not clear, since Idso et al (1969) have demonstrated, for a single data set, that the value depends on the method of data analysis.

E. SURFACE HEATING

Surface temperature, since it largely controls L_o, is a component of the radiation balance at the surface. At the same time it is greatly influenced by the other components of the balance. Hence L_o flux variations, unlike those of L_i, cannot be treated in

isolation from other factors. Surface temperature is dependent on the surface energy balance:

$$R_n = H + E + G + \Delta F, \tag{38}$$

where H = sensible heat exchange between surface and air,

E = latent heat exchange between surface and air,

G = heat exchange between the water surface and deeper layers,

and ΔF = the subsurface horizontal heat flux.

Since R_n is usually the main energy input to a surface, it largely controls T_s. The other energy fluxes, therefore, are mainly a response to radiatively induced surface temperature changes, although the temperature itself will be modified as a result of energy transfer by these fluxes. Hence, consideration of the rate of change of T_s with R_n is important for an understanding both of the cause of modification of the boundary conditions for the surface energy balance and of the influence of a surface on net radiation.

A parameter relating R_n to T_s can be defined directly as

$$\beta^* = dLo/dRn. \tag{39}$$

Monteith and Sceicz (1961) defined a 'heating coefficient' β, for use when measurements of R_n and Q_n (or L_n) only were available, as

$$\beta = -dLn/dRn. \tag{40}$$

They emphasized that this could be used only when L_i was approximately constant. In such conditions, equation 40 reduces to equation 39. Monteith and Sceicz (1961) considered β to be constant and predictable for a given surface. Since

$$\beta = (1-b')/b', \tag{41}$$

equation 34 could be rewritten as

$$R_n = a' + \beta Q_n. \tag{42}$$

Hence R_n values could readily be obtained from Q_n measurements if the β value were known.

β^*, and β in constant L_i conditions, will be constant from day to day only if either R_n completely controls T_s, implying constancy of the fluxes on the right hand side of equation 38 with time, or that these fluxes have approximately the same diurnal variation each day. Such a situation may occur in the absence of changes in the horizontal movement of air or water. Usually there is a smooth diurnal variation of R_n which will be similar from day to day. From the conservation of energy principle, the components H, E, and G must follow approximately the pattern of energy input. Consequently the diurnal variation of R_n and T_s should be similar, with a phase lag

in T_s maximum behind the R_n maximum of about three hours (Lettau 1951).

If variable horizontal air motion is present, however, H or E will vary either as a result of atmospheric advection or of wind speed changes. Similarly, changes in horizontal water movement will lead to changes in heat storage near the surface because of energy advection in the water. In these conditions, therefore, surface temperature will not be controlled by radiation, and β^* will not be an index of surface radiative heating.

CHAPTER 3

SITE, INSTRUMENTATION AND FIELD METHODS

A. SITE

The site chosen for the field study was about 15 km east of Grimsby, Ontario, off the junction of Martins Road and Lakeshore Road, in Clinton Township (43^{o} 13'N, 79^{o} 22'W) (Figure 1). At this point the Niagara escarpment, the major cause of horizon problems along the south shore of Lake Ontario, is about 4 km inland, and relatively low. The horizon from the site was open in all directions.

The site was selected so that there was: good potential instrument exposure, with low horizons in all directions; fairly deep water (>2 m) within 300 m of the shore; no major air or water pollution; low shoreline to facilitate cable laying; a dock facility for a small boat; absence of resort or recreational facilities in the area, for security; availability of A.C. power; and easy road access.

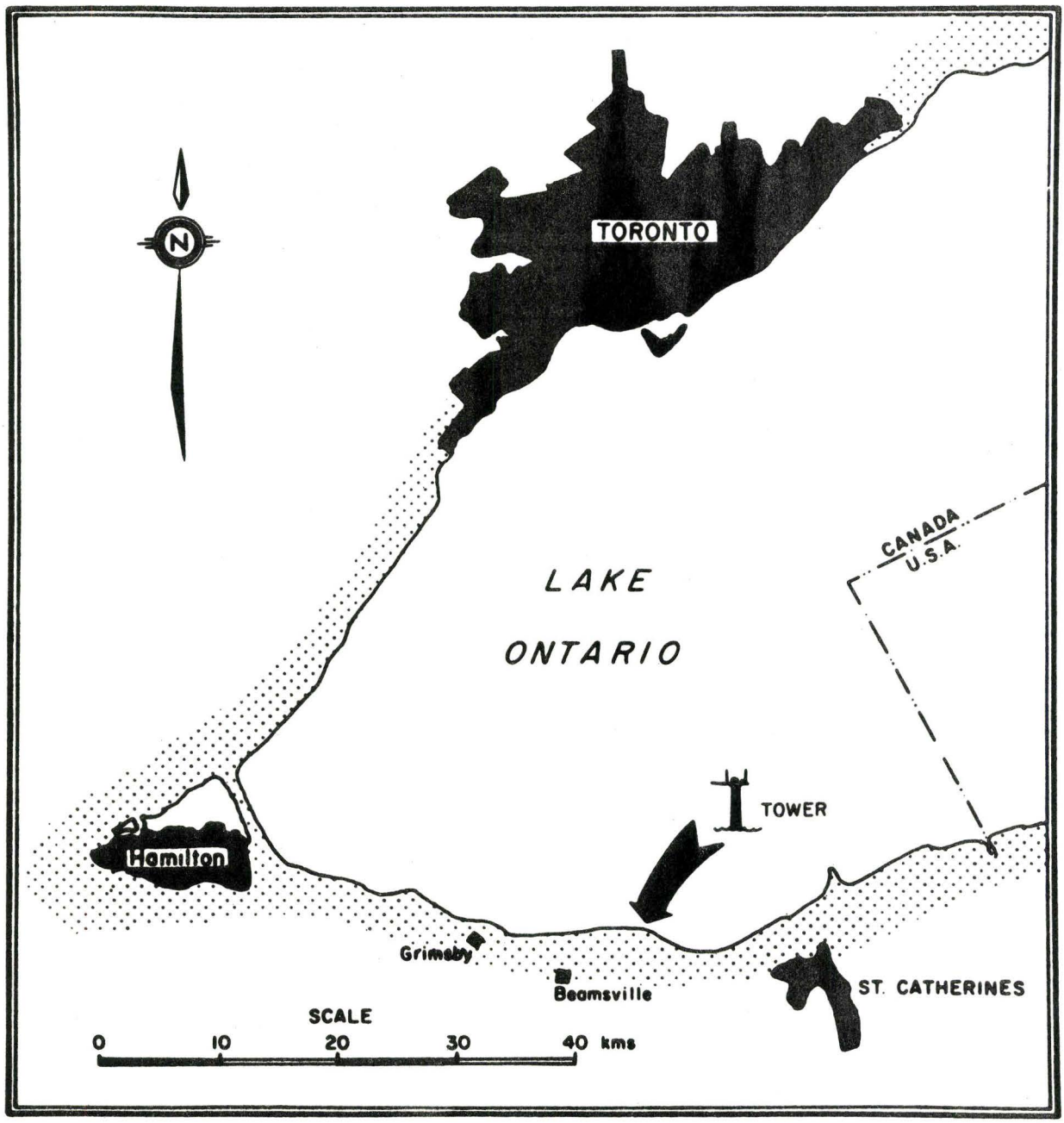

FIGURE 1 TOWER LOCATION

B. INSTRUMENTATION AND FIELD METHODS

1: Tower

The exact location of the instrument tower within the general area of the chosen site was determined after the lake bed had been examined by divers. It was placed about 500 m offshore. Water depth at the start of the season (July 1st) was about 4.5 m. The lake level feel steadily throughout the season, and the water was only some 3.5 m deep by November.

The aluminum tower was a 9 m high heavy duty sectional TV mast, 30 cm square (Figure 2). Three sets of anchor cables, at the top, middle and base of the mast were attached to four anchors set in concrete gabions weighing 1 ton each, and located approximately 7 m from the tower baseplate. This system ensured rigidity in all wave conditions likely to arise on the lake.

A 2 m square open-mesh platform for instrumentation was placed on the mast section. This was positioned with its sides aligned to the cardinal points of the compass. The north side was flush with the north side of the mast, to provide access from the mast. A radar reflector screen and a flashing warning light were provided for safety from lake craft.

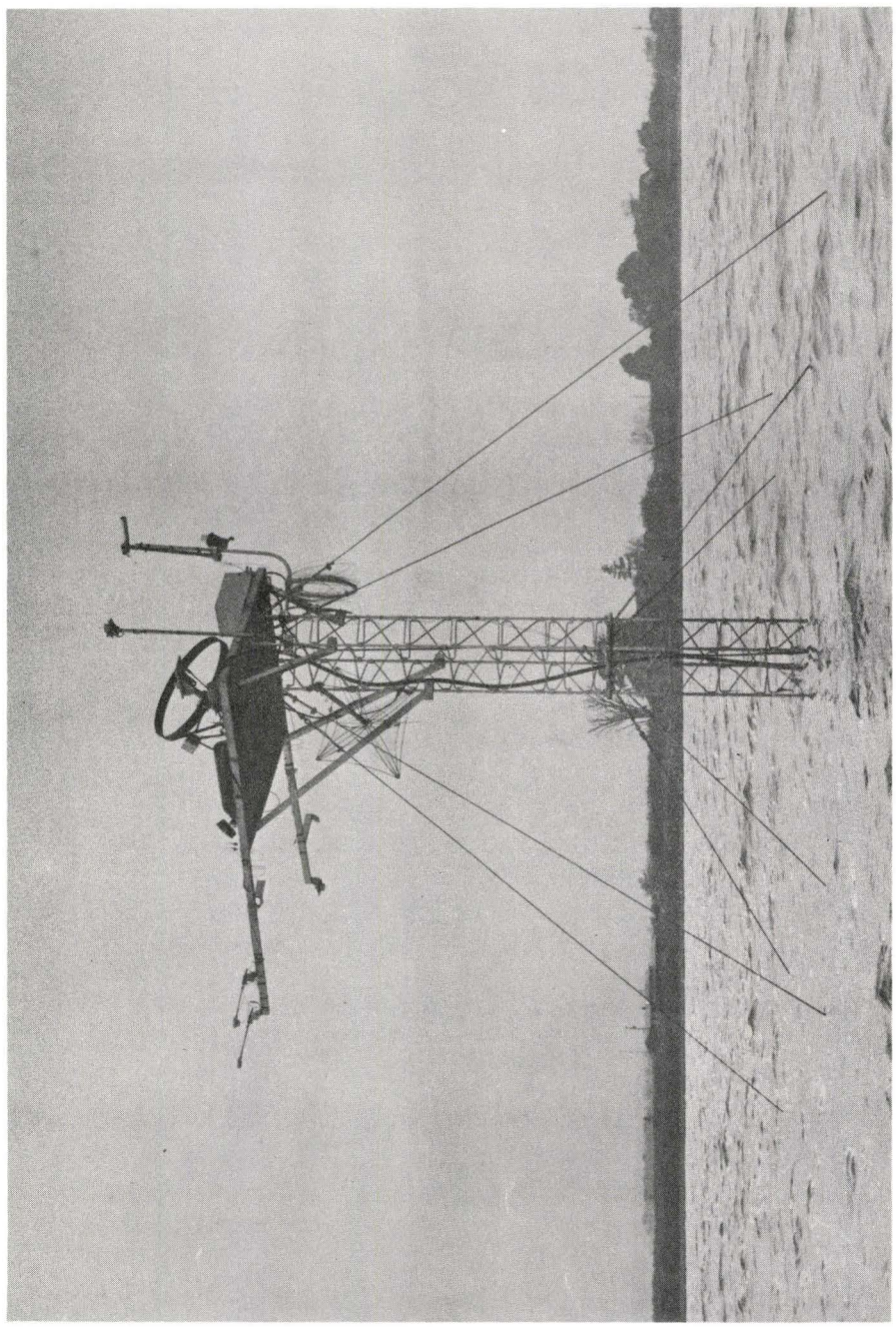

FIGURE 2. THE TOWER.

A. C. power was provided from the recording centre by underwater cable (Belden Shielded Cable). A circuit breaker was incorporated in the line which was automatically tripped if a power surge, caused possibly by a leak in the cable, occurred. This prevented damage to sensors and recorders through overloading. This circuit breaker was tripped several times during the season, sometimes for unknown reasons, but usually when there was lightning in the area.

2: Radiation Measurements

Two types of commercially available radiation sensors were used in this study (Table 1). Both are similar in that they operate on a differential thermopile principle. The output voltage V from a thermopile with temperature difference ΔT_* between the hot and cold junctions can be expressed in the simplified linear form

$$V = k_* \Delta T_* \ , \tag{43}$$

where k_* is a proportionality constant related to the thermopile materials. This equation, combined with an equation relating ΔT_* to a radiant flux, allows the flux to be measured in electrical units. The nature of the relationship depends on the energy balance of the

TABLE 1

RADIATION SENSORS AND CALIBRATIONS

Function	Sensor	Calibration Constant mV/cal $cm^{-2}min^{-1}$		
		Initial	Final	Adopted
Solar radiation*	Eppley, Model 8-48	7.45	7.57	7.51
Solar radiation**	Eppley, Model 6-90	17.60	17.80	17.70
Reflected solar radiation	Eppley, Model 8-48	6.00	6.13	6.06
Net radiation	Swissteco, Model S-1	23.0	23.0	23.0
Incoming total radiation	Swissteco, Model S-1	21.0	21.0	21.0

* July 1st - August 10th.

** August 11th - November 18th

sensor, and this differs for each type of sensor. Sellers (1965) gives details of these relationships, while Robinson (1966) considers the general desirable properties of instruments for radiation measurements.

(a) Eppley Pyranometer:

The thermopile of the Eppley Pyranometer (Eppley Laboratories Inc., Newport, R.I.) consists of radially wound copper plated constantan wire (Monteith 1959). The cold junctions are in good thermal contact with surfaces painted white with barium sulphate, and the hot junctions with surfaces coated with Parsons Optical Black (Figure 3) (Kimball and Hobbs 1923). The thermopile is located on an equatorial plane below a glass hemisphere which transmits only solar radiation. This hemisphere is provided with an O-ring moisture seal. Since there is no means of purging this instrument, should a moisture leak develop the instrument must be replaced. The instrument measuring incoming solar radiation during the lake program had to be replaced for this reason. The sensor measuring reflected solar radiation remained moisture-free throughout the season.

(b) Swissteco Net Radiometer:

The net radiometer (Swissteco Pty., Melbourne, Aust.) is a modified version of the C.S.I.R.O. instrument designed by Funk (1959).

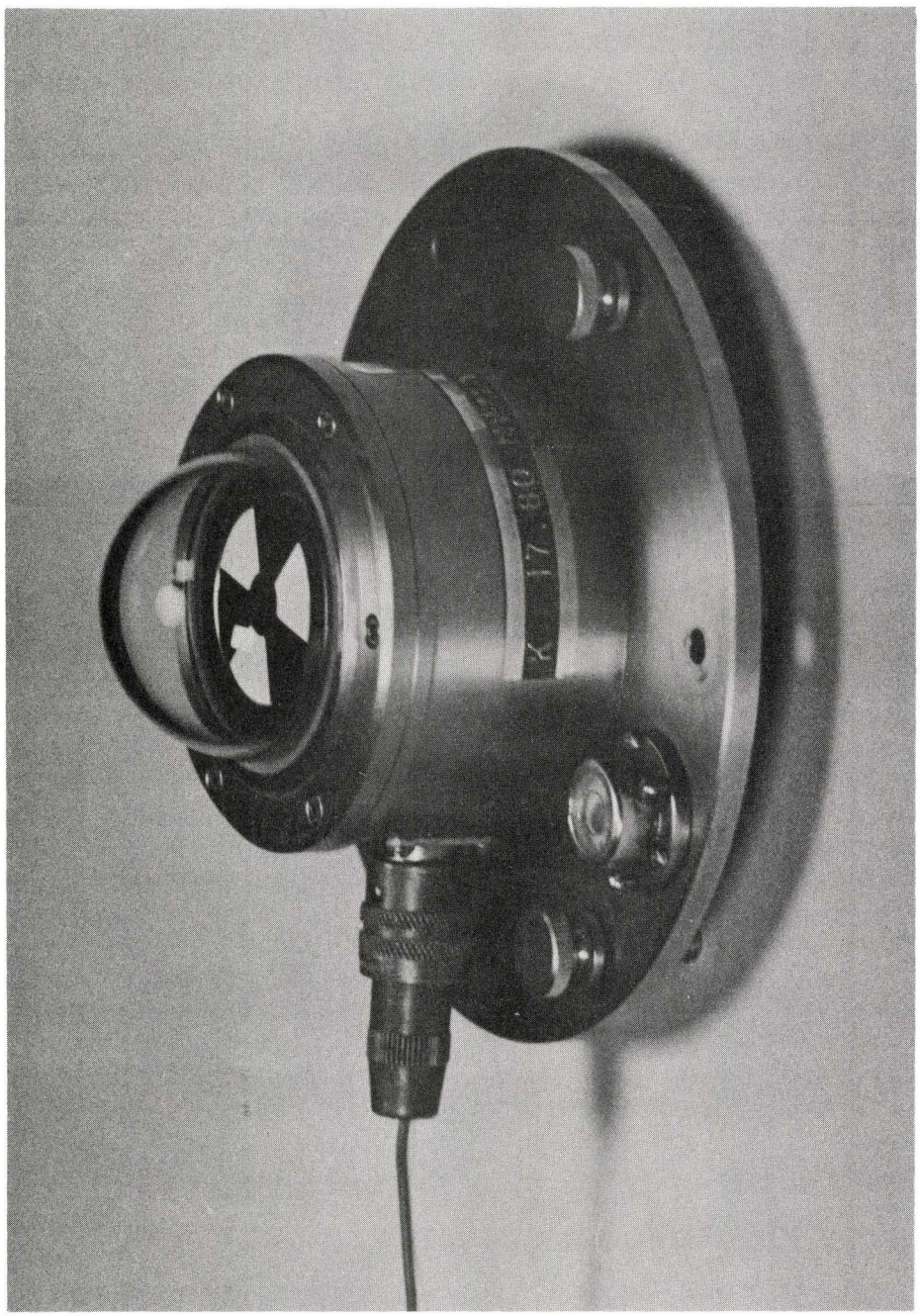

FIGURE 3. EPPLEY PYRANOMETER (MODEL 6-90).

The sensor (Figure 4) consists of a cross-shaped thermopile constructed by copper plating constantan wire as in the case of the Eppley instrument. In this design, one set of junctions is in good thermal contact with an upward facing blackened surface, while the other set is in contact with a blackened surface that faces the ground. The thermopile surfaces are enclosed within a pair of polyethylene hemispheres which transmit radiation of nearly all wavelengths. Portions of the sensor surface are painted white to equalize the long and shortwave calibrations. Ports are located within the head and handle of the instrument to allow purging of the inside of the domes with a dry gas and outer surface ventilation of the polyethylene.

One Swissteco instrument was used as a net radiometer with polyethylene domes covering both surfaces. The second instrument was converted to a total hemispheric radiometer, measuring incoming radiation of all wavelengths, by replacing the lower dome with a black-body cavity. The output of the instrument was then proportional to the difference between the total incoming radiation, T_i, and the radiation emitted by the inner surface of the cavity. If the cavity temperature, T_c, is known, the flux on to the lower surface can be calculated by the Stefan-Boltzmann law. The incoming flux is given by

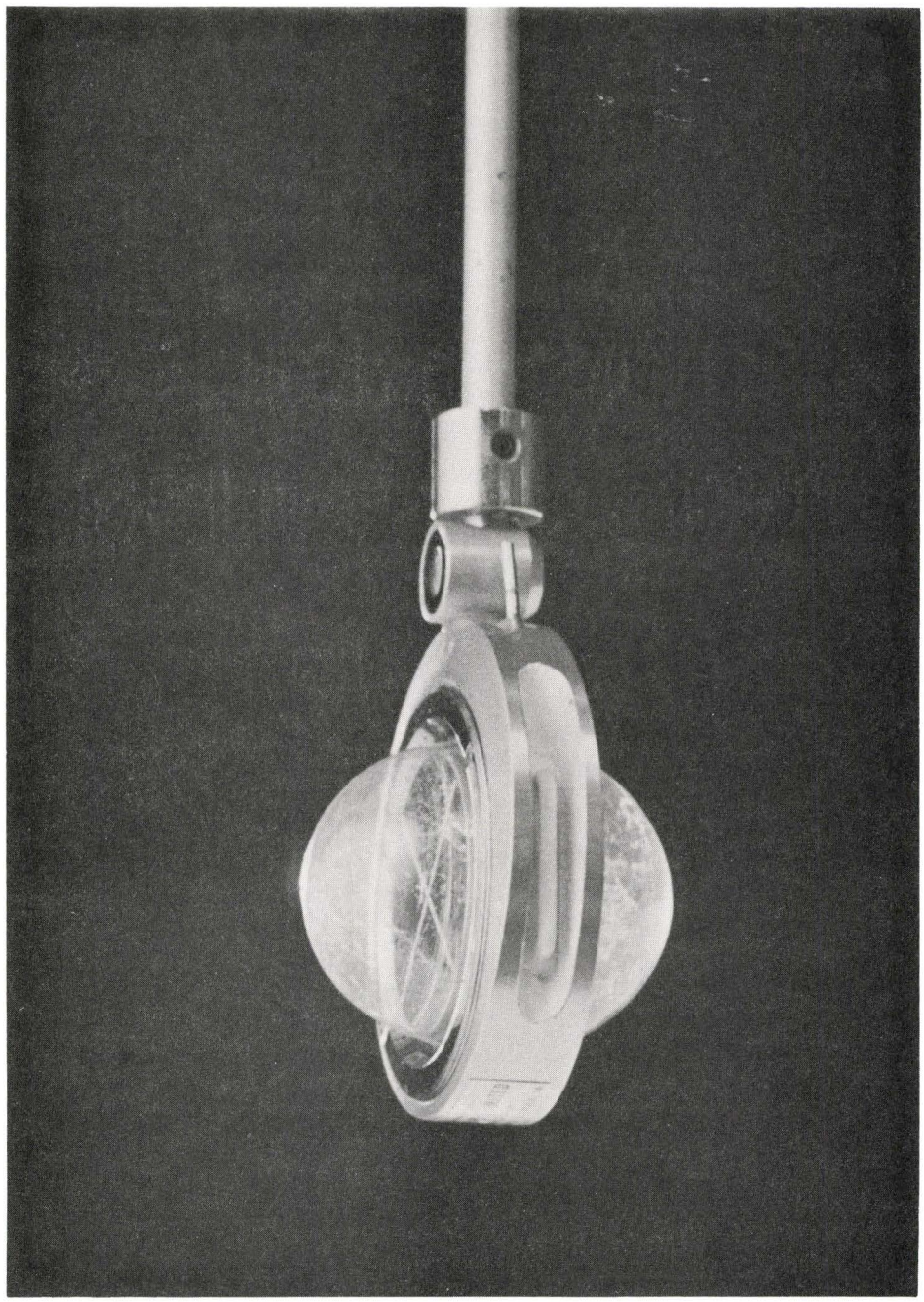

FIGURE 4. SWISSTECO NET RADIOMETER (MODEL S-1)

$$T_i = T_i^1 + \sigma T_c^4 , \qquad (44)$$

where T_i^1 is proportional to the radiometer output. T_c was measured by a thermistor embedded in the cavity.

The cavity is designed to minimize internal temperature fluctuations, hence T_c was sampled once every five minutes. The temperature trace, however, indicated that rapid fluctuations were occasionally possible, especially in alternately cloudy/bright conditions when the outer surface of the cavity received direct solar radiation. Such rapid fluctuations suggest that convection is present within the cavity, and consequently a single measurement of T_c may not be adequate for calculation of the flux on to the lower thermopile surface. Better insulation of the cavity from solar radiation effects may lead to less fluctuation and hence allow a better estimate of the flux from the cavity.

Nitrogen for purging the interior of the instruments was obtained from 0.1 m^3 cylinders, one for each instrument, located on the tower platform. A regulator was attached to each cylinder, and the flow rate, as measured by a bubbler, was controlled to approximately 15-50 bubbles per minute, slightly faster than the minimum rate recommended by the manufacturer.

Towards the end of the experimental period the nitrogen purging system for the T_i measuring radiometer was replaced by a 7 W aquarium pump, passing air through a silica gel container into the radiometer. A similar bubble rate was maintained. There was no apparent change in instrument output or performance caused by this change. The pump system was therefore as effective as the nitrogen system, and was considerably better suited to work on the confined space of the platform. Little maintenance was needed beyond the replacement of the silica gel approximately every three days. On no occasion did the drying agent appear excessively wet when replaced. With the pump in operation the thermopile surfaces are protected. Pump operation could be monitored remotely, and hence any malfunctions speedily rectified. If a nitrogen system is used, however, the cylinder can quickly drain if a small leak appears in the system. The thermopiles are then unprotected, and this condition may remain undetected if there is no regular surveillance.

The outer surfaces of the instrument domes were aspirated to prevent moisture condensation and to equalize heat transfer to the atmosphere from both upward and downward facing domes. During initial tests on the instruments it was found that low aspiration rates altered the calibration constant slightly, the minimum flow for constant output being equivalent to four litres per second. This flow rate was exceeded throughout the work. Any data collected at times when the A.C. powered compressor used for aspiration was inoperative were discarded.

Since the domes of the Swissteco instruments are subject to ageing, leading to a change in transmission properties, they were replaced at four week intervals. The domes were also cleaned regularly, to prevent an accumulation of dirt and dust. In no case could ageing or dirt and dust accumulation be detected before the domes were replaced.

(c) Instrument Calibration:

The Eppley instruments were calibrated by the manufacturers, and these values were accepted at the commencement of the field season (Table 1). The initial calibration of the Swissteco instruments was carried out at the National Radiation Laboratory by Mr. J. R. Latimer. At the end of the season all sensors were recalibrated. The calibration constants for the Swissteco instruments remained constant throughout the season (Table 1). The Eppley calibrations increased by about 2 percent. Since the accuracy of these instruments is about 5 percent, this small change is negligible, and the means of the two calibration sets were used.

(d) Instrument Mounting :

The pyranometer measuring incoming solar radiation was located on the north side of the platform and raised one metre above platform

level, to minimize interference with other sensors. The remaining sensors, measuring R_n, T_i, and Q_o, were placed on booms projecting from the southern edge of the platform, and were about 4 m from the tower structure. Hence only a small portion of the radiation incident on the downward facing surfaces came from the tower instead of from the water. The booms were hinged close to the platform so that the sensors were readily accessible for maintenance.

With this mounting system the instruments on the booms could be levelled only to within 2^{o} of horizontal. Although the instruments are cosine dependent the error caused by this small deviation is less than 1 percent. A retrospective check on levelling was possible, since on clear days Q_i, T_i and R_n should be at a maximum at solar noon. The data suggest that this was the case, maxima usually being within a few minutes of this time.

(e) Calculation of non-measured fluxes:

The instruments used in this study gave direct measurements of R_n, T_i, Q_i, and Q_o. The other components of the radiation balance (equations 1 and 2) could then be calculated from:

$$Q_n = Q_i - Q_o; \tag{45}$$

$$L_i = T_i - Q_i; \tag{46}$$

$$L_o = T_i - R_n - Q_o; \tag{47}$$

and

$$L_n = L_i - L_o = R_n - Q_n. \tag{48}$$

3: Temperature Measurements

The temperature sensors used in the study had to be rugged, waterproof, and capable of operating continuously for extended periods without maintenance. Although accuracy was desirable, rapid response was not considered necessary. Thermistors (Yellow Springs Instruments, Yellow Springs, Ohio) were selected. The leads attached to the thermistor beads by the manufacturer were extended to the required length with standard electrical conductors.

The thermistors were calibrated prior to installation, with the lead extensions in place, in a constant temperature water bath. All had similar characteristics, despite the slight difference in lead length, and a single, linear, calibration curve could be used.

(a) Air Temperature Measurement

Yellow Springs Instruments Model 406 thermistor, with the bead at the end of a 12 cm stainless steel tube of 0.4 cm O.D., was used.

The time constant was 2.5 sec. With a large temperature sensing element, radiation errors are likely to be large (Tanner 1963). The sensor was therefore placed in a tubular styrofoam shield, 2.5 cm O.D., and 23 cm long, coated externally with reflecting mylar tape. The sensor was aspirated to prevent a stagnant air layer forming around it, by a small electrical motor drawing air through the shield.

(b) Humidity Measurement

The psychometric method of humidity measurement was adopted, since this allows continuous measurement. A second model 406 thermistor was placed in the radiation shield, parallel to and slightly below the dry bulb sensor. Distilled water was fed from a closed plastic container adjacent to the shield to the sensor along a wick. The wick was enclosed in vinyl tubing to prevent evaporation. Close to the thermistor bead Kleenex tissue replaced the wick. This was replaced at monthly intervals. The tissue had to be changed at least every four days to prevent an accumulation of dirt, which would lead to uncertain humidity values.

From the measurement of wet and dry bulb temperature the humidity was calculated by the Groff-Gratch formula (List 1966).

The system generally performed adequately during the field season. At times, however, data were lost as a result of drying of the wet bulb. A slight kink in the wick was sufficient to cause this. Various attempts to overcome this problem were made, but none appeared completely successful. This remains a problem for humidity measurement in remote locations.

(c) Surface Temperature Measurement

Water surface temperature was measured with an infra-red thermometer, and with temperature sensors on single and multiple sensor floats.

The infra-red thermometer (Barnes Engineering Co., Stamford, Conn., Model PRT 5) (Figure 5) was used on selected occasions as a standard method of surface temperature measurement. The instrument was used from the tower platform. Prior to each set of measurements the temperature of a convenient area of water was determined from a boat. The temperature of the same area was then determined from the platform. On no occasion were these determinations different, so flux divergence between the surface and the platform could be neglected.

A single thermistor was used in an attempt to monitor values continuously. The sensor was a Yellow Springs Instrument

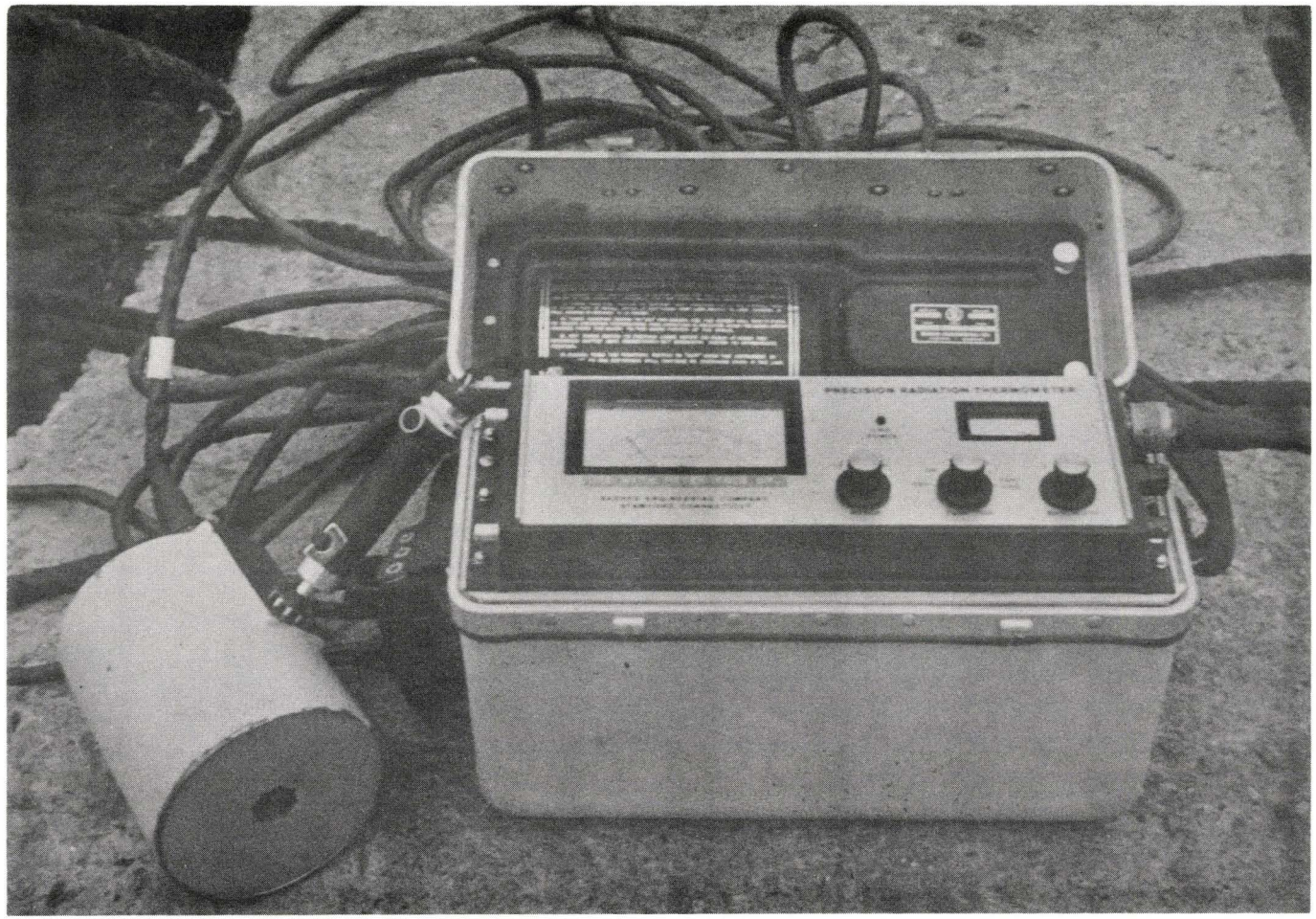

FIGURE 5. BARNES INFRA-RED THERMOMETER (MODEL PRT 5).

Model 401 general purpose waterproof thermistor, with a vinyl tip, radius 0.2 cm, and a vinyl covered lead, 0.3 cm O.D.. The time constant was 7 sec. The thermistor was threaded through a hole drilled in a styrofoam float 12 x 12 x 9 cm (Figure 6). The height of the sensor element was adjusted to correspond approximately with the water level. Close to the bead the hole was enlarged to allow free water movement. The float was anchored to the lake bed. Shortly after initial installation a leak was detected in the lead cable, and the sensor was replaced. At the same time the hole at the base of the float was enlarged to allow better water movement. The position of the thermistor was adjusted occasionally to compensate for changes in float level. It was regularly checked and cleaned to remove weeds that collected around the float and anchor cable.

A float system using five thermistors was designed. Four of these were placed at the centre points of the sides of a square aluminum frame, of side 63 cm, which had styrofoam floats (12 x 12 x 9 cm) at the corners (Figure 7). These four thermistors were fixed in position at the start of the season so as to be as close as possible to the water level. The fifth sensor (Yellow Springs Instruments Model 406) was at the intersection of the cross-members of the frame. The height was adjusted prior to each run. This float was used close to the tower, with the sensor cables linked directly to the tower

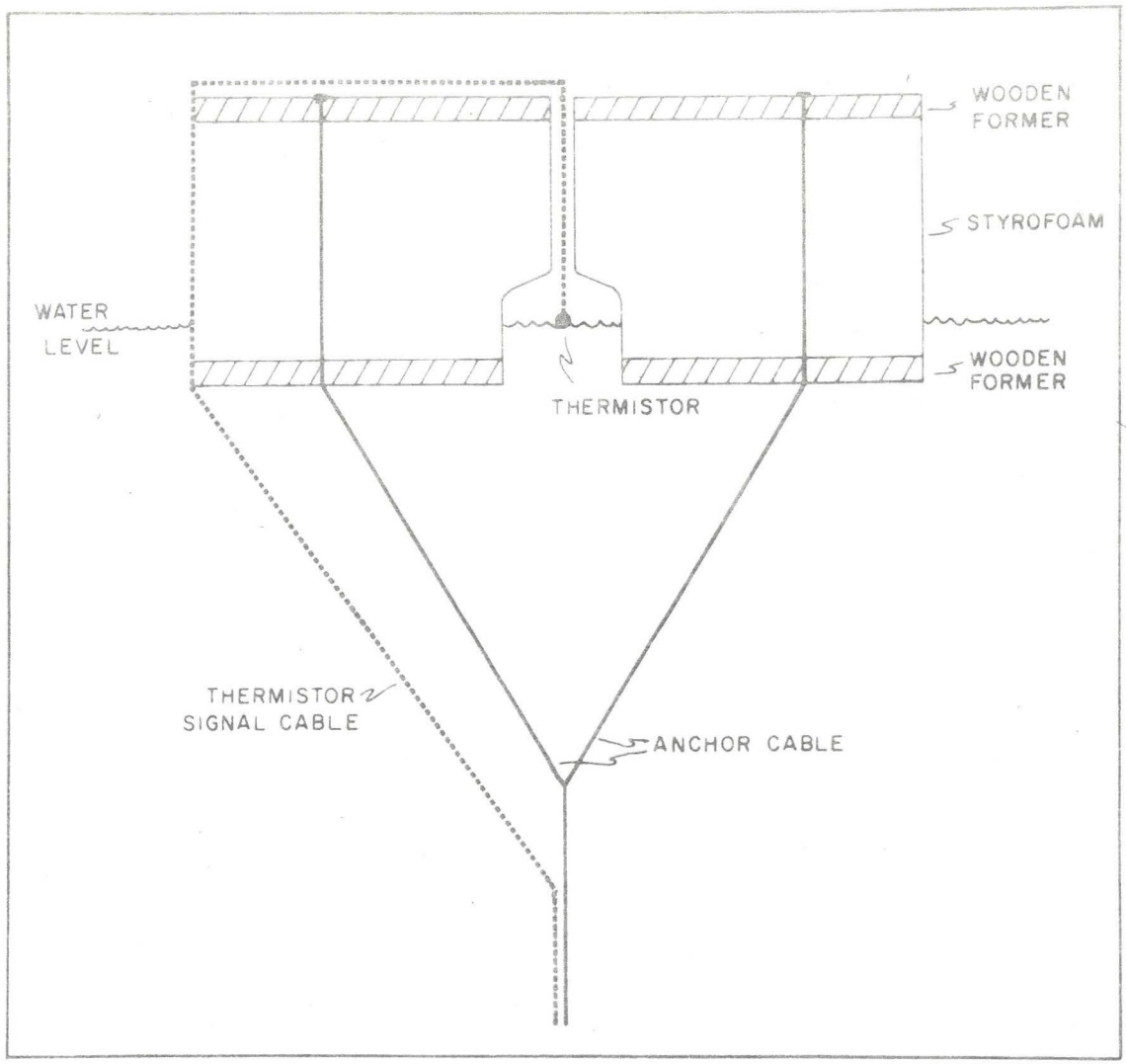

FIGURE 6 CONSTRUCTION OF SINGLE THERMISTOR FLOAT

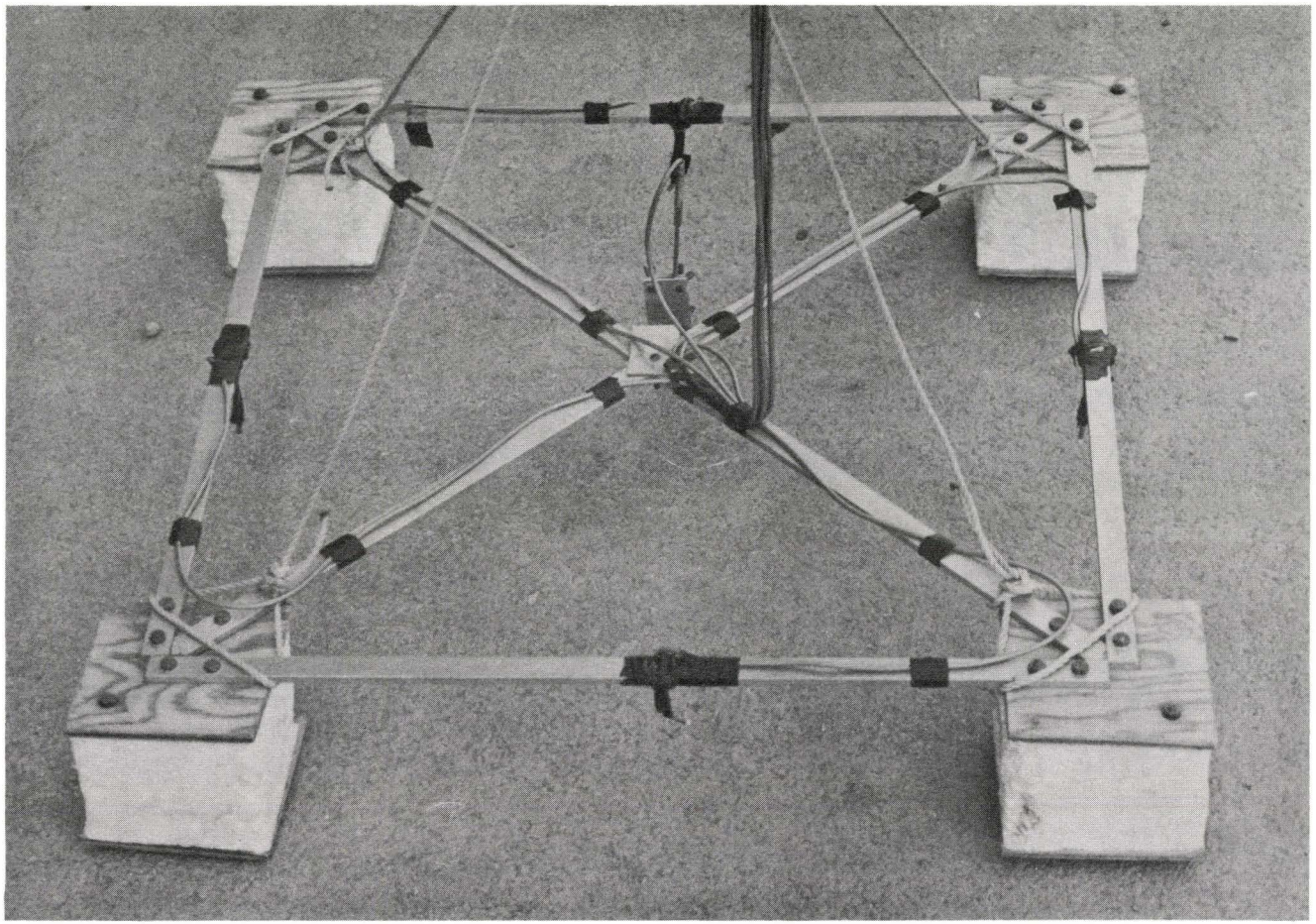

FIGURE 7. CONSTRUCTION OF MULTIPLE THERMISTOR FLOAT.

platform. It was only used for short periods at times when the infra-red thermometer measurements were made. It could not be used in rough conditions.

Although the sensors of both the single and multiple sensor floats were probably not at the exact interface, it seems likely that they were close to it and would, in all but completely calm conditions, alternate between in-air and in-water conditions. The resultant rapid temperature fluctuations were smoothed because of the sensor time constants, and the recorded output should therefore approach the true surface temperature. At night the smoothing process would probably give rise to accurate values, as at this time the temperature gradients at the interface are least steep. During the day evaporative cooling lowers the surface temperature slightly (Malevskiy-Malevich 1963), so that the sensors may overestimate the true value.

(d) Temperature Signal Scanning

The thermistor signals were wired into a scanning device (Yellow Springs Instruments Scanning Telethermometer) on the tower platform. Signals were normally scanned in the order: zero channel; wet bulb; dry bulb; water surface (single float); open channel. The scanning rate was one channel per minute. For the short period

runs, when the multiple sensor float was in position, eleven channels were used, with a second open channel used for ease of channel identification. The channels were then scanned at a rate of three channels per minute.

The scanner was housed in a white painted wooden box for protection, and operated throughout the season without attention. A direct readout dial on the instrument was used for routine checks of the thermistors. Internal circuitry converted the thermistor signals to millivolt signals which were recorded on shore.

4. Signal Recording and Reduction

All radiometer and temperature signals were passed through underwater cable to the onshore recording site. Eight, two conductor, p.v.c. covered, shielded cables (Boston Insulated Wire and Cable Co.) were laid, to record all signals and allow for two replacement channels. These replacements were not needed. The cables were taped together and threaded through strong p.v.c. tubing to give added protection against abrasion on the lake bed. The tubing was anchored with cement bags located at approximately 30 m intervals along its length. The position of the cable was marked by styrofoam buoys. At the shore the cables passed over a 2.5 m concrete retaining wall before entering the recording centre. Abrasion of the outer tubing

at this wall became evident as the season progressed. Consequently the vertical section and the first metre of underwater cable were embedded in concrete.

Throughout its route, the sensor cable was separated from the power cable, to prevent any interference with the sensor signals.

Signals were recorded on four dual-channel potentiometric strip chart recorders (Hewlett Packard Co., Model 7100B, with 17501A plug in modules). These were equipped with variable range spans and zero settings, and had electric writing. They were individually grounded to a cast iron water pipe, and the instrument rack was separately grounded, to eliminate spurious signals.

Time marks were put onto the charts each day from the broadcast signal of the Dominion Observatory. Whenever possible a zero check for the R_n and T_i records was performed daily. The appropriate adjustments were then made. Any necessary adjustments to the zero for the solar radiation records were made during the night. Rarely was zero drift detected, and in no case did it amount to a change in indicated flux of more than 0.005 cal cm^{-2} min^{-1} in any 24 hour period. Recorder accuracy was tested periodically throughout the season, using an accurate millivolt source. In all cases the accuracy was found to be within the manufacturers specification of one percent for full scale deflection.

The data were reduced from the continuous records to half-hourly averages, beginning on the hour, true solar time. The radiation records were planimetered, and the temperatures were read off by eye. The recorder chart drives were sufficiently accurate for time to be easily determined by distance from the time mark. The data are presented in Davies et al (1970).

The systems described worked well throughout the measuring period, despite the potential difficulties of passing signals under water. Recording on the tower would have removed these possible difficulties, but other, less accurate, types of recorder would have been needed. In addition, with the system chosen, a more continuous check on the instrument output could be maintained, and the performance continuously monitored. Consequently faults could usually be speedily rectified. This led to records with few breaks.

5. Errors in Radiation Flux Measurement

There are three possible sources of error in the determination of the radiation fluxes:

(i) Sensor error: The sensor error is difficult to determine, and depends to a great extent on the care taken to maintain the sensors (Robinson 1966). Values used here (Table 2) have been obtained from various sources (Abraham 1960, Funk 1959,1961,1962, Robinson 1966);

TABLE 2

ERROR ESTIMATES FOR RADIATION FLUX MEASUREMENTS AND CALCULATIONS

A. Measured Fluxes

Flux	Sensor error	Recorder error	Integration error	RMS error
Q_i	5%	1%	2%	5.6%
Q_o	5%	1%	2%	5.6%
R_n	10%	1%	2%	10.2%
T_i [1]	10%	1%	2%	10.2%
T_c	5%	1%	2%	5.6%

B. Calculated Fluxes

Flux	Error
Q_n	7.7%
T_i	6.6%
L_i	8.6%
L_n	12.8%
L_o	15.5%

(ii) Recorder error: This (Table 2) is based on the manufacturer's specification and the periodic checks during the season;

(iii) Integration error: The variation in the results obtained by plannimetry of the data suggested that two percent was a reasonable value for this error.

The results of the calculation of the root mean square error of the system for each flux (Table 2) shows that the shortwave fluxes and the incoming longwave flux can be measured to within 8 percent, but the other longwave fluxes and the net radiation have larger errors (10 to 16 percent).

6: Routine Weather Observation

Routine weather observations were taken at least hourly, on the hour, Civil Time. In rapidly changing conditions they were more frequent. Until the middle of September observations were taken, with few breaks, throughout the daylight hours. Later in the season fewer were recorded.

Early in the season two observers were available. Both took measurements independently and compared and checked the results. Later in the season this was not possible.

The observations taken were:

(i) Cloud type and amount. Values of cloud amount, for the three major levels separately and for total cloud cover, were obtained by the standard visual, highly subjective, method. Dominant type at each level was recorded;

(ii) Wave height and direction. The height and direction of dominant waves only were recorded. Frequently there appeared to be up to three sets of waves present, and the presence of minor sets was noted. Direction was divided into the 16 cardinal points, and height was estimated a few metres off the end of a dock, to the nearest 2 cm up to 12 cm and every 6 cm thereafter. Occasionally measurements were taken at the tower in addition to those at the dock. The results were rarely different;

(iii) Wind speed and direction. An anemometer and wind vane (Science Associates, Princeton, N.J., Nassau Windmaster) were installed above the roof of the recording centre. Visual readout meters were placed inside the centre and one minute averages of wind speed and direction obtained. Early in the season the fetch from the south-east appeared poor. However, comparison with a second anemometer at a nearby site which was clear in this direction, indicated no difference in reading.

7: Radiosonde Observations

Measurements of upper air temperatures and humidities were

obtained to allow calculation of vapour path lengths. Ascents were not made at a fixed time, and the length of time needed to prepare an ascent meant that it was not possible to predict cloud conditions during the ascent. Trouble with the receiver further limited the choice of ascent times.

The method of preparation, release and data recording followed standard Department of Transport procedures (Department of Transport 1962). The antenna, receiver, frequency converter, recorder and base line check equipment were loaned by the Department of Transport, which also provided maintenance personnel when required. These personnel also assisted with ascents at times. 403 megacycle VIZ radiosonde packages were used, carried below hydrogen-filled Darex balloons. The antenna was located on the roof of the recording centre, with the other instruments inside the building. The balloons were usually launched from the field adjacent to the centre. Because there was frequency drift during the ascent, the receiver had to be constantly adjusted, and poor signals occasionally were received for part of an ascent. All flights were monitored to 400 mb, judged from previous experience to be the upper limit for significant changes in precipitable water vapour. On some occasions good data were obtained to 100 mb, but changes in vapour content above 400 mb proved to be small.

Temperature, pressure and relative humidity at significant levels were obtained as outlined by the Department of Transport (1962). Specific humidity was calculated. The corrected optical depth for the i th layer, u_i, between two significant levels, was determined by

$$u_i = 10^{-3} \overline{q_i}(\overline{p_i}/p_o)\ \Delta p_i, \tag{49}$$

where p_o is the total atmospheric pressure (mb), $\overline{p_i}$ is the mean pressure of the i th layer, Δp_i is pressure thickness of this layer and $\overline{q_i}$ its mean specific humidity (g kg^{-1}).

The total corrected optical depth, or path length u, for j layers, is then

$$u = \sum_{i=1}^{j} u_i. \tag{50}$$

u below each significant level up to 400 mb was calculated, and the results applied to the radiation charts to provide a u:T curve. Since most of the downward flux to the surface originates at low levels, the portion of the ascent curve between the surface and the first datum level accounts for most of the area under the curve. Accurate observations at these levels, and accurate representation on the chart, are vital (Goody 1964). With the instrumentation used in this study the low levels were probably more accurately represented than the higher levels.

8: Emissivity Measurements

To determine emissivity in the field, three temperature measurements were needed (equation 27). The infra-red thermometer was used for these. This instrument assumes that the surface is a black-body and measures the radiation from the surface, and converts the result to a temperature. T_r (equation 27) was therefore measured directly by aiming the sensor at the surface under test and recording the temperature.

To determine T_u the sensor was used to obtain the apparent radiative temperature of the sky in several directions, and a representative value assigned to T_u, taking into account the presence of radiation from the tower and the boat (Lorenz 1966). This value was subjective, but whenever possible estimates were made by two people, and differences were rarely greater than 1 C. The methods of Buettner and Kern (1965) and Fuchs and Tanner (1968) are possibly more accurate, but were impractical for determinations over water.

The true surface temperature T_s was found by isolating the surface from sky radiation and allowing it to radiate as an apparent black-body (Fuchs and Tanner 1968). An aluminum cone was placed over the water and the temperature measured through a hole at the apex (Figure 8). It was assumed that the cone temperature was close to

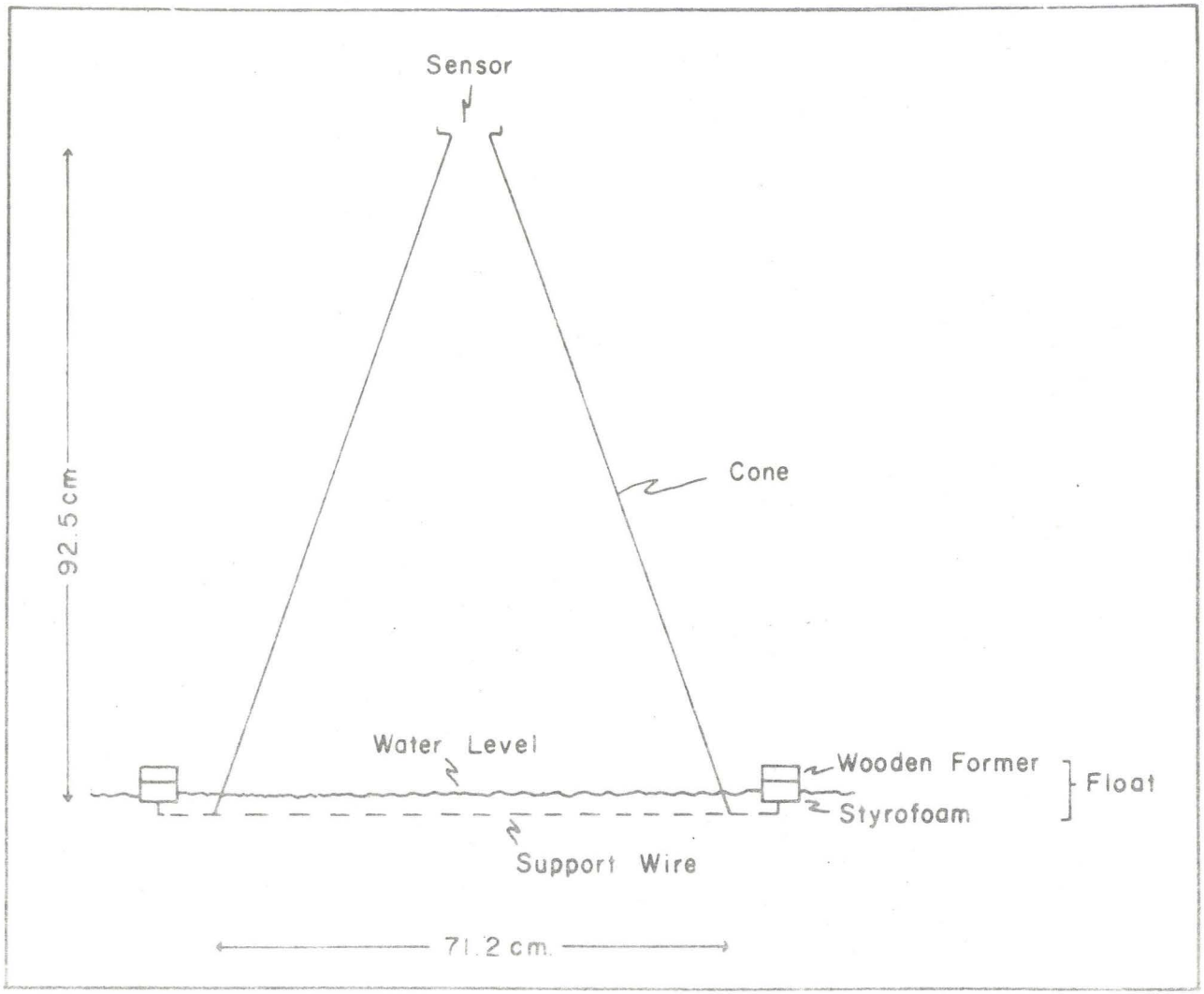

FIGURE 8 ALUMINUM CONE FOR EMISSIVITY DETERMINATIONS

that of the water surface. The effective emissivity through the apex of a cone, ε_c, as given by Fuchs and Tanner (1968) is

$$\varepsilon_c = 1-4\varepsilon_a(1-\varepsilon)(T_s-T_n)T_s^{-1}(\varepsilon_a+\varepsilon-\varepsilon_a\varepsilon)^{-1}, \qquad (51)$$

where ε_a is the apparent emissivity of the cone at temperature T_n, and ε is the emissivity of the surface at temperature T_s. The emissivity of aluminum is approximately 0.03, and for an apex angle 41^o, ε_a is approximately 0.24 (Sparrow and Jonsson 1963). Assuming a surface emissivity of 0.95,

$$\varepsilon_c = 1-0.05\ (T_s-T_n)T_s^{-1}\ . \qquad (52)$$

The effective emissivity therefore depends on the temperature difference T_s-T_n. If they are equal, $\varepsilon_c=1.0$. If the difference is 10 C at 300 K, $\varepsilon_c=0.998$, giving an error in T_s reading of 0.2 C, approximately within the limits of accuracy of the instrument. As 10 C was estimated as the maximum difference encountered, the surface covered by the cone can be considered a black-body cavity, and hence T_s could be determined.

The cone was supported on two fine wires stretched on a wood and styrofoam float (Figure 8). These support wires, fine nylon line, were several centimetres below the water surface so that they had a negligible effect on the temperature readings. Several holes were

drilled in the cone near the rim to allow water movement and to ensure a constant level water surface.

For each set of readings T_u was determined first, then T_r for the test surface, which was always the water surface inside the float. The cone was then put in place, a value obtained for T_s, and the cone removed as quickly as possible. Finally, a further set of T_u measurements were taken. Once the cone was in place there was a period of about 20 sec in which the T_s reading was constant, the temperature then starting to rise appreciably as the surface energy balance was altered. In calm conditions on the lake the placing of the cone, temperature reading, and cone removal could be accomplished in about 10 sec, the sequence taking slightly longer with a light swell. The method was not practical for wave heights greater than about 25 cm. On most occasions the readings were taken close to the dock, with the sensor circuitry and readout dial on land, and only the sensor head held from the boat. The dial was then not subject to movement, and the sequence could be somewhat more rapid.

Each set of readings was repeated at least three times to ensure consistent results. After each set there was a break of at least one minute to allow re-establishment of the normal surface energy balance. This was found to be necessary in calm conditions, although with waves present the readings could be almost continuous, presumably because of mixing of the water.

Any errors possibly introduced by flux divergence between the surface and the sensor were minimized by ensuring that T_s and T_r were measured at the same level. Hence the errors should be equal and self-cancelling, although in the atmospheric window region used, such divergence should be small.

Readings were taken under both clear and cloudy skies. In some instances of the former T_u could not be determined accurately for any part of the sky since the temperatures were below the lower limit of the radiometer scale (-20C). These data were discarded. On days with complete overcast this problem did not arise. Under these conditions T_s remained constant for a period of approximately 30 sec, and it is likely that these results are the most reliable. With partly cloudy conditions T_u estimates were highly subjective, but a value could be determined provided the cloud conditions were not changing too rapidly.

A small error in T_u can be tolerated, since ε is not very sensitive to changes in T_u. From equation 26,

$$\partial\varepsilon/\partial T_u = 4T_u^3(T_r^4-T_s^4)/(T_s^4-T_u^4)^2, \qquad (53)$$

and the result, using T_r = 22 C, T_s = 23 C and T_u = -20 C, suggests a variation in ε of 0.001 C^{-1}. Similarly,

$$\partial\varepsilon = 0.024\ \partial T_r, \tag{54}$$

and

$$\partial\varepsilon = 0.028\ \partial T_s. \tag{55}$$

Hence accurate determination of T_s and T_r is vital. The sensor has a stated absolute accuracy of 0.5 C, and a sensitivity of 0.1 C. Since differences are being considered, the sensitivity is the limiting factor. Readings were taken to 0.25 C, the practical limit enfored by dial needle movement in a moving boat.

High contaminant concentrations and surface films were not observed in the field, but they could be established in the laboratory, and any effect on ε could be observed experimentally. The spectral emissivity ε_λ of water samples was determined with a spectrophotometer (Beckman Instrument Company, Model IR 12), using equation 23. Measurements were obtained for 14 wavelengths in the 7.7μ to 14.3μ interval, which corresponds closely to the band used by the infra-red thermometer in the field program. Chromium was used as a standard surface. Its emissivity, assumed constant with wavelength, was taken as 0.95, slightly below the normal value (0.98) since the surface was slightly tarnished. Results, however, are insensitive to small changes in the assumed emissivity value.

CHAPTER 4

OUTGOING LONGWAVE RADIATION

With the data available from the Lake Ontario field program, it was possible to determine outgoing longwave radiation both as the residual of the radiation balance equation $L_o(R)$, using equation 47, and also from measurements of T_s, L_i and ε, $L_o(T_s)$ using equation 18. Hence comparison of two independent sets of results was possible. Good agreement implies first that the fluxes on the right hand side of equation 47 were measured to good accuracy, and, second, that, provided ε is known, simple methods of obtaining surface temperature can be used to calculate L_o. Some variation between the results can be expected, since flux divergence between the two measurement levels will occur, and a comparison of the results should give some indication of its magnitude. Since L_o depends on surface temperature, which in turn is influenced by the net radiation, consideration of causes of temporal flux variations will be postponed until Chapter 6. Surface emissivity and temperature results will be considered prior to a comparison of the two sets of L_o results.

TABLE 3: RESULTS OF THE FIELD DETERMINATION OF EMISSIVITY

Date	Time (L.T.)	Site	T_u °C	T_s °C	T_r °C	Cloud Type	Cloud Amount 10ths	Emissivity
Sept. 15	1430	D	-25.0	19.3	18.5	Ac Cu	4	.977
	1630	D	-20.0	20.5	19.7	Ac	4	.976
16	1240	D	-10.0	19.7	18.7	As Ac	9	.961
22	1130	T	-23.0	13.9	13.2	Clear	0	.977
	1330	T	-23.0	15.8	14.9	Clear	0	.972
25	1220	D	7.0	15.0	14.7	Sc	10	.961
Oct. 26	1600	D	0.0	9.4	9.3	As Ac	10	.989
	1650	D	-8.0	9.0	8.8	As Ac	9	.987
27	1230	D	-5.5	8.1	7.9	Sc	9	.984
	1350	D	-6.5	8.0	7.6	Sc	9	.970
	1604	D	-7.5	6.7	6.4	Sc	10	.977
	1700	D	-5.5	7.7	7.4	Sc Ac	10	.976
28	1200	D	-25.0	8.0	7.0	Ac	1	.964
	1515	D	-25.0	8.0	7.0	Ac Cu	2	.964
Nov. 3	1210	T	-20.0	8.8	8.3	Ac Sc	8	.980
	1230	D	-12.0	9.8	9.5	Ac Sc	8	.985
	1400	D	1.5	10.5	10.3	As	10	.977
	1410	T	-9.0	8.0	7.5	As	10	.968
	1505	D	8.0	10.1	10.0	As	10	.952
	1520	T	0.0	7.5	7.3	As	10	.972
4	1025	T	-7.0	8.0	7.5	As Ac	9	.964
	1040	D	0.0	9.8	9.5	As Ac	10	.968
	1330	D	-8.0	9.5	9.0	As Ac	9	.969
	1610	D	-20.0	9.5	9.0	As Ac	9	.980
5	1010	D	-15.0	7.5	7.0	Ac Cu	9	.975
	1315	D	-20.0	8.0	7.5	Cc Ac Cu	4	.979
	1505	D	-2.0	10.0	9.5	As Sc	10	.956

D = Dock T = Tower

A. EMISSIVITY

The results of the field determinations of emissivity are shown in Table 3. The values range from 0.952 to 0.989, with a mean of 0.972 and standard deviation 0.021. The instrumental accuracy suggests a maximum error in ε of about $\pm$ 0.02 when the similar absolute errors in T_s and T_r (equation 27) measurement are of opposite sign. Therefore, within the limits of the method, the surface emissivity is close to 0.97. No systematic variation of ε with cloud type or amount, or with sky temperature, could be found.

Although the values refer to only one site, they are probably quite representative. On four occasions measurements were taken close to a dock within a few minutes of a set taken at the tower (Table 4). Water conditions were visibly dissimilar, but only on one occasion was there a difference in ε greater than 0.01. All differences are within the error of the method.

TABLE 4: COMPARISON OF DOCK AND TOWER EMISSIVITY DATA

Dock	Tower	Difference
.985	.980	0.005
.977	.968	0.009
.952	.972	-0.020
.968	.964	0.004

The effect of the water composition of the surface layer upon ε is shown in Table 5. For the seven measurements no systematic variation in ε with any measured contaminant was found. This shows that the surface radiative character of the water is not related to any of the measured contaminants. However, the concentration of contaminant in the surface layer was generally low, and the effect of high concentrations and surface films could not be tested by field methods. The scatter of results appearing in Table 3 can probably be attributed to sensor errors. The mean value is identical with a value for Lake Hefner (Anderson 1954), the only value for a lake surface encountered in the literature.

Spectral emissivities for pure water obtained by laboratory methods (Figure 9) are virtually identical with those given by Bell (1957) and Kislovskii (1959). The spectral variation is also similar but shows a minimum at slightly longer wavelengths.

Emissivities for water with various additives and surface contaminants are given in Table 6. Emissivity was computed in three ways, to determine whether it was dependent on the spectral distribution of incident energy and upon sensor filters. The first method establishes true emissivity ε_t, which is the emissivity calculated assuming constant spectral incident energy. Equation 24 was used

TABLE 5. VARIATION OF EMISSIVITY WITH WATER CONDITIONS

Date	Time	Site	Emiss-ivity	Ortho-phosphate (ppm)	Nitrite+ Nitrate (ppm)	Dissol-ved Solids (ppm)	Susp. Solids (ppm)	Dissol-ved Oxygen (mg/litre)
Oct. 28	1515	D	.964	37	230	220	700	-
Nov. 3	1515	T	.972	0	164	205	446	12.9
	1530	D	.952	9	100	207	466	11.2
4	1605	D	.980	9	148	215	456	12.7
5	1020	D	.975	0	144	204	522	11.7
	1330	D	.979	-	-	-	-	11.7
	1515	D	.956	1	148	220	92	12.1

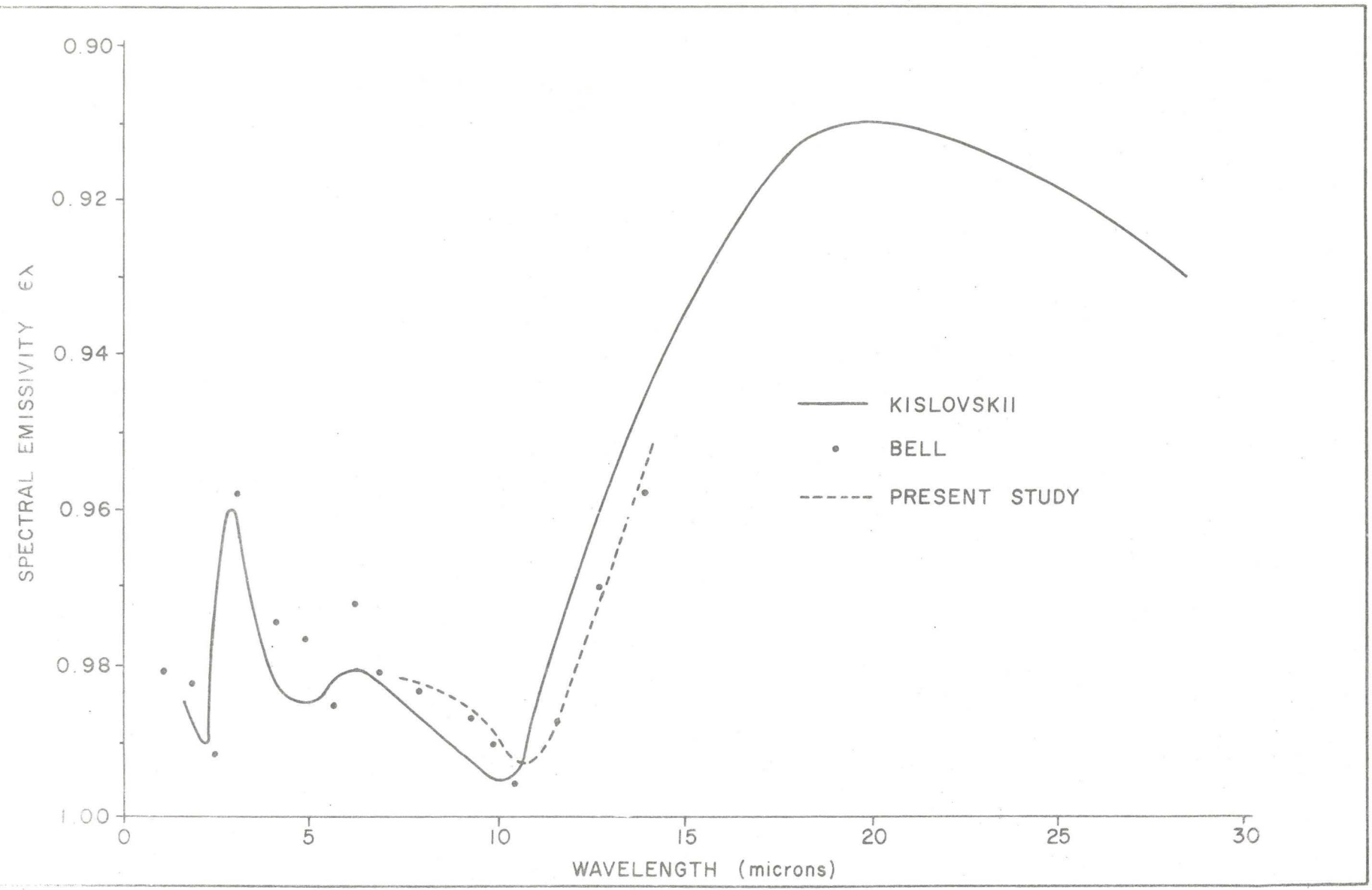

FIGURE 9 SPECTRAL EMISSIVITY OF WATER (AFTER KISLOVSKII 1959 AND BELL 1957)

TABLE 6

LABORATORY DETERMINATION OF EMISSIVITY

Water Sample	ε_T	ε_A	ε_B
Distilled	.980	.979	.980
Tap	.980	.979	.981
Dissolved detergent	.984	.982	.983
Surface scum of detergent	.983	.984	.984
Lake Ontario			
(1) Clear	.978	.978	.980
(2) Clear	.979	.978	.980
(3) Dirty, settled	.976	.979	.981
(4) Dirty, stirred	.976	.979	.980
Corn oil, surface film	.966	.968	.968
Corn oil & detergent mixed on surface	.979	.979	.979
Machine oil			
(1) Thin film (<1 mm) dispersed with toluene	.956	.960	.960
(2) Thick film (≃3 mm)	.958	.959	.960
Crude oil- Chedabucto Bay oil.	.952	.953	.954

directly. The second approach is to calculate the emissivity of a surface exposed to the atmosphere ε_A. This was computed using equation 24 with the known spectral variation of incident energy from the atmosphere (Sloan, Shaw and Williams 1955) as a weighting factor. The third method gives the emissivity as detected by an infra-red thermometer ε_B. This was found in the same way as ε_A, but the additional effect of the spectral transmissivity of an infra-red thermometer filter (Lorenz 1966) was incorporated.

The results show that the inclusion of the weighting factors used in the second and third methods has little effect on the emissivity. The three sets of values confirm the field finding that emissivity is independent of composition. This was true even when a detergent scum covered the surface, although there is the possibility that the scum may have had such a high water content that water was the major radiatively active component. The presence of surface oil lowered the emissivity by about 3 percent. The type of oil had little effect, in that emissivity differences between crude oil and machine oil were less than one percent.

Laboratory determinations of emissivity for lake water samples agreed with the field results to within one percent. From both sets

of measurements the writer concludes that the emissivity of water lies between 0.97 and 0.98. Furthermore, unless the results contain significant undetected error, this value should apply to all fresh water surfaces. Therefore the variation of outgoing longwave radiation from a water surface will depend solely on one variable, water surface temperature.

B. SURFACE TEMPERATURE

Several times, during relatively calm conditions, the three methods of obtaining surface temperature discussed in Chapter 3 were used simultaneously. The values that were used from the infra-red thermometer measurements were the mean of at least three instantaneous readings. The float data were means obtained over 15 minutes, the time period needed for the infra-red thermometer measurements.

Although the five thermistors of the multiple sensor float were unlikely to be at the same height relative to the water surface, and hence could be influenced by the steep temperature gradient at the interface (Malevskiy-Malevich 1963), the results from each compared to within 0.2 C, and have a small standard deviation of 0.09 C.

Interrelationships between the data obtained by the several methods are shown in Figure 10. Float temperatures are higher than those obtained from the infra-red thermometer in the temperature range where most of the observations were made. Emissivity corrections applied to the infra-red thermometer data produced little change.

1. Comparison of Methods over 24-hour Periods

Comparisons of the methods over 24-hour periods were made on July 16th - 17th (Run 1) and July 30th - 31st (Run 2) (Figure 11). For Run 1 the values at night by the three methods compare to within 0.5 C, but during the day the temperature from the single sensor float, $T_{s(s)}$, and the multiple sensor float, $T_{s(m)}$, exceed the infra-red thermometer value $T_{s(b)}$ by several degrees. Some systematic difference between contact and remote methods can be expected. Marlatt (1967) and Malevskiy-Malevich (1963) have drawn attention to the reduction of surface temperature by evaporative cooling. The latter quotes a maximum surface temperature reduction of 1.5 C for water in an evaporation pan. The present data represent conditions of relatively high solar heating, and some degree of cooling by this mechanism can be expected. Its extent can be postulated only if the infra-red thermometer and float results are compared, assuming that the float data represents the regime some distance from the interface. In the case

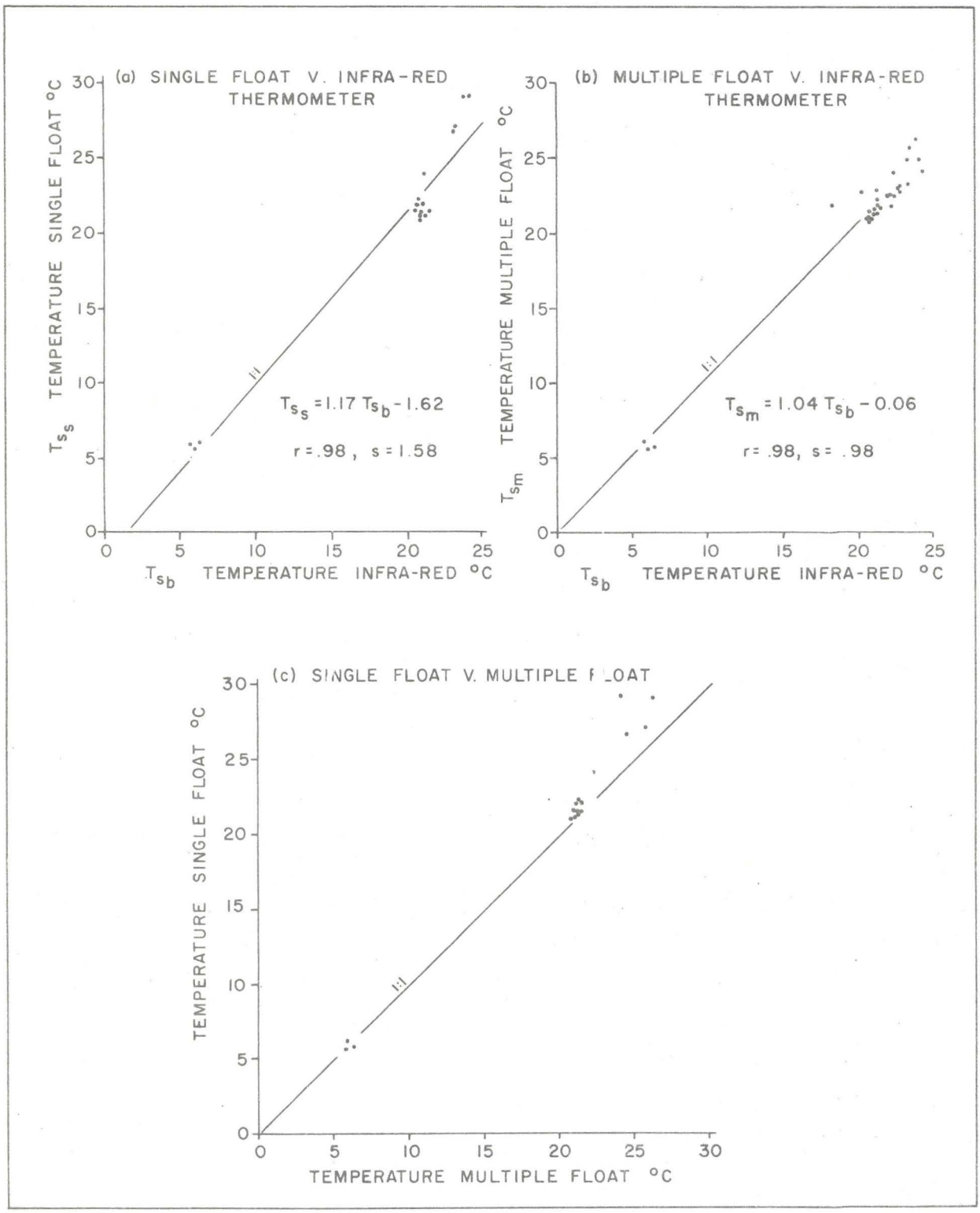

FIGURE 10 COMPARISON OF SURFACE TEMPERATURE MEASUREMENTS BY THREE METHODS

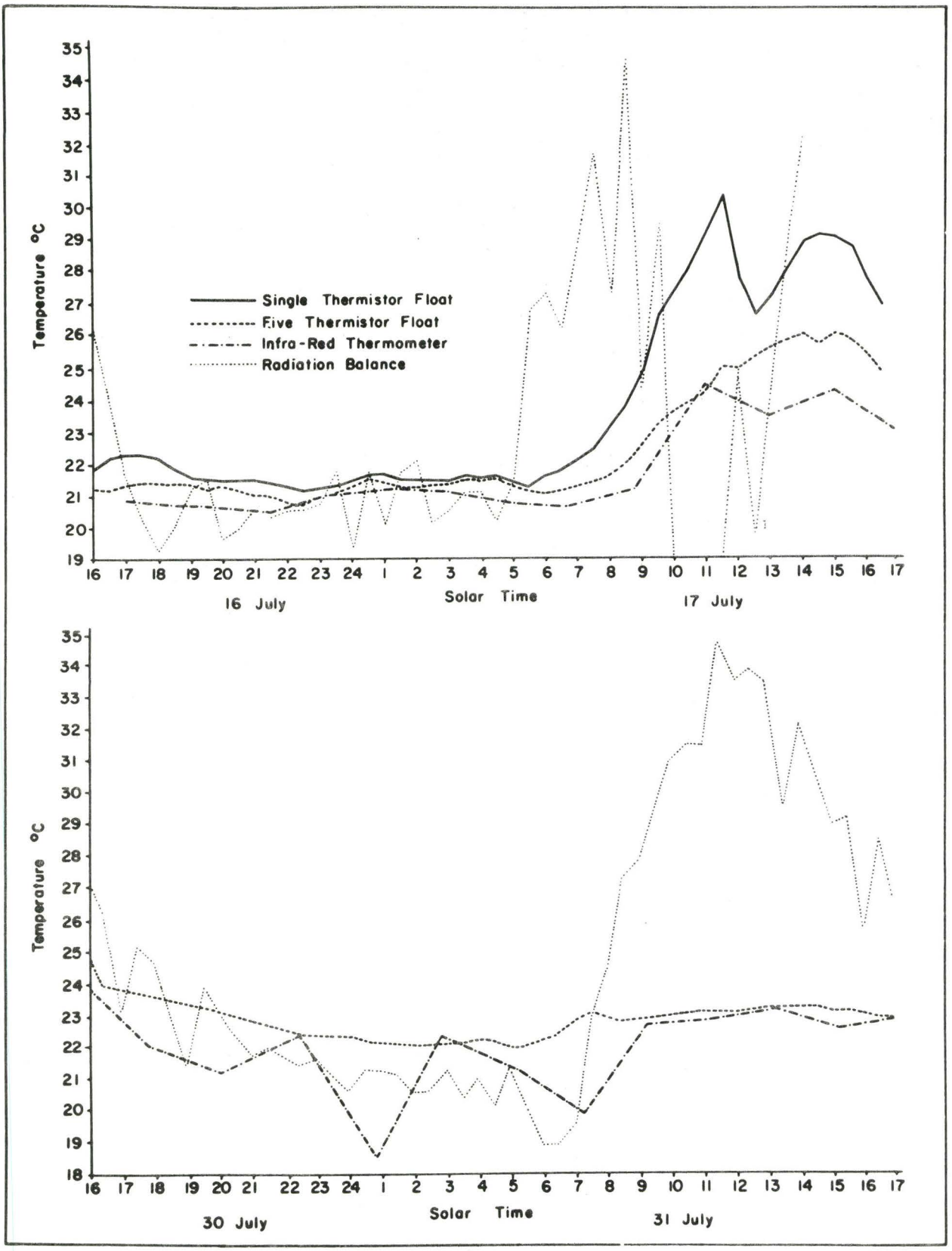

FIGURE 11 SURFACE TEMPERATURE VALUES FOR 16-17 JULY AND 30-31 JULY 1969.

of the multiple sensor float the observed maximum difference of 2 C is consistent with the Malevskiy-Malevich findings. The differences indicated by the single sensor float are too large to be accounted for in this manner, and suggest systematic error possibly due to incorrect location of the sensor, or to direct solar heating of the float. However, there is evidence that temperatures from this run are anomalous. This was the only day in July when the lake was calm. Other data for this period indicate much smaller temperature ranges (Table 7). On these days waves washed over the float and probably reduced the effect of solar heating, producing temperatures close to the true surface temperature.

TABLE 7: DAILY SURFACE TEMPERATURE RANGES FOR JULY (^{o}C)

(Single Sensor Float Data)

Date	17th	18th	19th	20th	21st	22nd
Maximum	30.5	25.9	25.0	20.4	23.3	22.3
Minimum	21.5	22.5	20.8	17.8	19.1	19.6
Range	9.0	3.4	4.2	2.6	4.2	2.7

The single sensor float was inoperative during Run 2. $T_{s(m)}$ only slightly exceeded $T_{s(b)}$ during both daylight periods, and there was close agreement at night (Figure 11).

Intercomparisons using the modified single sensor float which was available later in the program were made on October 29th (Table 8). The three sets of data compare favourably to within 0.5 C. This suggests that the modified sensor in operation from August 27th gave reasonable estimates of surface temperature.

TABLE 8 : SURFACE TEMPERATURE MEASUREMENTS, OCTOBER 29th (^{o}C)

Time (T.S.T.)	Infra-red Thermometer	Single Sensor Float	Multiple Sensor Float (Average)
1110	5.6	5.9	6.1
1245	6.2	6.2	5.9
1515	6.0	5.7	5.8

2. Errors in Surface Temperature Measurement

If it is assumed that the infra-red thermometer gave true surface temperatures, a measure of the accuracy of T_s measurement by the other methods is given by the standard error of the regression relationships shown in Figure 10. For $T_{s(s)}$ this value is approximately $\pm$ 1.5 C. Figure 11 indicates that better accuracy is probably achieved at night, and possibly this is also the case when waves are present. An estimate of the accuracy of the single sensor float for the second part of the season, when only three intercomparisons were available, was more difficult. The error, however, is then probably less than that of the first period, and better than $\pm$ 1 C.

Surface temperature values $T_{s(r)}$ were also obtained for Runs 1 and 2 from the radiometric determinations of L_o, by using equation 19 in the form

$$T_{s(r)} = (L_o/\varepsilon\sigma)^{1/4}. \tag{56}$$

$T_{s(r)}$ was determined as the average value for the half-hour period during which $T_{s(b)}$ was measured. The data, included in Figure 11, are in poor agreement with the other evaluations. The wide range and fluctuations of $T_{s(r)}$ can be explained using equation 20. Differentiating equation 20 gives

$$\partial T_s/\partial L_o = T_s/4L_o. \tag{57}$$

Hence, small errors in radiation measurement will result in quite large errors in temperature. For example, with T_s=300 K, L_o = 0.66 cal cm^{-2} min^{-1}, and a 5 percent error in L_o leads to an error of over 15 K in T_s. Consequently equation 20 is unsuitable for accurate T_s determination when the error in L_o measurement may be large. If L_o is directly measured with a radiation thermometer the error is considerably reduced.

Equation 20 can be used, however, to obtain L_o accurately from T_s measurements. An error in T_s measurement of about 1 C, the error

suggested for the modified single sensor float, results in an error in L_o estimate at 300 K of about 0.007 cal cm^{-2} min^{-1}, or about 1 percent. Hence, best estimates of L_o can be obtained from surface temperatures measured to an accuracy of 1 C.

C. COMPARISON OF METHODS FOR OBTAINING OUTGOING LONGWAVE FLUX

Radiometrically measured outgoing longwave radiation, $L_o(R)$, was compared to L_o obtained using equation 18, $L_o(T_s)$. In addition, the simplified form of equation 18, equation 20, was used, since this includes fewer parameters and may be more generally useful. The results of the two measurement methods were used in a comparison on the regressions of $L_o(R)$ and $L_o(T_s)$, and for a comparison of estimates of half-hourly values.

Correlation coefficients (r) between $L_o(R)$ and $L_o(T_s)$ are given in Table 9. Part (a) refers to pooled half-hourly data for each month, and part (b) refers to daily totals. Insufficient data were available for July and August in part (b). Equation 18 gives slightly better results than equation 20 for both sets, and therefore will be used subsequently.

TABLE 9 : CORRELATION COEFFICIENTS BETWEEN $L_o(R)$ and $L_o(T_s)$

	JULY	AUGUST	SEPTEMBER	OCTOBER	NOVEMBER
(a) Half-hourly values					
Equation 18	.28	.50	.79	.83	.81
Equation 20	.29	.45	.76	.81	.76
(b) Daily Total values					
Equation 18	-	-	.88	.96	.90
Equation 20	-	-	.87	.95	.85

Lower correlations were obtained in part (a) of Table 9 than in part (b). The explanation is apparent from time series plots of $L_o(R)$ and $L_o(T_s)$. A typical example (Figure 12) shows that whereas $L_o(T_s)$ is fairly constant throughout the day, $L_o(R)$ may fluctuate considerably. However, when the data are summed over the day, the discrepancy is reduced.

The correlation coefficients for half-hourly data have a marked seasonal trend. In July the value was low, but as the season progressed it increased to greater than 0.8. The low July value may be attributed partly to the anomalously high surface temperatures recorded during the daylight period of July 17th. Later in the season the improved single

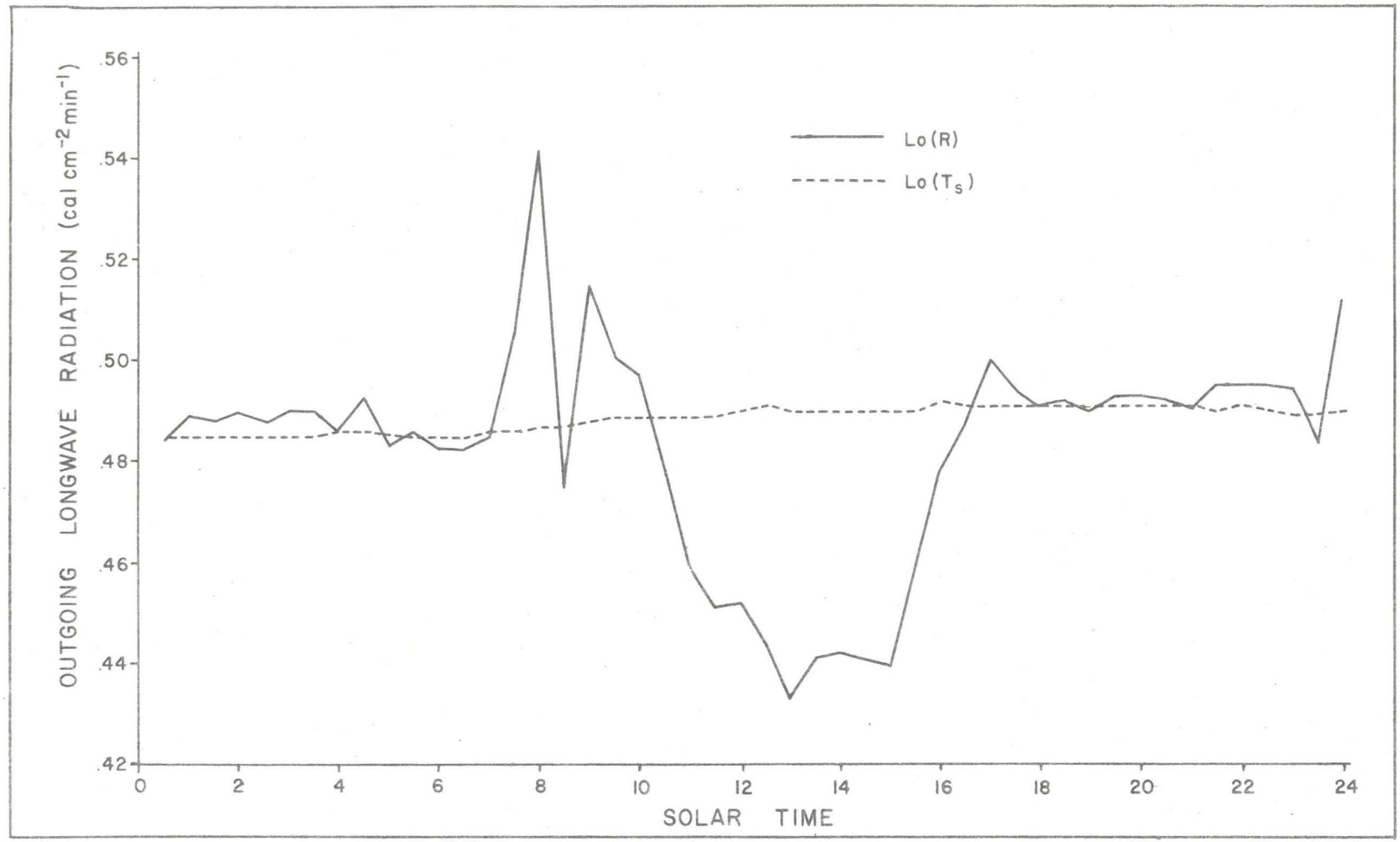

FIGURE 12 DIURNAL VARIATION OF OUTGOING LONGWAVE RADIATION DETERMINED FROM RADIOMETRIC MEASUREMENTS Lo(R) AND FROM SURFACE TEMPERATURE Lo(T_s) FOR OCTOBER 30, 1969

sensor float gave more accurate T_s measurements probably because solar intensities were less and hence radiational heating errors were reduced.

Slope values for the regressions were expected to approach unity, since the two variables are independent measures of the same entity. For the half-hourly data they were considerably less than unity (Table 10). This must be the result of different diurnal variations for the two sets. Figure 13 shows that $L_o(R)$ has the greater diurnal variation in all months. The slope value increases as the difference between the diurnal variation decreases. The points where the regression lines and the 1:1 lines intersect were also calculated (Table 10). At L_o values higher than the intersection point the regressions show that $L_o(R)$ exceeds $L_o(T_s)$. Since the majority of data lie within the range 0.45 to 0.60 cal $cm^{-2}min^{-1}$, $L_o(R)$ generally exceeds $L_o(T_s)$ in the first three months. The opposite is the case for October and November.

In order to obtain more detail regarding differences between $L_o(R)$ and $L_o(T_s)$, times when the two differed by more than 10 percent were investigated. Such differences were found for 14 percent of the time when the original single sensor float was in operation, and 2 percent of the time when the modified float was in use.

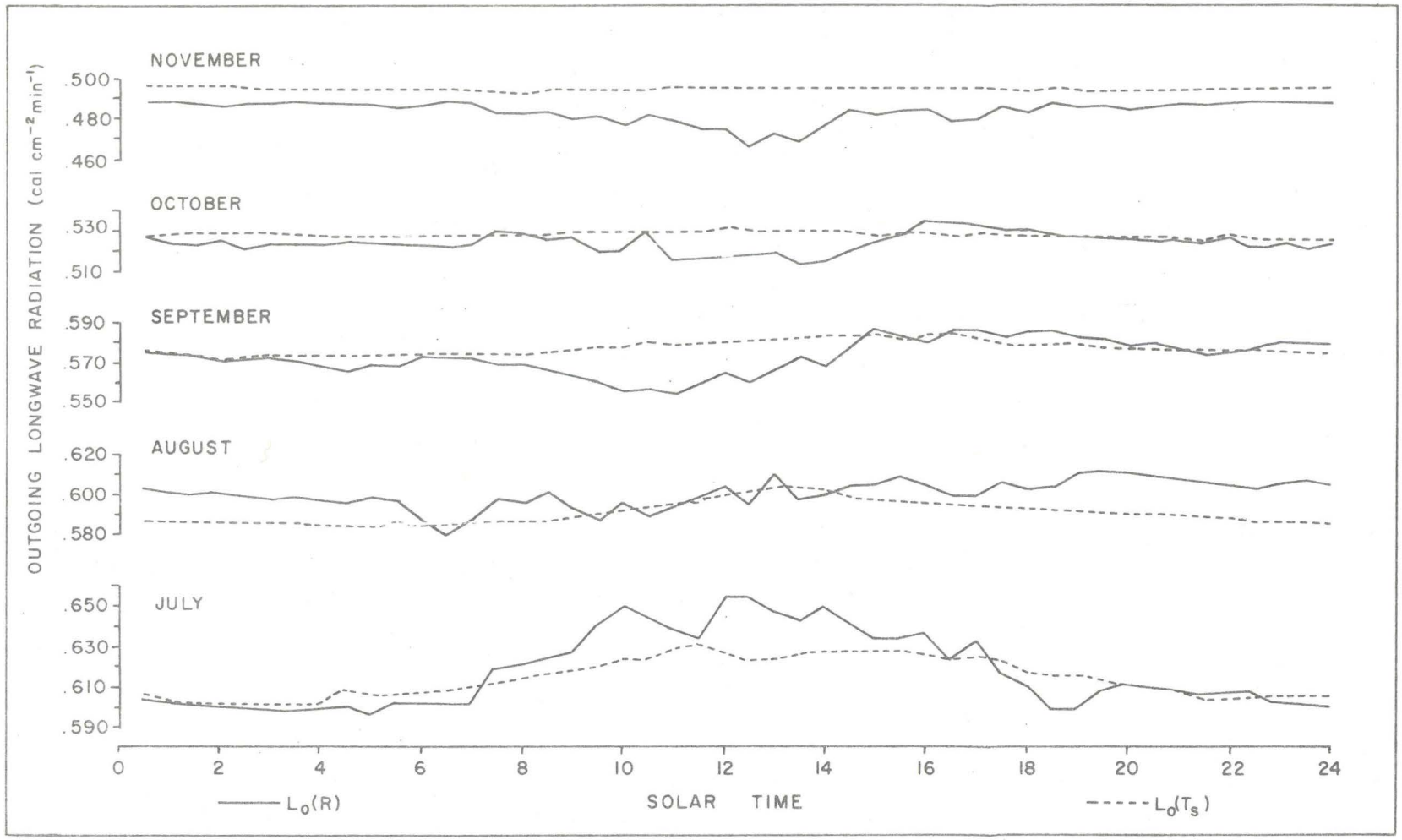

FIGURE 13 MONTHLY AVERAGE DIURNAL VARIATION OF OUTGOING LONGWAVE RADIATION DETERMINED FROM RADIOMETRIC MEASUREMENTS $L_o(R)$ AND FROM SURFACE TEMPERATURE $L_o(T_s)$

TABLE 10: REGRESSION CONSTANTS AND COEFFICIENTS OF $L_o(T_s)$ ON $L_o(R)$

(For Half-hourly Data)

	JULY	AUGUST	SEPTEMBER	OCTOBER	NOVEMBER
Intercept	.52	.43	.24	.20	.32
Slope	.15	.28	.59	.64	.35
$L_o(R) = L_o(T_s)$	.61	.59	.59	.44	.50

In July the differences all occured in daylight. All occasions except those of the afternoon of July 17th indicated greater outgoing radiation of 5 m than at the surface. This is contrary to what would be expected if T_s was in error because of radiative heating of the float or evaporative cooling of the surface. These results again suggest that the July 17th data were anomalous.

For the second measurement period, after August 27th, again differences occurred mainly in daytime, but they usually occurred sporadically over periods of less than one hour. They were found in a variety of wave conditions, and seemed unrelated to L_i. No relation between large flux differences and humidity at radiometer level or with T_s : T_a differences, both of which may influence the transfer process between measurement levels, could be found. The differences, therefore, are not likely to be totally environmental. On four occasions differences occurred directly after a break in the radiometer

record caused by lack of aspiration. Condensation may then have occurred on the sensor domes, which would have increased the calculated $L_o(R)$. Soon after aspiration restarted, differences in estimate by the two methods became small. However, on many occasions the differences are probably environmental, and these, along with the differences commonly occurring during July, must be explained in terms of radiative flux divergence.

D. DIVERGENCE OF OUTGOING LONGWAVE RADIATION

Greatest divergence is likely when there is a large temperature difference between the two measurement levels (Malevskiy-Malevich 1963). The temperature difference $\Delta T(=T_s-T_a)$ was therefore compared to differences in flux estimate. On September 23rd between 1430 and 1500 hours, T_a exceeded T_s by over 10 C, and $L_o(R)$ exceeded $L_o(T_s)$ by 13 percent, suggesting that divergence was significant. However, on several other occasions when the two flux estimates differed considerably ΔT was small. Also, large ΔT values did not necessarily produce large differences in flux estimate. Marked divergence is also likely when large water vapour amounts are present between the 2 measurement levels. Although day to day fluctuations in vapour pressure were frequently about 5 mbs, they were poorly correlated with divergence. The lack of agreement between divergence of L_o and temperature or humidity may indicate errors in the measurements, especially in $L_o(R)$, since errors up to $\pm$ 15 percent are possible (Table 2).

While the present data do not allow an examination of short term changes in divergence with temperature and humidity changes, the regression comparison of the two methods of L_o determination suggested that there were differences that varied with season. When long term averages of $L_o(R)$ are used, the random measurement error is considerably reduced, and the measured average value should approach the true value. Therefore the daytime and nighttime average values of the ratio $L_o(R)/L_o(T_s)$ were found separately for July, and for the August to November period (Table 11). A student's t test indicated that the difference between the means of L_o obtained by the two methods was significant at the levels indicated in Table 11. The differences are highly significant in all cases except for the nighttime data for the August - November period. The results indicate that divergence is commonly present. The $L_o(R)/L_o(T_s)$ ratio mean for the July period is greater than 1.0, but it is less than 1.0 for the rest of the season. This shows a change from divergence to convergence between the two periods. Divergence will occur if the surface is cooler than the air (Davies et al 1971). The converse follows for convergence. The monthly mean air and surface temperatures for the times when $L_o(R)/L_o(T_s)$ was determined (Table 12) show that divergence is likely in July and August, and convergence in the other months. As only 6 percent of the observations in the second period were in August, these temperature data support the conclusion that convergence is present in the second period.

TABLE 11: AVERAGE $L_o(R)/L_o(T_s)$ FOR DAY AND NIGHT

	JULY		AUGUST - NOVEMBER	
	Daylight	Night	Daylight	Night
$L_o(R)/L_o(T_s)$ - Mean	1.033	1.016	0.988	0.995
$L_o(R)/L_o(T_s)$ - Standard deviation	.071	.011	.043	.025
$L_o(T_s)$ - Mean cal cm^{-2} min^{-1}	.622	.607	.550	.539
$L_o(R)$ - Mean cal cm^{-2} min^{-1}	.641	.616	.543	.537
No. of Observations	177	106	1667	1726
Student's t test	5.486	4.716	3.961	1.846
Significance Level percent	0.1	0.1	0.1	5.0

TABLE 12: MONTHLY MEAN SURFACE AND AIR TEMPERATURES (^oC)

(For times of $L_o(R)/L_o(T_s)$ determination)

	JULY	AUGUST	SEPTEMBER	OCTOBER	NOVEMBER
Surface Temperature T_s	21.8	18.8	17.2	10.8	6.1
Air Temperature T_a	22.2	24.4	17.1	9.9	5.9
$T_s - T_a$	-0.4	-5.6	0.1	0.9	0.2

Divergence values calculated from the means of $L_o(R)$ and $L_o(T_s)$ with an assumed difference in measurement level of 5 m, are shown in Table 13. For July, divergence at night is weaker than during the day, since $L_o(R) - L_o(T_s)$ differences are a maximum during the day (Figure 13). For the August to November period convergence is generally weak, with daytime values exceeding those at night. The larger absolute daytime values in both seasons may possibly be explained by a slight increase in vapour path length between the 2 levels during the day. Vapour pressure at midday exceeded nighttime values by up to 4 mb in July. The variation was weaker and less consistent later in the season.

TABLE 13 : ESTIMATES OF OUTGOING LONGWAVE FLUX DIVERGENCE BETWEEN SURFACE AND RADIOMETER

(cal cm^{-2} min^{-1} m^{-1})

	JULY		AUGUST-NOVEMBER	
	Daylight	Night	Daylight	Night
Measured	.0038	.0018	-.0014	-.0004
Deacon Chart estimate	.0004	.0002	-.0001	-.0002

The only other published values of upward flux divergence are those of Funk (1960), who obtained values around 0.001 cal cm^{-2} min^{-1} m^{-1} for 3 measurements over grass at night in winter. The present night value for the August - November period is considerably less than this value. Although Funk gives no values of the temperature gradient when L_o divergence was measured, data he presents for similar times and conditions indicate that it was probably greater than in the present study, leading to greater divergence. Estimates of L_o divergence from the Deacon (1950) chart for the four periods considerably underestimate the divergence (Table 13). Funk (1960) found a similar result, and, following Robinson (1950), concluded that undetected haze near the surface was present at night. This effect is possibly more marked over water than over land. However, investigation of this hypothesis requires detailed measurements of radiative and heat flux divergence, similar to those carried out by Funk (1960). The present data indicate that divergence is commonly present near the surface throughout the season.

CHAPTER 5

INCOMING LONGWAVE RADIATION

In this chapter measurements of incoming longwave radiation by two independent methods are compared, and the influence of radiative flux divergence and cloud on L_i considered. Fluxes calculated from charts and formulae are compared to the measured values. The formulae are also used to obtain estimates of the net longwave flux.

A. MEASURED VALUES

The tower measurements permit two separate estimates of the flux from

$$L_i(R) = T_i - Q_i, \tag{58}$$

and

$$L_i(T_s) = (R_n+Q_o-Q_i+\varepsilon\sigma T_s^4)/\varepsilon. \tag{59}$$

The two methods are virtually independent. Although Q_i appears in both, it is the component of the radiation balance that can probably

be measured with the least error (Table 2). Equation 58 would normally be preferable to equation 59 since fewer measurements (three rather than four) are needed.

The two methods of estimation were compared, using the ratio $L_i(R)/L_i(T_s)$, for times when differences were greater than 10 percent. All such differences occurred in daylight. As with the comparison of the two methods of L_o determination, however, two distinct regimes were present, the first for July, and the second for the rest of the season. In July the differences occurred for most of the daylight period for each day, and $L_i(R)$ exceeded $L_i(T_s)$. This, as with L_o, is contrary to what would be expected if differences were the result of radiative heating of the single sensor float measuring T_s. Later in the season, large differences were sporadic in occurrence, and $L_i(T_s)$ usually exceeded $L_i(R)$. These differences are probably the result of flux divergence between the measurement levels. The T_a:T_s differences (Table 12) confirm that convergence of L_i is likely in July and divergence in the other months. Further, since temperature differences are likely to be at a maximum during the day, divergence is likely to be at a maximum at that time. The L_i divergence is therefore opposite in sign to that found for L_o in each period. However, it is not possible to calculate the actual divergence of L_i, since equation 59 utilises data from both measurement levels. Hence the divergence of the net longwave flux cannot be determined.

While the measurement by both methods indicates a distinct diurnal variation in L_i in July and August, the $L_i(T_s)$ data are insufficient for generalization. The monthly average $L_i(R)$ values for each half-hour (Figure 14) show midday minima in July and August, but no distinct diurnal pattern in the other months. Anderson (1954) found that L_i over Lake Hefner consistently reached a minimum near noon. He rejected the daytime data, since he believed that the variation was due to a dependence of radiometer paint reflectivity on solar zenith angle. It is unlikely that the similar pattern in the present July and August data is due to instrument response since the minimum does not occur at a preferred time, and disappears later in the season. An alternative explanation may be offered.

Swinbank (1963,1964) suggested that $\varepsilon_\lambda(u)$ could be regarded as approximately constant close to the surface. This is probably true for the large vapour paths likely near a water surface. Hence L_i is determined by temperature only. This temperature can be approximated by the temperature at the 'centre of gravity' of emission of the atmosphere (Paltridge 1970). The position of this centre of gravity will vary diurnally, and, on average, will be lowest at night, when inversion conditions are common, and will increase in height during the day as convection increases. Consequently the temperature controlling L_i will be lowest during the day, leading to an L_i minimum. Two cloudless periods in August (Figure 15) show some evidence of this

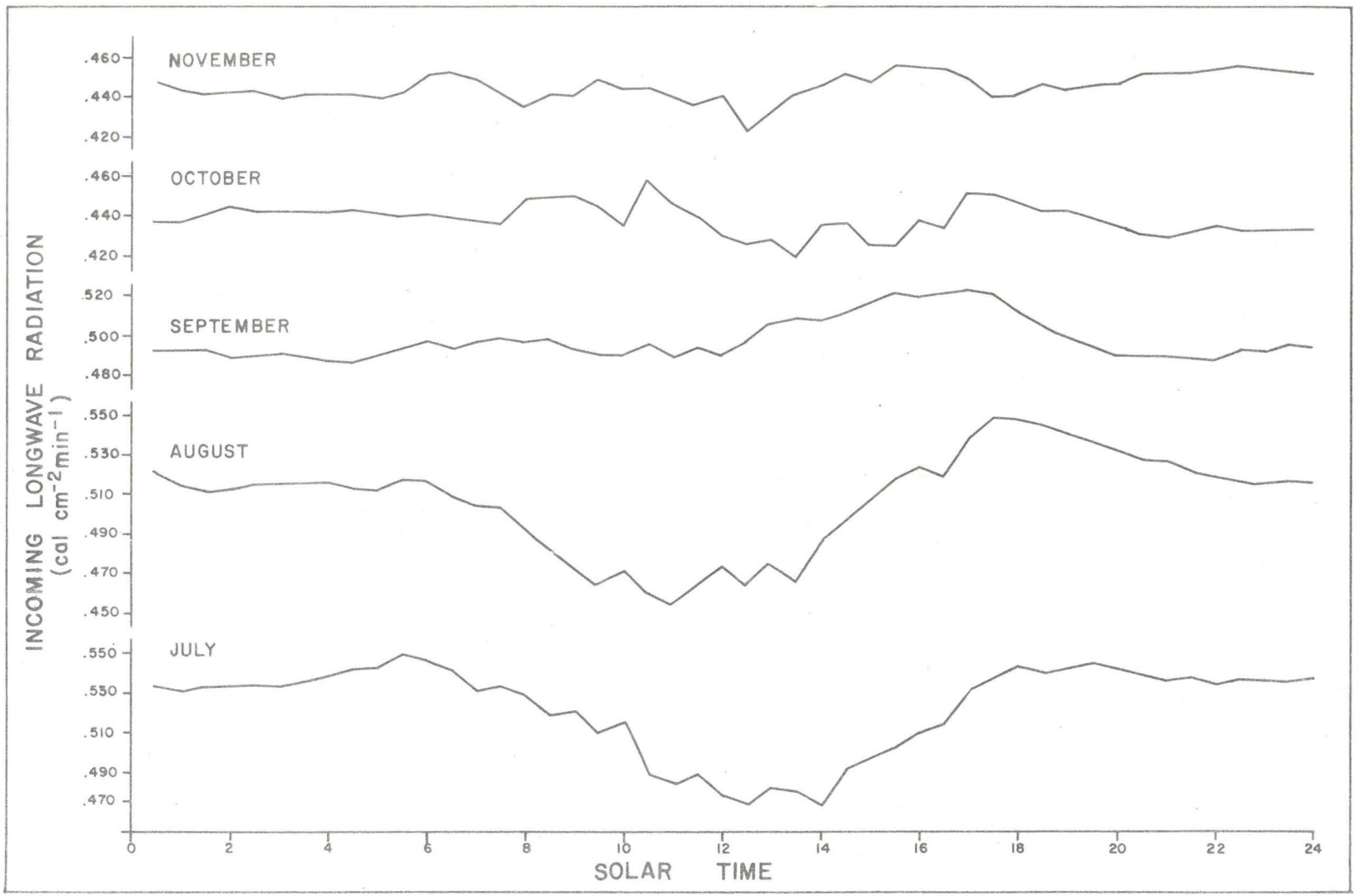

FIGURE 14 MONTHLY AVERAGE DIURNAL VARIATION OF INCOMING LONGWAVE RADIATION

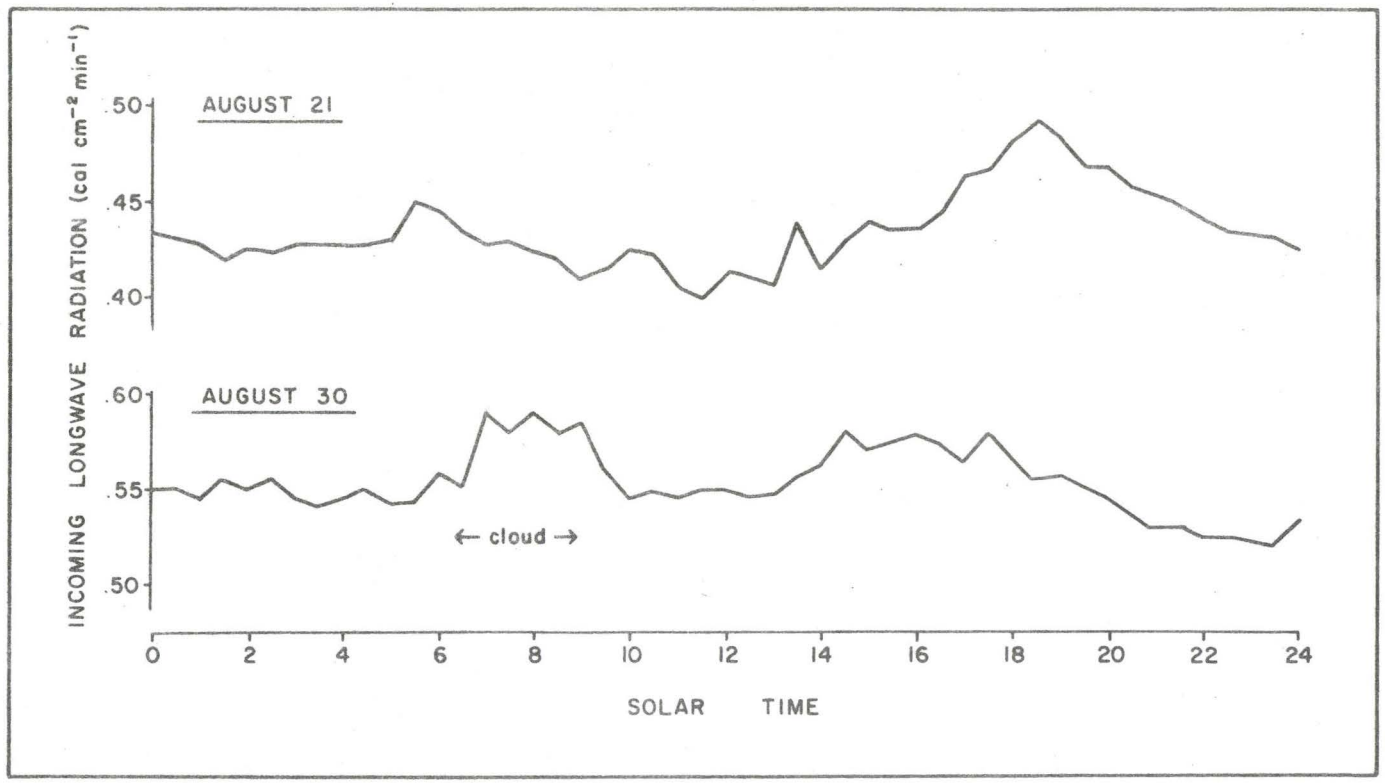

FIGURE 15 DIURNAL VARIATION OF INCOMING LONGWAVE RADIATION FOR TWO CLOUDLESS PERIODS

pattern. However, when this mechanism is most well developed, with strong convection, cloud formation is likely, and the clouds themselves will cause a change in L_i. Although the influence of cloud is difficult to summarise, the cloud observations suggest that amounts were commonly a minimum around midday in July and August, which may have led to the midday minimum L_i in these months.

Clouds have a higher emissivity than water vapour, so an increase in L_i with cloud amount is likely. In addition, low clouds, having higher temperatures and emissivities (Allen 1971), should have a greater effect on L_i than high clouds. Radiation from the clouds will be added to that from the cloudless portions of the atmosphere. Hence the influence of cloud on incoming longwave radiation at the surface should be determined with this 'clear atmosphere' radiation approximately constant. With the present data there is no means of ensuring this condition, and Figure 15 demonstrates that even with a cloudless atmosphere changes in the position of the centre of gravity of emission lead to temporal variations in L_i of as much as 20 percent.

The influence of cloud on L_i was therefore determined for periods of a few hours when cloud amount changed rapidly, since use of short periods should ensure approximate constancy of clear atmosphere radiation. The results are ambiguous for periods when only high clouds were present (Figure 16a - Figure 16c). There are indications that

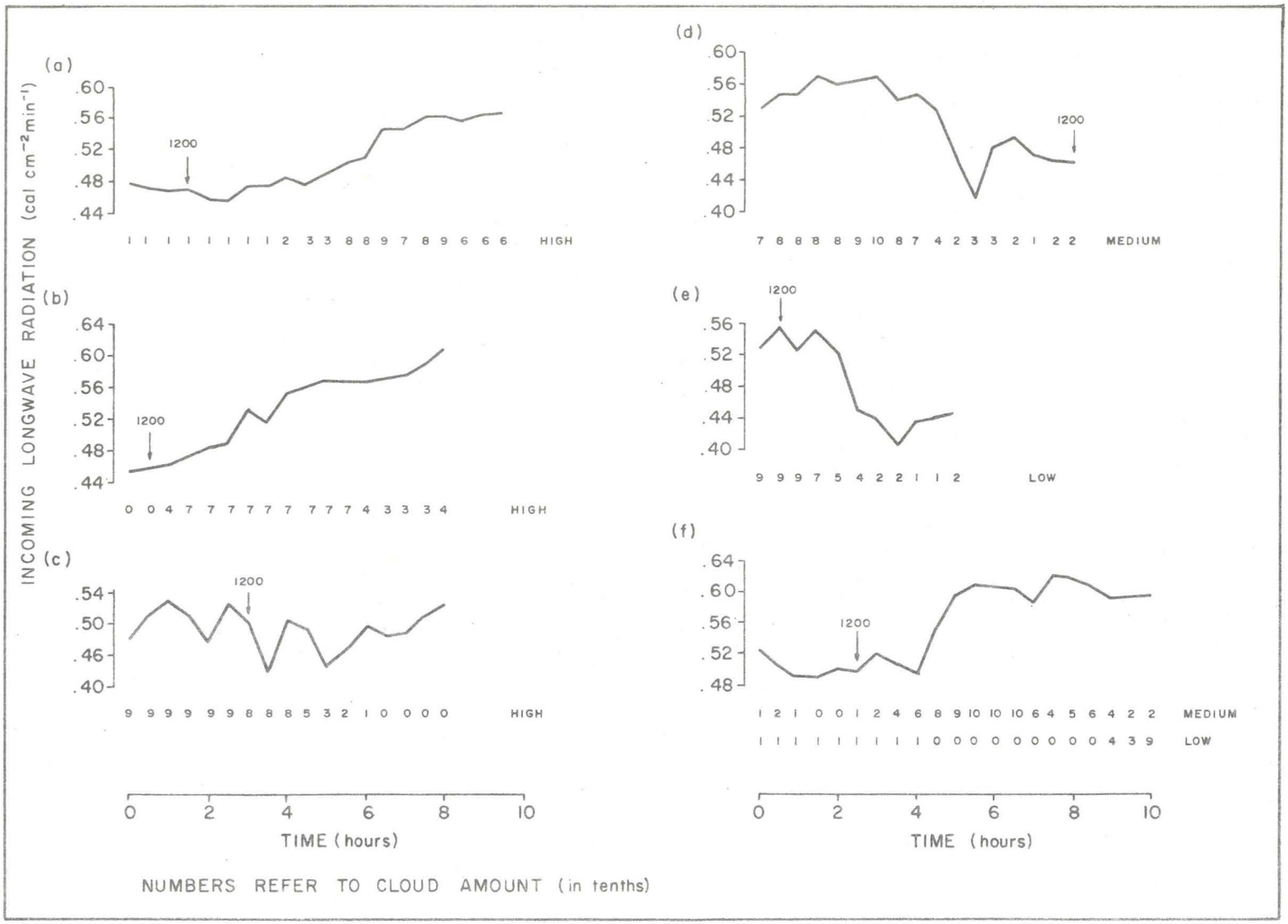

FIGURE 16 TEMPORAL VARIATION OF INCOMING LONGWAVE RADIATION WITH CLOUD AMOUNT

L_i increases, decreases and remains constant as cloud amount increases. For the first two cases L_i was at a minimum near noon and increased in the afternoon. This suggests that the variations were controlled by a variable centre of gravity of emission rather than by the amount of high cloud. Few data were available when only medium or low clouds were present. With medium cloud (Figure 16d and Figure 16c) the variation is approximately the same as that occurring in a cloudless atmosphere with an L_i minimum near noon. The distinct increase in L_i as cloud amount increases however, is rather more rapid than would be expected in a cloudless atmosphere. A strong increase in L_i occurs as amounts of low cloud increase (Figure 16f). Hence, although few data are available, it appears that low clouds strongly influence L_i, medium clouds have some effect, but the influence of high cloud is negligible.

A similar conclusion follows from a consideration of the influence of average daily cloud amounts on daily total L_i. 17 days in July and August had complete records of cloud amount. The average daily amount for each level was determined. The value at each level was weighted and the three weighted values summed. The correlation between this sum and daily total L_i for the 17 days was established. This procedure was repeated several times with different weightings for each level and the highest correlation (0.69) occurred when the

weightings were: low x 3; medium x 2; high x 0. Although the sample was small and the correlation low, the strong influence of low cloud and the negligible influence of high cloud is again demonstrated.

The monthly mean influence of total cloud amount was determined for July and August. The mean L_i in cloudless conditions, $L_{i(c)}$, was determined, and the ratio $L_{i(n)}/L_{i(c)}$, where $L_{i(n)}$ is L_i with cloud amount n, obtained for each L_i observation when cloud amount was known. A mean and standard deviation was found for this ratio for each n. These, with the regression relationship between the ratio and cloud amount, are shown in Figure 17. An increase in L_i with cloud amount is apparent in both months. However, high standard deviations of the ratios emphasize the difficulty of determining cloud influence on incoming longwave radiation. Variations in both clear atmosphere radiation and cloud types and distributions must have a great influence on L_i.

B. ESTIMATED VALUES

1. Radiation Charts

Results from calculations using various charts are listed in Table 14. Since a radiosonde ascent takes approximately one hour, the

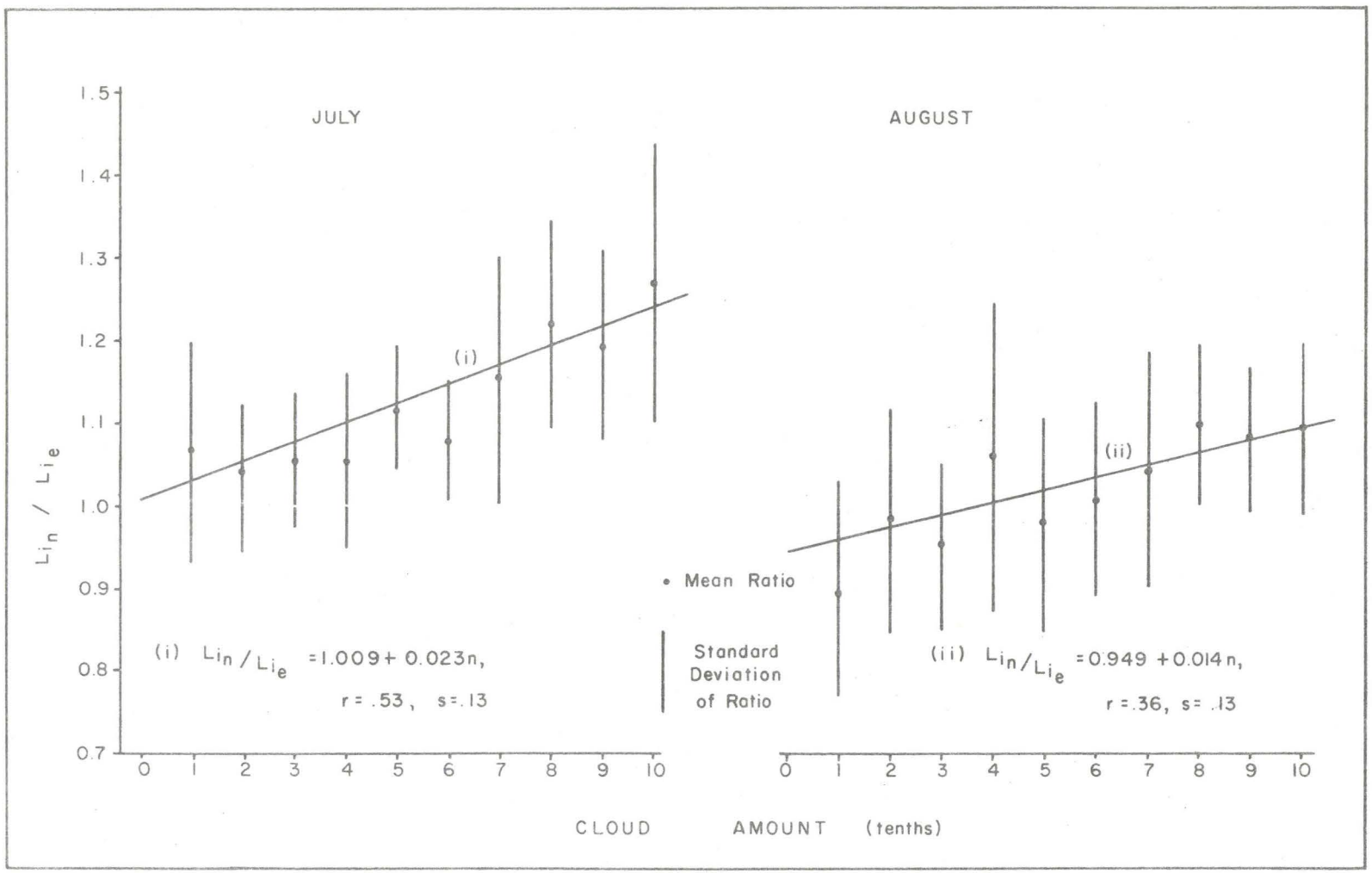

FIGURE 17 VARIATION OF L_{in} / L_{ie} WITH CLOUD AMOUNT : JULY & AUGUST

TABLE 14

ESTIMATES OF INCOMING LONGWAVE RADIATION BY CHART METHODS

Date	Launch Time T.S.T.	Elsasser L_i	Yamamoto L_i	Measurement Period	Measured L_i	Cloud Type	Cloud Amount (Tenths)
22-7	1436	.490	.485	1430-1530	.430	Cu	1
23-7	1302	.485	.457	1300-1400	.433	Cu	1
30-7	1213	.520	-	1200-1300	.452	Cu,Ac	3
15-8	1303	.509	-	1300-1400	.532	As	10
18-8	1510	.531	-	1500-1600	.528	Cu,Cc	8
19-8	0949	.472	.453	0930-1030	.374	Cc	1
19-8	1543	.488	.489	1530-1630	.434	Cu	1
21-8	1440	.476	.476	1430-1530	.438	-	0
26-8	0540	.454	.445	0530-0630	.483	Ci	1
27-8	1331	.487	.419	1330-1430	.440	Ci	1
9-9	1322	.465	-	1300-1400	.530	Cu,As	9
13-9	1142	.491	.486	1130-1230	.480	Ci	1
15-9	1758	.512	-	1800-1900	.577	As,Ci	6
16-9	1758	.512	-	1800-1900	.581	Cu,Ac	10
17-9	1800	.417	-	1800-1900	.450	As	7
19-9	0613	.398	-	0600-0700	.434	As,Cc	9
19-9	1737	.418	-	1730-1830	.422	As	3
20-9	0608	.424	-	0600-0700	.464	As	10
20-9	1744	.442	.437	1730-1830	.453	As	2
29-9	1153	.404	-	1200-1300	.430	As	9
10-10	1306	.469	.452	1300-1400	.453	-	0
13-10	1314	.483	-	1300-1400	.507	Cs	9
15-10	1327	.389	-	1300-1400	.331	Ci	4
27-10	1423	.370	-	1400-1500	.470	St	10
28-10	1357	.344	.326	1330-1430	.274	Cu	1
29-10	1409	.361	-	1400-1500	.349	Ac,Cc	10
31-10	1614	.416	-	1600-1700	.447	As	4
4-11	1447	.376	-	1430-1530	.362	Sc,As	8
5-11	1204	.369	-	1200-1300	.339	Cu,Sc	4
10-11	1230	.402	-	1230-1330	.488	Sc	6
11-11	1613	.417	-	1600-1700	.487	Sc,Ac	7
12-11	1154	.412	-	1130-1230	.471	Sc,Ac	6

measured flux for comparison with chart calculations was determined as the hourly average flux, from the radiometer records, for the approximate time of ascent.

The charts, as indicated earlier, are strictly applicable only to cloudless skies. Inspection of the radiosonde records and visual observations during the ascents indicated that ascents when cloud cover was less than three tenths did not pass close to the cloud, and hence the conditions should approximate to cloudless.

The Elsasser chart generally overestimates L_i in cloudless conditions (Figure 18a). About half the measured values differ from calculated values by more than 10 percent. In cloudy conditions the chart underestimates L_i. It is apparent that the accuracy of the chart bears little relation to cloud amount.

The Yamamoto chart gave similar results (Figure 18b), with about 40 percent of the cloudless estimates differing from measured values by more than 10 percent. Hence a slightly better agreement is possible.

Elsasser's values generally exceeded those of Yamamoto (Figure 18c), by up to 15 percent. This was approximately the difference found by Yamamoto (1952).

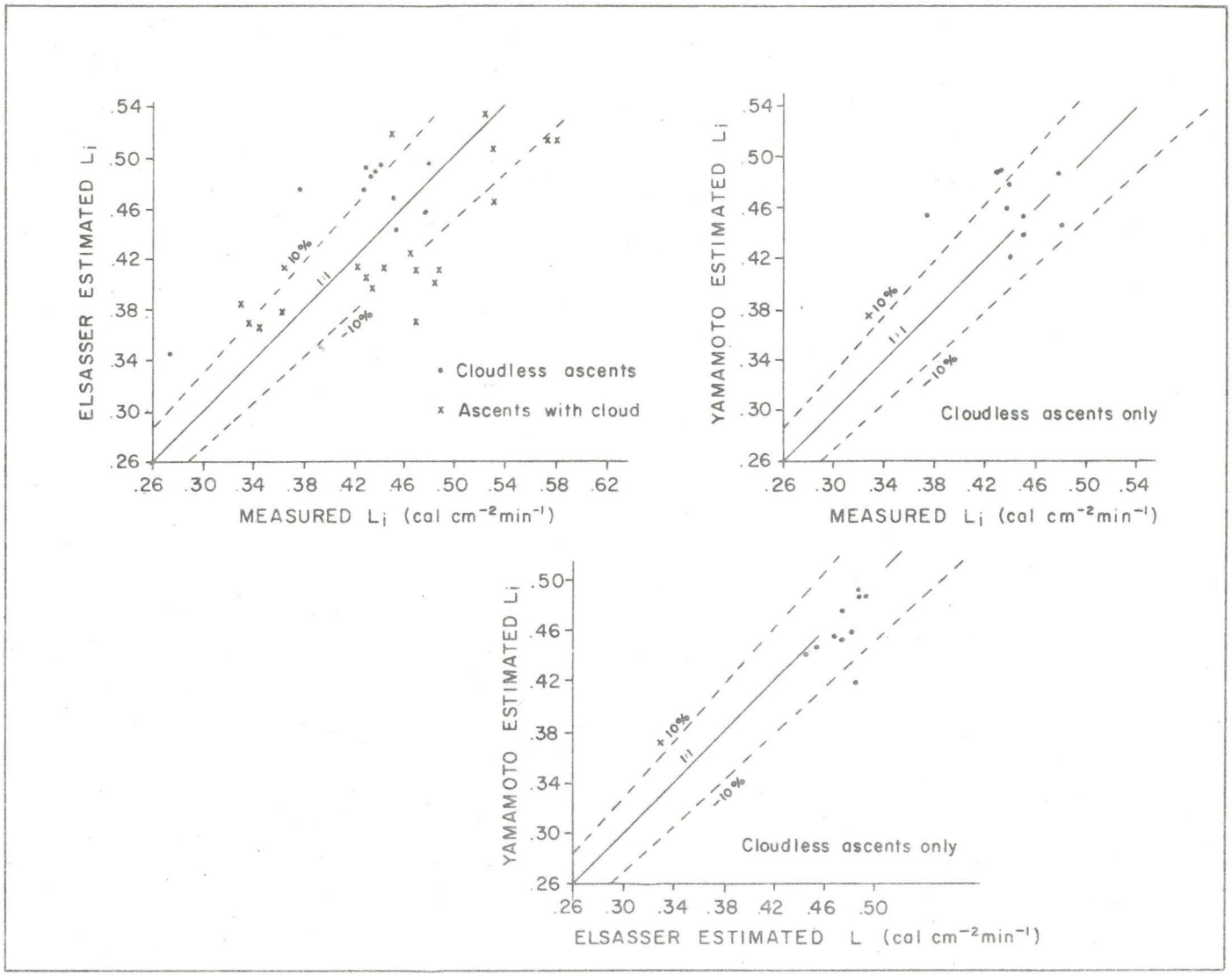

FIGURE 18 RELATION BETWEEN CHART ESTIMATES AND MEASUREMENTS OF INCOMING LONGWAVE RADIATION L_i (cal $cm^{-2}min^{-1}$)

On days with complete overcast, the downward flux was also calculated for the Elsasser chart, assuming that the cloud was a black-body at the cloud base temperature (Table 15). On two occasions the results are considerably better than those assuming a cloudless atmosphere, but on the other occasions there is little improvement. The major uncertainty in using the radiosonde data in this way lay in estimating the time at which the sensing package entered the cloud, and hence determining the cloud base temperature. On October 27th the time of entry was accurately determined since it was possible to follow the ascent visually. Also, the cloud base temperature at that time was determined by the radiation thermometer, which agreed with the temperature obtained from the ascent to within 0.5 C. The chart for this ascent appears to give a good estimate of the flux.

TABLE 15. DETERMINATIONS OF INCOMING LONGWAVE RADIATION L_i FOR OVERCAST CONDITIONS (cal cm^{-2} min^{-1})

DATE	MEASURED L_i	ELSASSER ESTIMATES	
		Using Cloud Base Temperatures	Assuming Cloudless Conditions
15-8	.532	.613	.509
16-9	.581	.595	.512
20-9	.464	.518	.424
27-10	.470	.463	.370
29-10	.349	.471	.361

Prediction of L_i from the charts generally, however, was disappointing. Since other charts, not used here, usually give L_i values proportional to those used, it is unlikely that they would yield more accurate L_i determinations. However, Morgan et al (1971) compared measured L_i to chart calculations and found that the Elsasser chart performed very well, suggesting that the theory underlying chart construction is adequate.

Since professional personnel supervised several of the ascents, there is no reason to suggest that the present radiosonde data are unreliable. Discrepancies between the present measurements and chart predictions may result from differences in atmospheric conditions between the launch and tower sites. The radiosonde launch site was over land and consequently the data for the surface and first datum level are possibly more representative of land than water. Since most L_i originates at low levels, correct determination of conditions at these low levels is vital (Goody 1964). Possible differences between conditions at the launch site and the tower were therefore examined. The data records indicated that air temperature at the release point was usually higher than at the tower, and use of the tower air temperature as the surface temperature of the sounding decreased L_i estimates by 1 or 2 percent. This adjustment, however, is not sufficient to give close agreement with the measurements. Further, the adjustment is probably partly compensated by the lower

vapour path length over land since the vapour pressure at the launch site was slightly lower than that at the tower. On three occasions the sensor package drifted over the lake at a height of 100 m. Since on these occasions the charts overestimated by 4,8 and 9 percent, it seems that the radiation regime controlled by the land surface dominated the ascent. It appears that the chart estimates obtained are more representative of the land atmosphere than of the lake atmosphere.

2. Empirical Formulae

Constants for the empirical formulae (equations 9 to 14) were calculated for cloudless conditions from the lake data, using half-hourly average fluxes. Cloudless conditions were defined from visual estimates of sky cover. Hence, the data are limited almost entirely to daytime. This method was preferred, however, to any definition of cloudless conditions based on smooth solar radiation traces, since smooth traces can occur when cloud is present. Since the cloud can occur in the clear sky between observations, the half-hour averaging period of L_i may contain data collected with some cloud present. It is unlikely that this occurred during the first three months of record, since frequent sky observations were made. Some cloudy periods may have occurred in October in apparently cloudless conditions. No cloudfree periods were recorded in November.

The formulae of Ångström, Brunt and Elsasser relate the effective emissivity of the atmosphere ε_f to surface (screen level) vapour pressure e. A plot of ε_f against e (Figure 19) shows a wide scatter of points. The three formulae and a linear relationship derived from the present data have been included in Figure 19. Their performances are similar. All have low correlation coefficients, as is to be expected from the data scatter. The correlation coefficient for the Brunt formula is lower than in the majority of previous determinations, a selection of which are shown in Table 16. This result implies that the present data scatter is greater than that found by previous workers. Also shown in Figure 19 are equations obtained by Anderson (1954) and Reuter (1950). The former was obtained over a lake surface and gave the highest correlation between ε_f and e of any equation tested. Although the slope of the line is identical to that of the present linear regression line, it considerably overestimates L_i. Reuter's (1950) Brunt-type equation was determined for Toronto, but the slope value is higher than the present data suggests, so that L_i is overestimated. The present relationship of the Brunt-type, however, is in reasonable agreement with several previous determinations (Table 16). The present Ångström-type relationship agrees well with that found by Anderson, but differs somewhat from other determinations (Table 16). Much of the general scatter of points in Figure 19 is the result of clustering of data points for individual days in a relatively small portion of the figure. Three days are separately identified in Figure 19, and these will be considered in detail below.

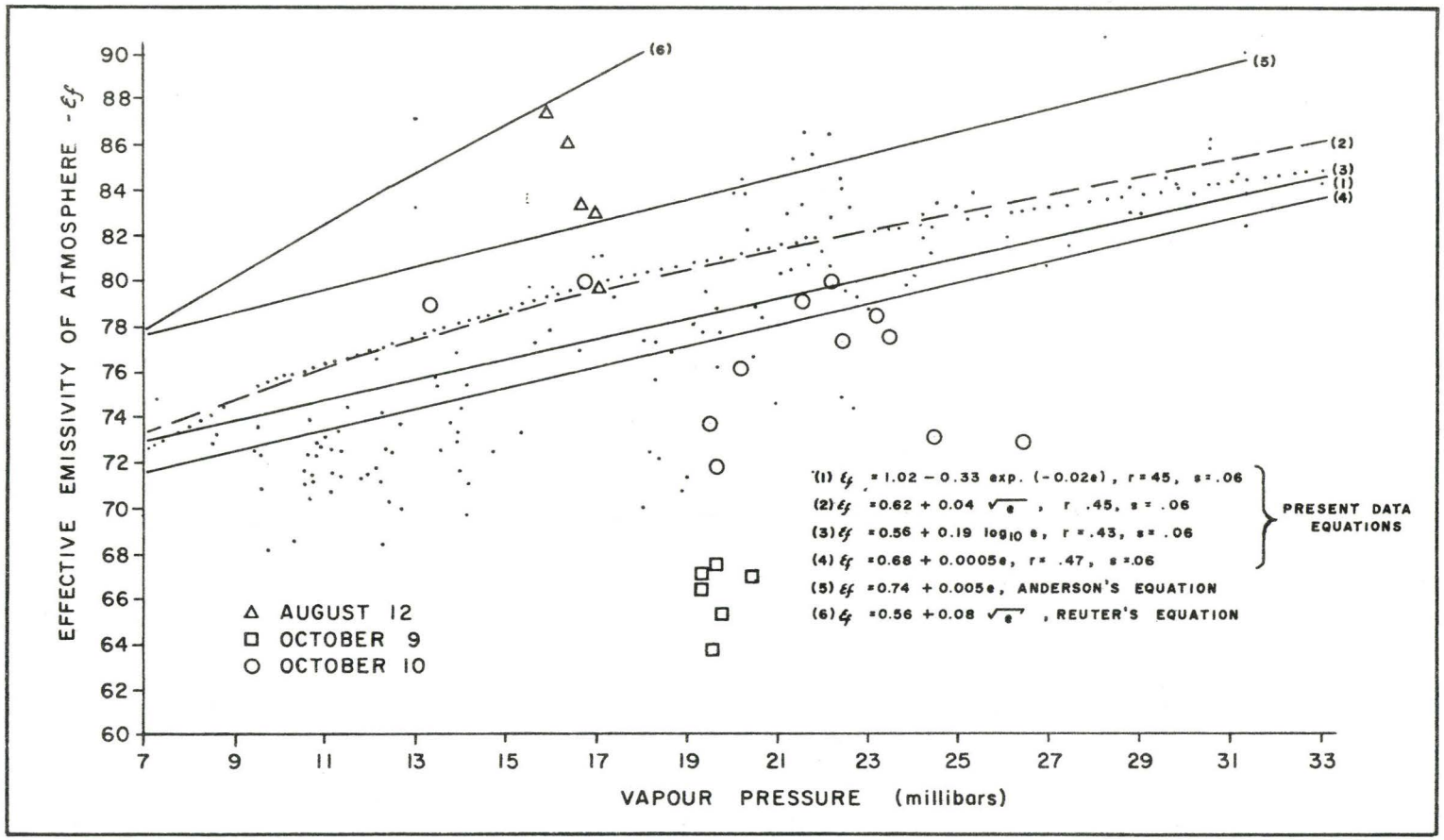

FIGURE 19 RELATION BETWEEN EFFECTIVE EMISSIVITY OF ATMOSPHERE (ε_f) AND VAPOUR PRESSURE (e) HALF HOURLY AVERAGE VALUES FOR CLOUDLESS OBSERVATIONS

TABLE 16

SOME PREVIOUS VALUES OF CONSTANTS IN BRUNT AND ÅNGSTRÖM ATMOSPHERIC RADIATION FORMULAE

BRUNT (Equation 10)				ÅNGSTRÖM (Equation 9)			
	a_b	b_b	r		a_a	b_a	γ
Anderson	0.68	0.036	0.92	Anderson	1.107	0.405	0.022
Ångström	0.48	0.058	0.73	Ångström	0.806	0.236	0.115
Ångström	0.50	0.032	0.30	Eckel	0.71	0.24	0.163
Asklof	0.43	0.082	0.83	Kimball	0.80	0.326	0.154
Boutaric	0.60	0.042	-	Raman	0.79	0.273	0.112
Brunt	0.53	0.065	0.97				
Eckel	0.47	0.063	0.89	Present Study	1.017	0.331	0.020
Kimball	0.44	0.061	0.29				
Raman	0.62	0.029	0.68				
Reuter	0.56	0.08	-				
Present Study	0.62	0.042	0.49				

Following Swinbank (1963), a much better relationship is obtained between L_i and σT_a^4 (Figure 20). The two functional forms of Swinbank's relationship (equations 12 and 13) were fitted to the Lake Ontario data (Figure 20). Compared to the humidity-based equations, correlation coefficients are high. The two equations originally obtained by Swinbank are also shown in Figure 20. They indicate a greater rate of increase of L_i with T_a, but give almost identical results at low L_i. Hence the Swinbank equations are likely to overestimate early in the season and in the middle of the day (Figure 21). Paltridge (1970) notes that the data used by Swinbank were collected at night, and are therefore biased towards inversion conditions. Daytime data would have a higher centre of gravity of emission, lower temperatures, and hence less L_i. Since the present data were collected during the day, L_i should be less than the value predicted by Swinbank. No nighttime cloud data were obtained, and no direct comparison with Swinbank's results is possible. A wide range of position of the centre of gravity is likely during the day, and hence L_i will vary even in cloudless conditions. Moreover the correlation between L_i and T_a should be lower than that found by Swinbank. Frequently cloudless mornings and afternoons were separated by cumulus formation near midday, so that the highest centres of gravity would not be encountered. If a large number of cloudless midday data were available, the slope would be further reduced.

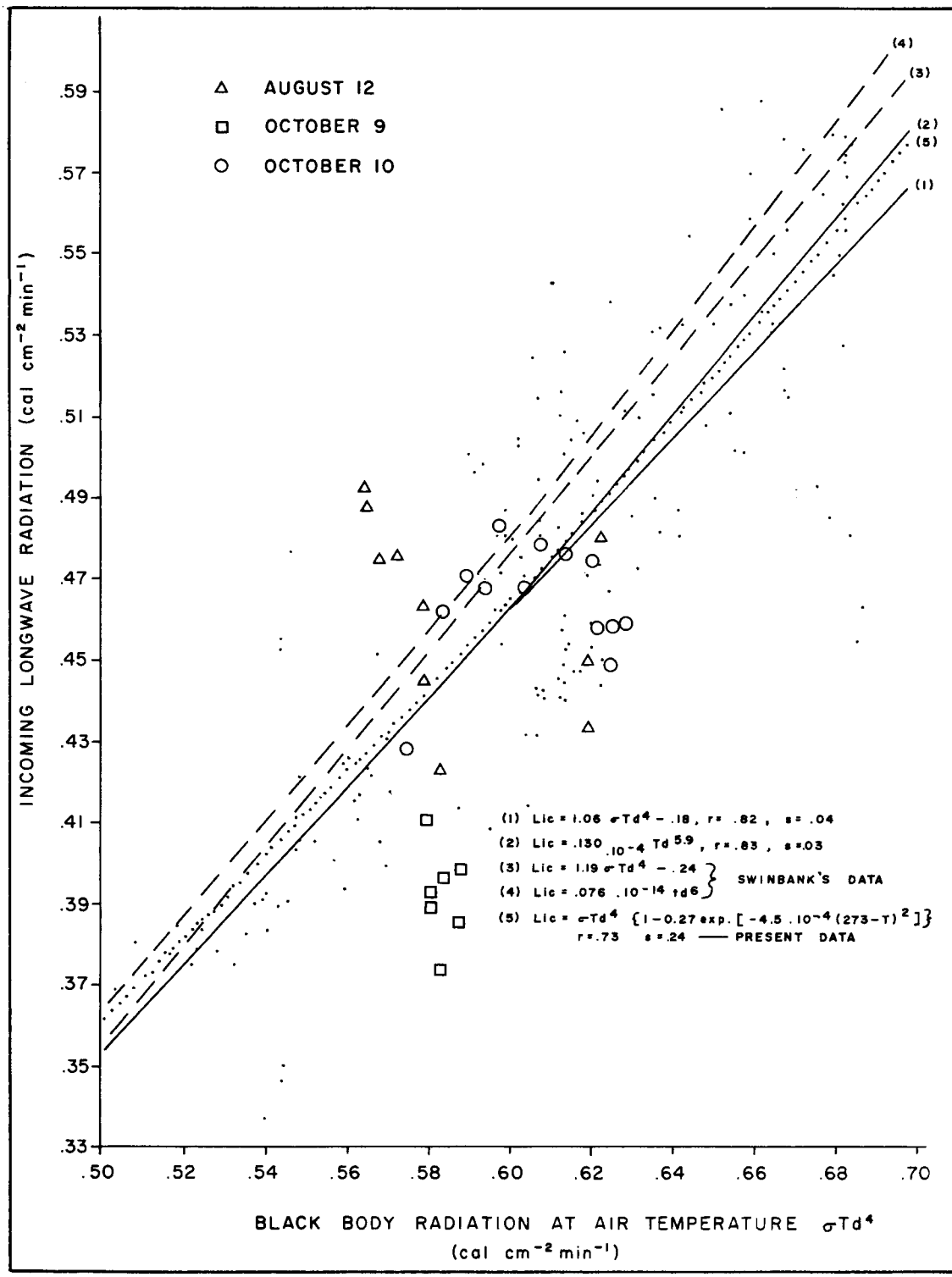

FIGURE 20 RELATION BETWEEN INCOMING LONGWAVE RADIATION AND BLACK BODY RADIATION AT AIR TEMPERATURES – FOR CLOUDLESS CONDITIONS (Half-hourly average fluxes)

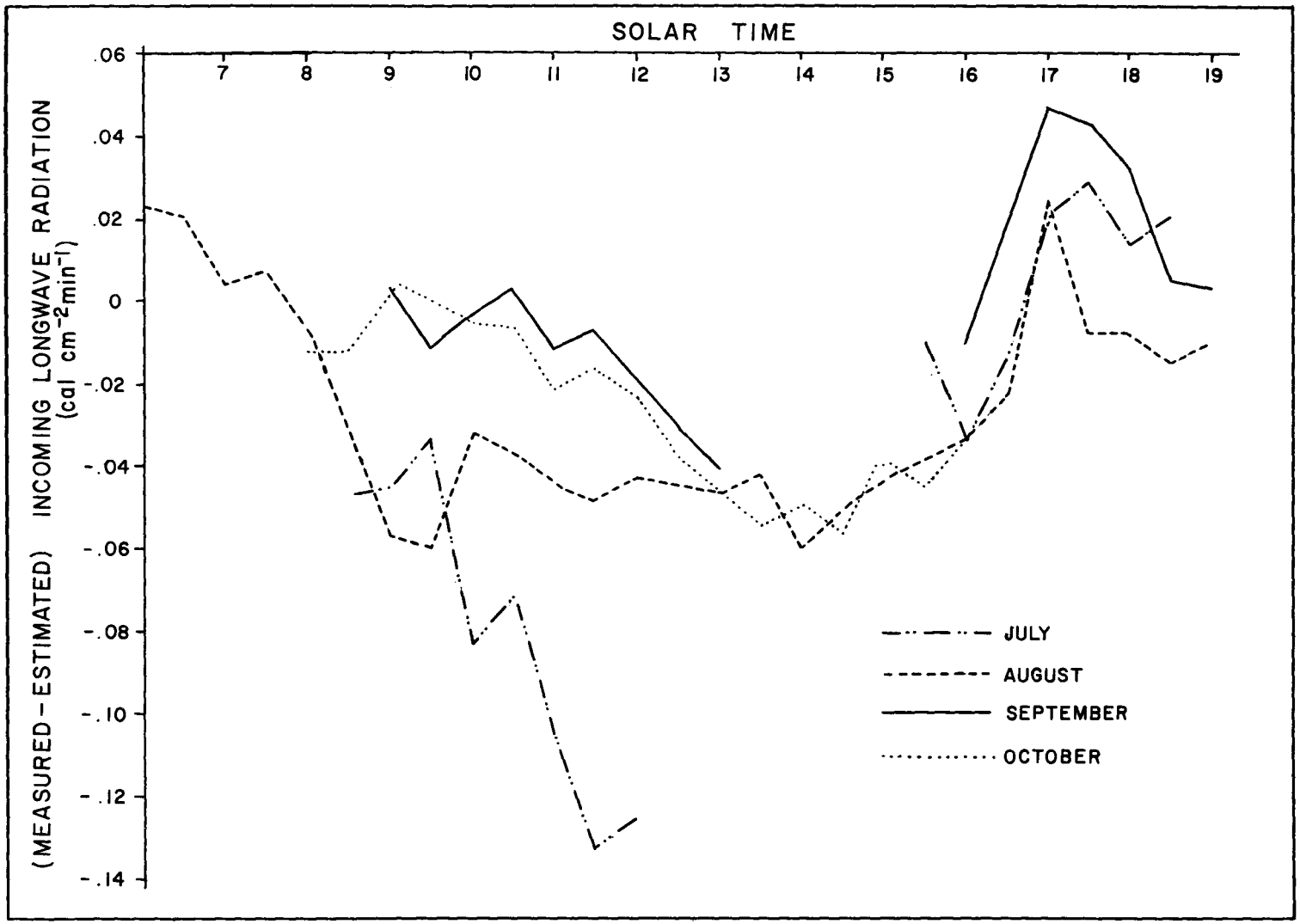

FIGURE 21 DIURNAL VARIATION OF DIFFERENCE BETWEEN MEASUREMENTS AND SWINBANK ESTIMATES OF INCOMING LONGWAVE RADIATION

The daytime data used here demonstrate the dependence of L_i on approximately the sixth power of the screen level temperature. Swinbank suggested this as a possible universal relationship. The lack of dependence on vapour amounts over a water surface is not surprising since for most of the time vapour contents will be sufficiently high in the lower atmosphere for $\varepsilon_\lambda(u)$ to be constant and a maximum. The theoretical basis for dependence on T^6 in these conditions has been argued by Gates (1965). He states, from consideration of equation 4, that while the total energy emitted by a black-body is controlled by the fourth power of the body's temperature, the monochromatic emission will depend on a power that varies with wavelength. For the modal wavelength of emission this power is the fourth, and it is respectively greater and less than the fourth for shorter and longer wavelengths. Since the atmosphere has a temperature around 300 K, its modal wavelength is about 10μ. However, the atmosphere is not a black-body, but has highest emissivity around 6.3μ, the strong water vapour absorption band. Hence the temperature dependence should be higher than the fourth power.

The alternative expression relating L_i to T_a given by Idso and Jackson (1969), equation 14, gives similar results to those of the Swinbank-type equations. The correlation coefficient, however, is lower. Idso and Jackson (1969) claim that their equation is better suited when a wide range of atmospheric temperatures, and hence

L_i, occur. Since the present data contain samples approaching the limits of conditions likely to be commonly encountered in the atmosphere, the simpler Swinbank equation appears preferable as a general equation.

Since it is difficult to compare the performance of the humidity-based and Swinbank-type equations from the correlation coefficients presented above, measured L_i values were compared to values predicted by the Brunt and Swinbank formulae. The results,

$$L_i \text{ (Brunt)} = 0.12 + 0.75\ L_i \text{ (measured)}, \quad r=0.79, S=.03, \quad (60)$$

and

$$L_i \text{ (Swinbank)} = 0.11 + 0.76\ L_i \text{ (measured)}, r=0.83, S=.03, \quad (61)$$

indicate that there is little difference between the two methods of estimation, since the intercepts, slopes and correlation coefficients are similar. Both show that L_i is overestimated at low L_i values. This is to be expected for the Swinbank equation, since low L_i values imply a high centre of gravity of emission of the atmosphere, and hence lower L_i values than those predicted from air temperature measurement. Since the Brunt equation is also strongly dependent on air temperature, a similar explanation follows. However, since the Swinbank equation requires simpler measurement, it appears to be the best predictive equation for L_i so far proposed.

Departures from the overall relations are shown by the data for the three cloudless periods given in Figures 19 and 20. These days were chosen to indicate some of the possible reasons for variation between formulae estimates and measurements. The temporal relations between measured values and estimates by the Brunt and Swinbank formulae are shown in Figure 22. October 9th was unusual since both formulae greatly overestimate L_i throughout the cloudless period. Air temperature slowly increased throughout the period, while vapour pressure remained approximately constant at 18 mb. The results suggest that the air above the surface was cold and dry, or that there was a high centre of gravity of emission of the atmosphere. No upper air data were available at this time. The closest ascent data were for a launch at 1306 on October 10th. At this time again the formulae overestimated L_i considerably, although earlier in the day agreement was good. The ascent data indicated a weak inversion at about 830 mb. Since other ascents near this date suggested that near surface inversions occurred early in the day, it is possible to suggest that the inversion rose slowly during the morning, the increase in L_i being associated with an increase in surface and air temperatures as shortwave radiation increased. It is possible that the inversion was removed prior

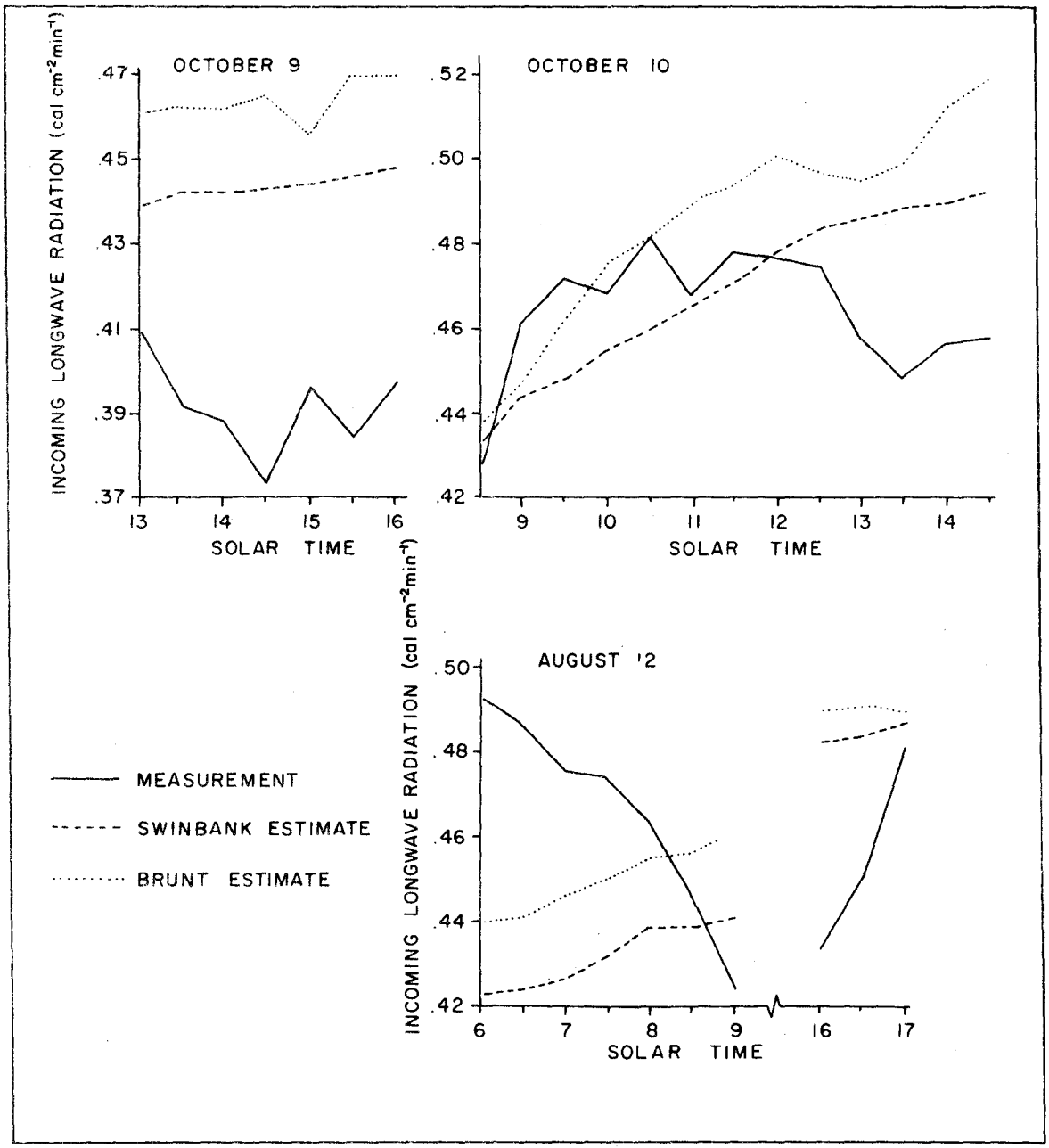

FIGURE 22 TEMPORAL VARIATIONS OF INCOMING LONGWAVE RADIATION AS MEASURED AND AS ESTIMATED BY THE BRUNT AND SWINBANK FORMULAE

to 1430, since cumulus appeared thereafter. This would establish convection currents and a higher centre of gravity of emission and result in lower L_i values than those predicted from surface values.

The effective emissivity of the atmosphere appears almost independent of vapour pressure for August 12th (Figure 19), while there is little relation between L_i and σT_a^4 (Figure 20). Figure 22, however, suggests that there was a well-developed relationship of the type discussed with reference to Figure 21. It seems likely that the centre of gravity of emission of the atmosphere rose rapidly in the morning, when convection was well-developed and led to cumuliform cloud for the period 0900 to 1600.

The data presented in Figure 22 demonstrate that the L_i estimates of Swinbank and Brunt generally have similar trends. This is to be expected since, as noted by Swinbank (1963), the dependence of L_i on $\sqrt{e}$ in the Brunt formula is relatively weak, so that L_i variations are caused mainly by T_a variations. The data here support his conclusion that direct determination of L_i from T_a is preferable.

Equations of the Brunt and Swinbank type were used for measurement periods less than the full season to determine if the constants obtained by such equations are stable with the time period of record. Swinbank's second form, equation 13, will be used, since it gives a higher correlation with the present data than does the first form. Swinbank has suggested that it is better founded physically. The full season equations, obtained from Figures 19 and 20 are

$$\varepsilon_f = 0.62 + 0.04 \sqrt{e}, \quad r=.45, \tag{62}$$

and

$$L_{i(c)} = .130.10^{-14} T_a^{5.9}, \quad r=.83. \tag{63}$$

For monthly periods the constants of the Brunt equation approach those of the full season data in August and September (Table 17). The results for the other two months, and the July results for the Swinbank equation appear to be anomalous. Correlation coefficients are generally lower for these months than for the others. There is no relation between the number of observations and either the correlation coefficients or the constants.

The constants were also evaluated on a daily basis for days that were almost completely cloudless (Table 18). These show great variation. This is to be expected since only a small number

of values are considered for each day. However, within the range of temperature encountered in the atmosphere, predicted values of L_i by the Swinbank type formula are similar, whichever set of constants are used, and are similar to values from the full season equation. For example, using the constants from Table 18 and those of equation 63, L_i differs by less than 4 percent at 20 C. A similar prediction, using the Brunt formula at 20 C and 16 mb leads to differences approximately three times as great. The difference between formulae must be a result of the better correlation between L_i and T_a than between ε_f and e. Hence, while the constants of the Swinbank equation cannot be considered stable for short periods, this equation provides a satisfactory method of L_i determination that holds for periods upwards of one day.

TABLE 17: MONTHLY VALUES OF CONSTANTS IN ATMOSPHERIC RADIATION EQUATIONS OF BRUNT AND SWINBANK

	JULY	AUGUST	SEPTEMBER	OCTOBER
		BRUNT		
a_b	.188	.630	.619	.738
b_b	.137	.042	.045	.003
Correlation coefficient	.45	.43	.67	.05
No. of Observations	20	85	22	38
		SWINBANK		
Log A_s	2.678	-14.578	-16.756	-12.161
B_s	-1.211	5.773	6.664	4.785
Correlation coefficient	- .30	.77	.90	.78
No. of Observations	25	96	25	42

TABLE 18

CONSTANTS OF ATMOSPHERIC RADIATION EQUATIONS OF BRUNT AND SWINBANK FOR CLOUDLESS DAYS

DATE	BRUNT (Equation 20)				SWINBANK (Equation 13)			
	a_b	b_b	Correlation Coefficient	Number of Observations	log A_s	B_s	Correlation Coefficient	Number of Observations
21-8	.593	.043	.50	15	-4.114	1.517	.42	15
22-8	.780	-.007	-.07	15	-21.829	8.699	.97	15
28-8	.649	.037	.53	14	-5.759	2.211	.22	14
30-8	.763	.017	.28	20	-4.893	1.872	.59	20
13-9	.521	.065	.84	11	-18.832	7.506	.96	11
5-10	.456	.087	.74	16	-12.642	4.984	.78	17
10-10	.833	-.010	-.16	13	-2.215	.762	.17	13

The above discussion indicates that a Swinbank-type formula is the best estimation procedure for L_i available, and that there is theoretical justification both for the general form and for diurnal variations in the results obtained. The standard errors associated with the formula, given in Figure 20, indicate that L_i can be determined to about $\pm$ 10 percent. While this is almost twice the error likely from direct measurement (Table 2), the measurement of screen level temperature is considerably easier than direct radiation measurement in remote locations.

3. Cloud Conditions

The difficulties of estimating the influence of cloud on L_i have already been considered. However, the present data were used with equations 15, 16 and 17 in an attempt to define predictive equations for L_i when cloud is present. Pooled data for the whole season were used, and L_i in cloudless conditions was obtained from both the Brunt and Swinbank formulae. The results of the determination of a bulk cloud coefficient (equation 15) and coefficients for each level (equation 16) were disappointing, since all had standard deviations which exceeded absolute values by several hundred percent. Using the coefficients of Bolz (1949) and Morgan et al (1971) (Table 19), and the square of the cloud amount (equation 17), the results of a comparison of estimated and measured values are

$$L_i \text{ (Brunt)} = 0.19 + 0.64\ L_i \text{ (measured)}, \quad r=.73, \quad S=.04, \qquad (64)$$

and

$$L_i \text{ (Swinbank)} = 0.19 + 0.63\ L_i \text{ (measured)}, \quad r=.70, \quad S=.05. \qquad (65)$$

The two results are not significantly different. The standard errors are small, and not greatly in excess of those of equations 60 and 61. They indicate that L_i in cloudy conditions can be estimated to within about $\pm$ 15 percent for the season as a whole. The results for shorter periods were very variable and equations similar to equations 64 and 65 have high standard errors. Hence the Bolz coefficients, which give most weight to low cloud, can be used to obtain estimates of L_i in all conditions if long period averages are needed. For short periods the variation in cloud distribution and clear atmosphere radiation decreases the accuracy of estimates and direct measurement is preferable.

TABLE 19. CLOUD COEFFICIENTS OF BOLZ (1949) AND MORGAN, PRUITT AND LOURENCE (1971)

Cloud Type	Coefficient
Cirrus (Ci)	0.04
Cirrostratus (Cs)	0.08
Altocumulus (Ac)	0.16
Altostratus (As)	0.20
Cumulus (Cu)	0.20
Cumulonimbus (Cb)	0.20
Stratocumulus (Sc)	0.22
Stratus (St)	0.24
Nimbostratus (Ns)	0.25

C. ESTIMATION OF NET LONGWAVE RADIATION

The Brunt and Swinbank equations were used to obtain relations between L_n and surface parameters. The resulting equations for cloudless data for the whole season are

$$L_{n(c)}/\sigma T_a^4 = .062\sqrt{e} - .451, \qquad r=.50, \quad S=.07, \qquad (66)$$

and

$$L_{n(c)} = 10^{-23} T_a^{10}, \qquad r = .36, \quad S = .21. \qquad (67)$$

The correlation in the Brunt equations is approximately the same as for prediction of L_i by this type of equation (equation 62), but Swinbank's equation gives lower correlation than equation 63. Kondrat'yev (1965) points out that for L_n determination it is necessary to take into account the stratification of the atmosphere, and that it cannot be assumed, as with L_i, that the flux is largely controlled by conditions close to the surface. The present data indicate that the vapour pressure at screen level probably represents conditions in the whole depth of the atmosphere better than does temperature.

While T_a appears to be an adequate parameter to use to determine L_i by empirical methods, its use in L_n calculations implies that the underlying surface is at the same temperature as the air at screen height. Taking the temperature difference into account (equation 30), the two equations become

$$L_{n(c)} = \sigma\{T_a^4(0.145\sqrt{e} - .768) - (T_s^4 - T_a^4)\}, \qquad r=.76,\ S=.10, \qquad (68)$$

and

$$L_{n(c)} = 10^{-178}\ T_a^{72} - \sigma(T_s^4 - T_a^4), \qquad r=.55,\ S=1.05. \qquad (69)$$

The inclusion of the temperature difference increases the correlation coefficient for both formulae. The coefficient for Swinbank's equation, however, is still significantly lower than that for the Brunt equation. Hence an equation of the Brunt type appears to provide the better predictive equation of L_n.

The relationships between measured L_n and L_n predicted by the Brunt equations are

$$L_i(\text{eq.66}) = 0.26\ L_n(\text{measured}) - 0.08, \qquad r=.54, \quad S=.019, \qquad (70)$$

and

$$L_i\ (\text{eq.68}) = 0.46 L_n\ (\text{measured}) - 0.04, \qquad r=.62, \quad S=.014. \qquad (71)$$

Both results indicate that the predictive equations underestimate at large (negative) values of L_n. This suggests that L_i is overestimated when the incoming flux is small, as found for the L_i prediction equations. The standard error of equation 70 indicates that L_n in cloudless conditions can be generally predicted to better than 20 percent. If surface temperature measurements are available, the accuracy increases to $\pm$ 15 percent. However, since L_o can be determined to within about 1 percent from surface temperature measurements, and L_i can be

obtained to within $\pm$ 10 percent with the Swinbank formula, L_n can then be estimated, through its componenets, to about $\pm$ 11 percent. Empirical methods cannot be used with any confidence when clouds are present. Table 2 indicates that L_n determined radiometrically as $R_n - Q_n$ has an error of about $\pm$ 13 percent. However, using L_i measured from $T_i - Q_i$, and L_o from surface temperature measurements, the accuracy of L_n is within about $\pm$ 8 percent. Hence separate measurement of the components of L_n appears to be the best method at present for L_n determination.

CHAPTER 6

RELATION BETWEEN LONGWAVE RADIATION AND NET RADIATION

Variations in net radiation at night involve only longwave flux variations. These variations and their controlling factors were considered in Chapters 4 and 5. During daylight however, variations in R_n also involve the shortwave fluxes, and it is relevant to access the relative importance of changes in short and longwave fluxes. These components are interrelated, since L_o depends on the surface energy balance and hence, indirectly, on the other components of R_n. Consequently, consideration is given in this chapter to the relationship between the long and shortwave fluxes and between longwave fluxes and net radiation.

A. RELATIONSHIP BETWEEN SHORTWAVE AND LONGWAVE FLUXES

λ_n was calculated as the slope of the regression line between L_n and Q_n for each daylight period with complete data. Frequency distributions of λ_n are shown in Figure 23. Values lie between -0.2 and 0.2. The distributions are quite compact in July and August,

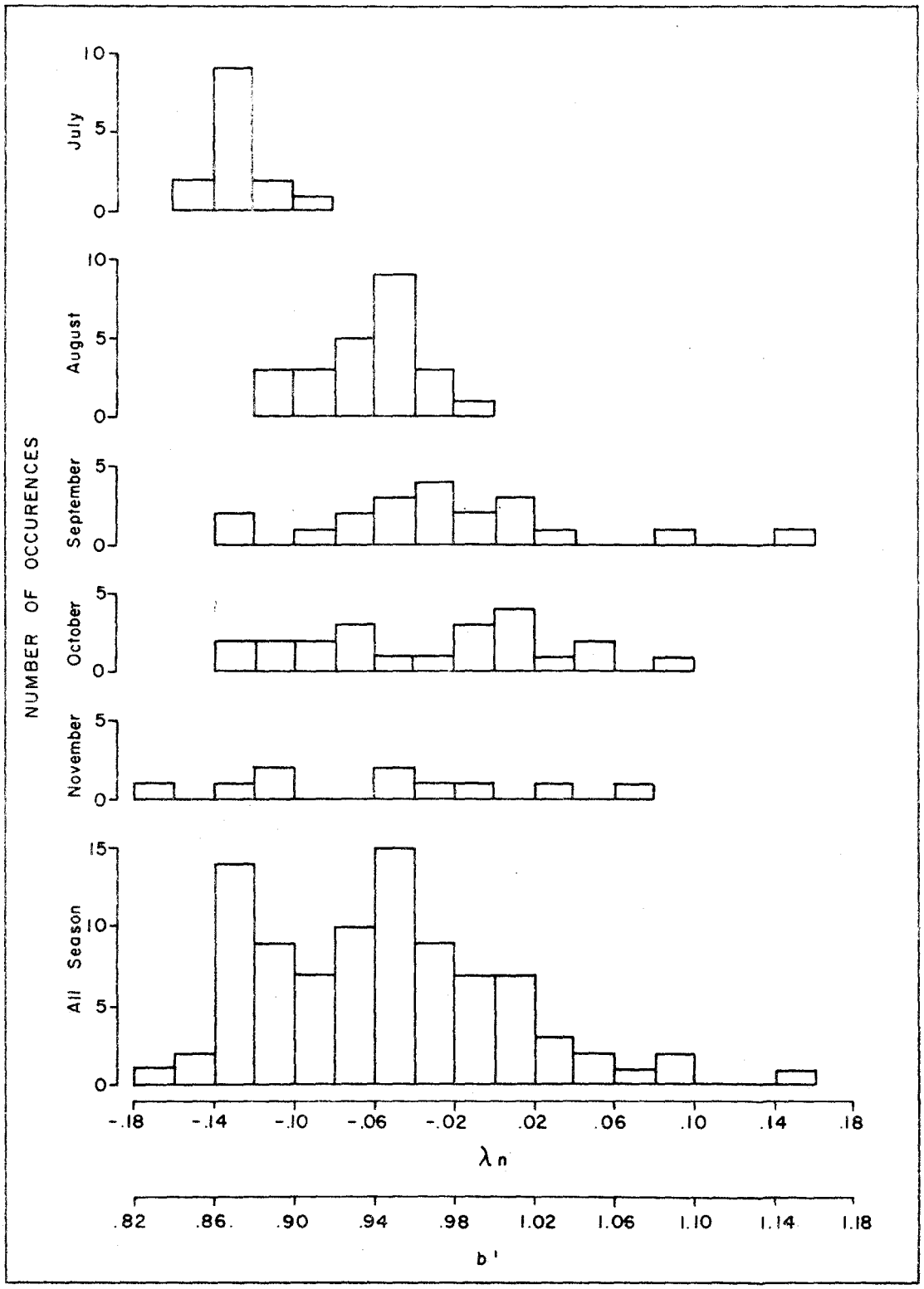

FIGURE 23 FREQUENCY DISTRIBUTION OF λn AND b' FOR EACH MONTH

indicating that L_n variations decreased the diurnal R_n variation by about 13 and 6 percent respectively. For the other months the values have considerable spread, and R_n variations are both increased and decreased by L_n variations, although the influence of L_n is usually less than 15 percent of that of Q_n. In order to isolate factors causing variations in λ_n, four idealised situations are defined, on the basis of diurnal L_n variations, (Figure 24):

(a) L_n constant, $\lambda_i = \lambda_o$, $\lambda_n = 0$;

(b) L_n maximum (lowest minimum value) at noon, $\lambda_i > \lambda_o$, $\lambda_n > 0$;

(c) L_n minimum at noon, $\lambda_i < \lambda_o$, $\lambda_n < 0$;

(d) L_n minimum after noon, $\lambda_i < \lambda_o$, $\lambda_n < 1$, λ_n is greater for a given L_n amplitude, than for type (c).

λ_n values for (b), (c) and (d) depend on the amplitude of the L_n variations. The value for type (d) depends in addition on the lag of the L_n minimum behind the Q_n maximum. While these indealised types demonstrate the dependence of λ_n on flux variations, they do not isolate the causes of such variations. Although changes of L_i in a cloudless atmosphere have been noted in Chapter 5, one of the major causes of L_i variation is cloud amount. At the same time, cloud will also modify Q_n, which in turn influences surface temperature and hence the outgoing longwave flux.

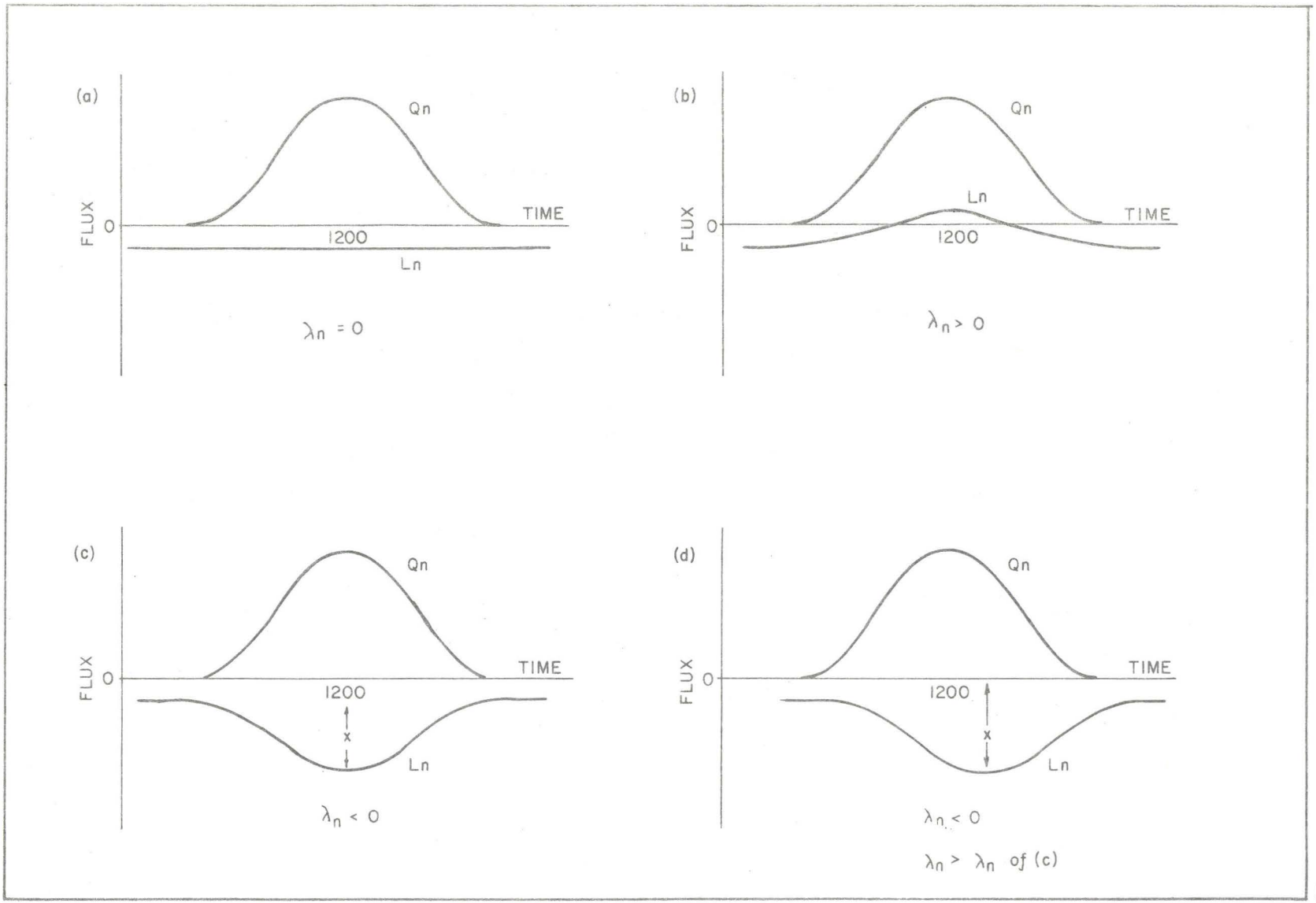

FIGURE 24 IDEALISED DIURNAL VARIATION OF NET SHORTWAVE (Q_n) AND NET LONGWAVE (L_n) FOR FOUR DAYS

The data for each day fit one of the four idealised types above. Four days were selected as examples and these indicate possible causes of variation. The relevant data are shown in Figure 25 (L_o is shown as negative for clarity):

(a) This day shows the minimum L_n variation found in the field season. Complete stratus cover throughout the day led to almost constant L_i and also decreased Q_i so that diurnal surface heating was negligible. In these conditions, although Q_n was assymetrical about noon, R_n was controlled by Q_n and λ_n approaches zero.

(b) A small amount of high cloud cover had little influence on L_i and this flux was approximately constant throughout the day. Hence $\lambda_i=0$. $|L_o|$, however, exhibited a minimum in the middle of the day, leading to a negative λ_o. Hence L_n was in phase with Q_n and $\lambda_n>0$.

(c) This represents a cloudless day with L_i approximately constant. Surface heating gave a positive λ_o, and an L_n minimum just after noon. λ_n was negative.

(d) A marked decrease in cloud amount during the morning resulted in an L_i minimum after noon. Consequently L_i was out of phase with Q_n and λ_i was negative. Although L_o was not constant no clear trend was discerable. Hence $\lambda_o \simeq 0$. Although the L_n minimum occurred later than on the day classified as (c), implying that for a time λ_i was positive, the greater amplitude led to a smaller λ_n value than in case (c).

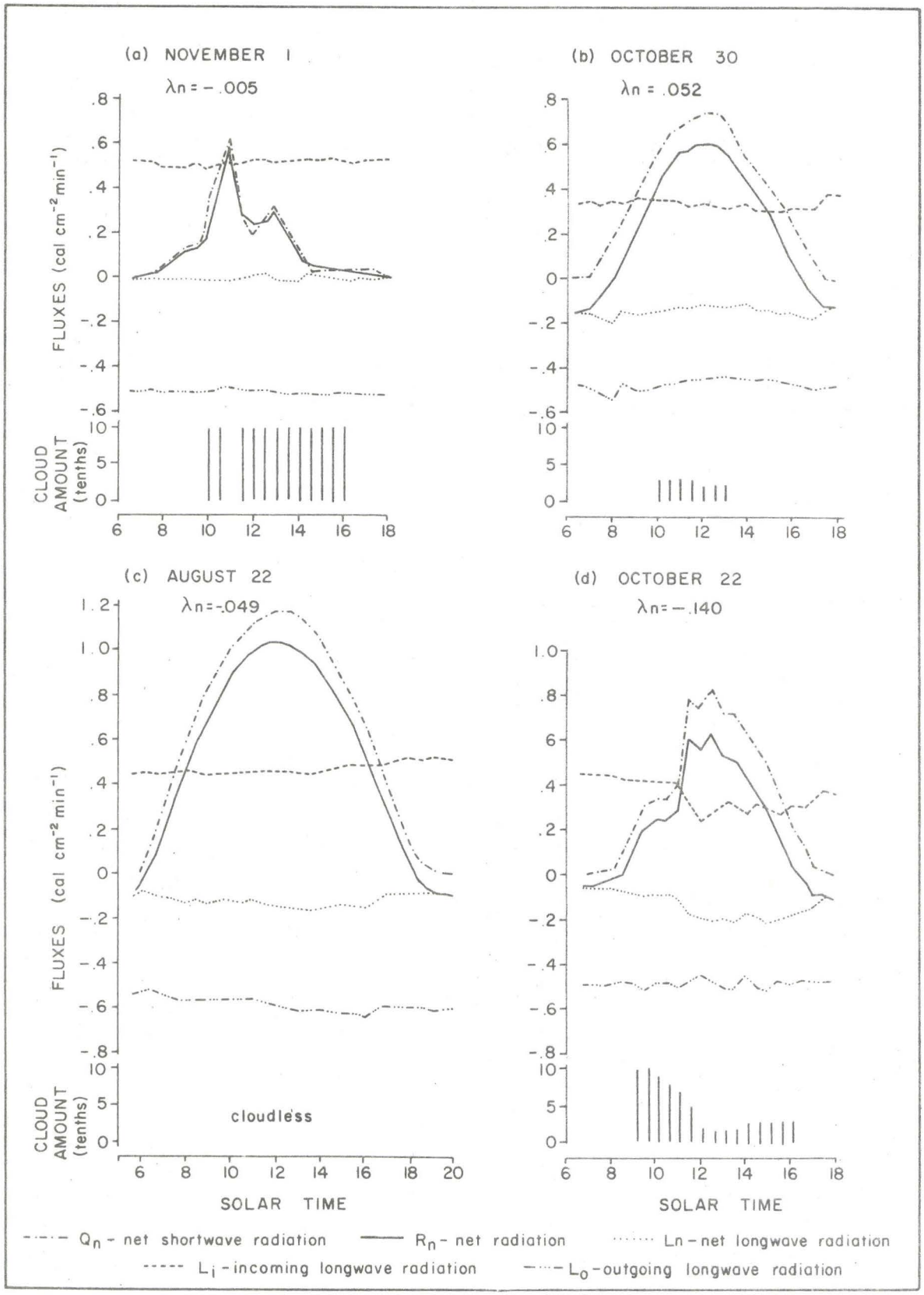

FIGURE 25 : DIURNAL VARIATION OF NET RADIATION, NET SHORTWAVE RADIATION AND LONGWAVE FLUXES FOR SELECTED DAYS

These four examples demonstrate the dependence of λ_n on absolute and relative changes in both L_i and L_o. Example (d) emphasizes the controlling influence of cloud. The results for these four days may now be generalized to explain the pattern of results shown in Figure 23.

In July there was a distinct diurnal pattern of cloud amount, leading to an L_i minimum around midday (Figure 14). Also, high Q_i values gave an L_o maximum close to this time (Figure 13). These two influences both act to give negative λ_n values. Since this pattern was found for most days during the month, the variation in λ_n is slight (Figure 23). The rate of change of both L_o and L_i were less in August than in July, although the diurnal patterns were similar. Consequently the λ_n value is closer to zero. For the other months, surface heating is less marked and $\lambda_o \simeq 0$. Hence λ_n was controlled mainly by λ_i. Since no diurnal L_i pattern occurred in these months, λ_n was highly variable.

Examples (c) and (d) in Figure 25, and the data for July and August, suggest that when L_n has an approximately smooth diurnal variation and a minimum close to noon, λ_n depends mainly on the amplitude of L_n variations, since maxima and minima of L_n and Q_n occur at approximately the same time. The combined effects of cloud and surface heating for July and August can therefore be determined

by the variation of λ_n with the amplitude of the diurnal L_n variation, L_n(range) (Figure 26). The regression between L_n(range) and λ_n is significant at above the 0.1 percent probability level. For the other months surface heating is less and cloud amounts do not have a distinct diurnal pattern. Hence L_n and Q_n maxima and minima do not occur simultaneously, and L_n(range) cannot be directly related to λ_n (Figure 26).

The relatively stable λ_n values for July and August, therefore, can be attributed to the approximately symmetrical variation of L_n about noon for each day, with a relatively small L_n (range) variation from day to day. There were 2 important factors which could account for such L_n conditions: first, the diurnal variation in surface heating which produced L_o changes and second, diurnal variations in cloud amount which produced L_i changes. As a result of these two influences R_n variations were reduced by 13 percent in July and by 6 percent in August. In the other months, since L_n variations were controlled by L_i variations which showed little diurnal pattern, the effect of L_n on R_n varied, but was usually small compared to the influence of Q_n changes.

Gay (1971) calculated λ_n in cloudless conditions for 3 land surfaces. He concluded that the results, -0.15 for desert, -0.03 for forest and +0.06 for an irrigated cotton field surrounded by desert,

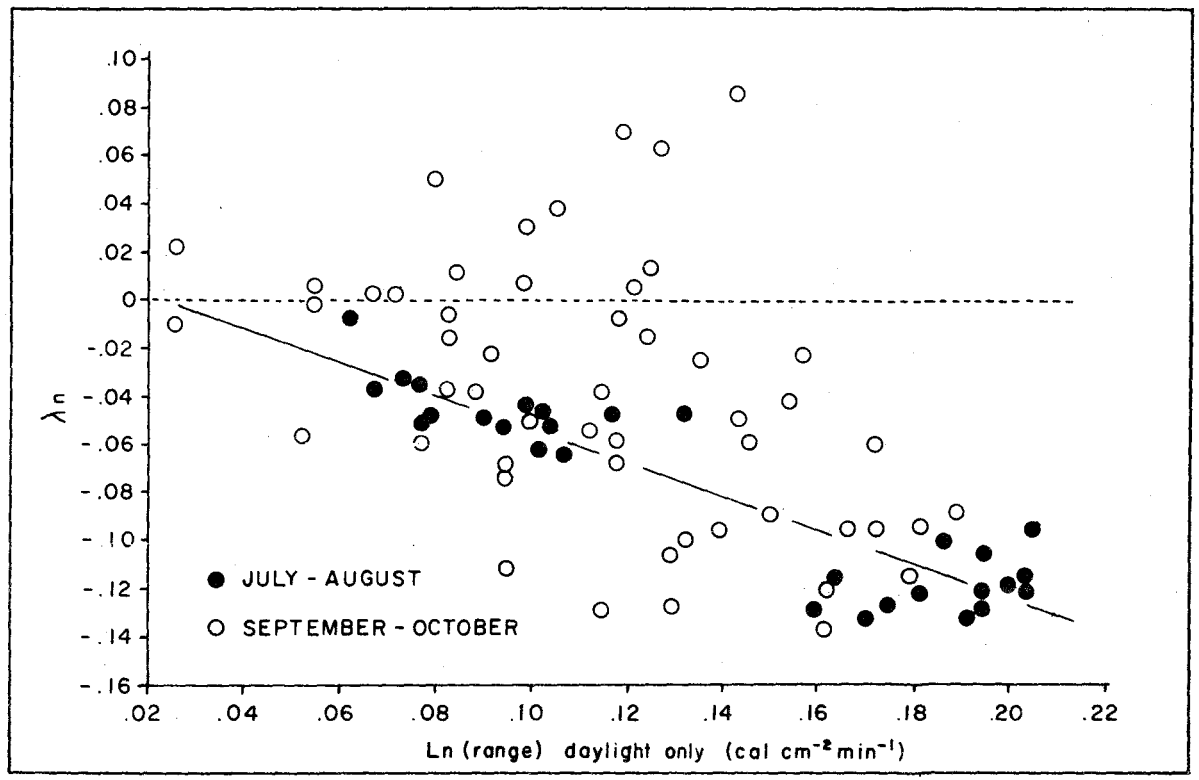

FIGURE 26 RELATIONSHIP BETWEEN λn AND DIURNAL RANGE OF NET LONGWAVE RADIATION Ln (range) FOR DAYLIGHT HOURS

were representative of such surfaces. These values cannot be compared directly to the present data since Gay did not take diurnal L_i variations into account. He suggested, however, that the positive value for the cool, evaporating cotton field was produced by a marked diurnal L_i cycle. This would result from a diurnal cycle of heat transfer and longwave emission from the surrounding desert surface. It appears, therefore, that λ_n generally increases as the surface water content increases. The value, however, is very sensitive to changes in L_i and this is not directly controlled by surface characteristics.

B. SURFACE HEATING

Since one of the objectives of this study is to understand the causes of R_n variations, with particular reference to the longwave fluxes, consideration has been given to the relative importance of L_n and Q_n on R_n variations. Further, reasons for the variation of the L_i component have already been advanced. So far, however, no attempt has been made to explain the causes of temporal changes of L_o. Understanding of such changes demands a knowledge of the surface energy balance (equation 38). The only component of the surface energy balance that can be studied in detail in the present work is the major energy input term, R_n. This can be related to surface heating, or surface temperature change, by the β^* and β coefficients (equations 39 and 40). These coefficients were calculated from the field program data for

each day with complete records of R_n and L_n or L_o. Although the true influence of R_n on T_s, and hence on L_o, can be determined only in 'ideal' conditions, when the other components of the energy balance do not change with time (Idso 1968), the use of all days should give some indication of the magnitude of the coefficients in ideal conditions, and reveal variations caused by departures from the ideal.

The frequency distribution of β values was almost identical to the distribution of λ_n values shown in Figure 23. This is to be expected since the two are directly related by

$$\beta = -\lambda_n/(1+\lambda_n). \qquad (72)$$

There is therefore some indication that β decreases towards the winter season, as found by Stanhill et al (1966). The median value is close to 0.05. Several values for land surfaces have appeared in the literature, the majority being higher than this value. Monteith and Sceicz (1961) found lower values for a moist crop surface than for a dry bare soil, which suggests that moisture generally lowers β coefficients. A contributory factor to this must be the long time lag between maxima of R_n and T_s, which, according to Lettau (1951), is larger for water (3 hours) than for soil (2 hours). The β value must decrease as R_n and T_s become increasingly out of phase.

Since temporal changes in λ_n have been explained in terms of L_n variations, these variations also control β. When β is small, the usual case in the present data, there is little variation in L_n. Hence minor changes in L_i will be important. Idso et al (1969) suggested that the atmosphere in many cases controls the β value, even for values up to 0.20. Hence β is only partially a function of surface characteristics, and cannot be used to determine the influence of R_n on surface heating.

The coefficient β^* does not depend on L_i, and hence is a more realistic measure of surface heating by radiation. β^* was calculated by equation 39. Outgoing longwave radiation was determined both from the radiometric measurements, giving $\beta^*(R)$, and from surface temperature, leading to $\beta^*(T_s)$. The resulting frequency distributions are shown in Figure 27. Both indicate that β^* decreased throughout the field season.

Advection of energy by air and water, and changes in sensible and latent heat flux exchange rates resulting from wind speed changes, must influence the surface temperature. They therefore lead to variable β^* values. However, since wind speed and direction were not constant for any month, these changes would both increase and decrease β^*. Consequently it is possible to suggest that the values close to the median of the distribution for each month are representative of 'ideal' atmospheric and water conditions.

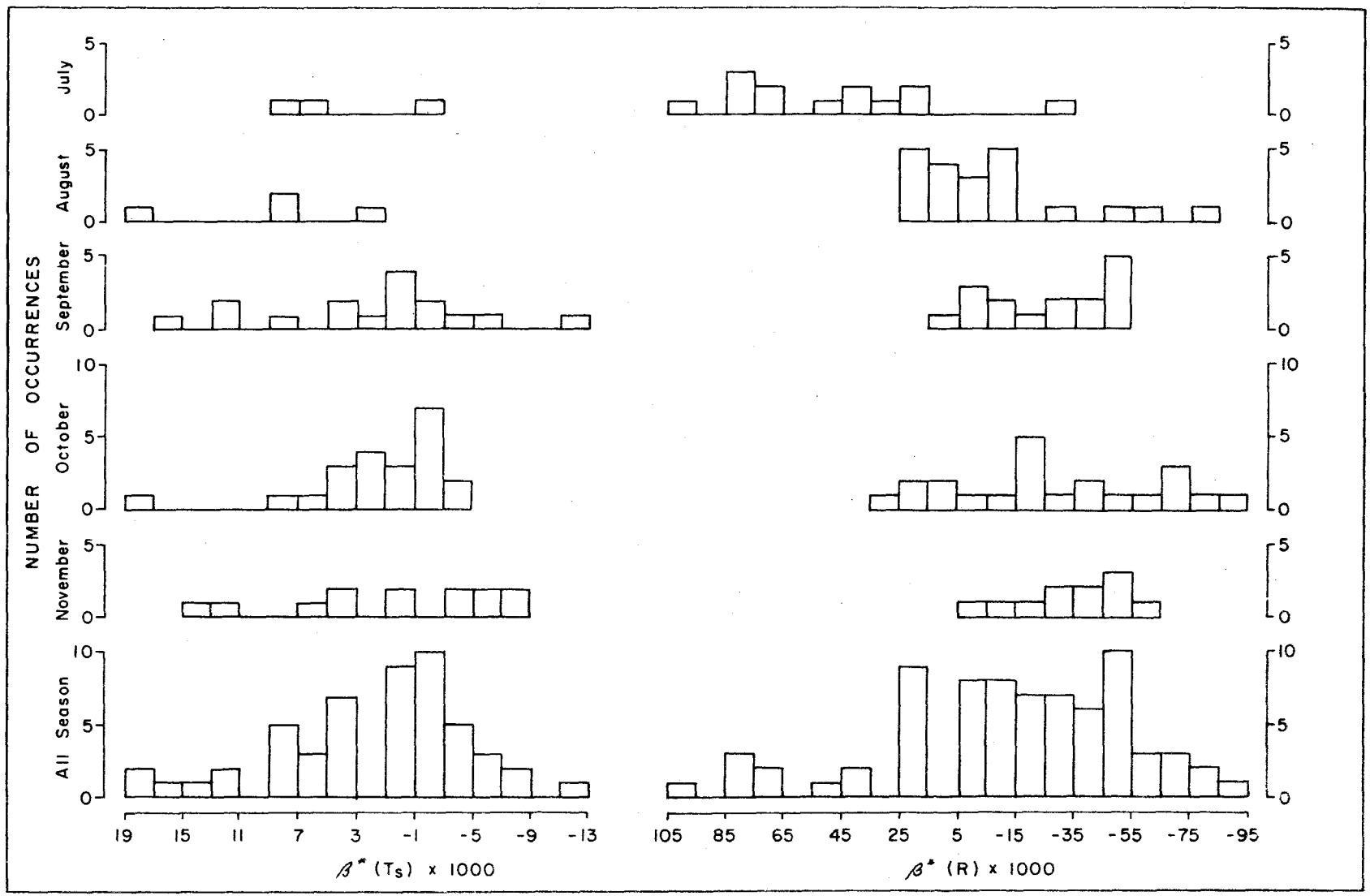

FIGURE 27 FREQUENCY DISTRIBUTIONS OF $\beta^*(T_s)$ AND $\beta^*(R)$ FOR EACH MONTH

TABLE 20. MEDIAN β^* VALUES FOR EACH MONTH

	July	August	September	October	November
$\beta^*(T_s)$	.0067	.0084	.0009	.0007	.0004
β (R)	.0475	-.0012	-.0303	-.0218	-.0383

The seasonal trend of median values (Table 20), however, cannot be explained by radiative considerations alone, since β^* should be independent of amount or intensity of net radiation. During July and August β^* is generally positive (Figure 27), and the air is warmer than the water (Table 12). Hence there will be no upward directed sensible heat flux, and much of the incident radiation will be used to heat the water. In the following months the water is warmer than the air, so that both sensible and latent heat fluxes are upwards, causing surface cooling. Most of the incident energy will be used to drive these fluxes, and not for surface heating. Hence β^* values will be low. Further, when the air is cooler than the water there will be a tendency for T_s to decrease as energy is used in an attempt to establish equilibrium with T_a. In the absence of incident energy, this would lead to surface cooling throughout the day. However, the common diurnal pattern of R_n will lead to a T_s maximum some 3 hours after noon. These two effects combined may lead to a diurnal variation in T_s with a minimum near noon, hence giving negative β^* values.

Figure 27 and Table 20 indicate that β^* values depend on the method of L_o determination. For July

$$dL_o(R)/dR_n > dL_o(T_s)/dR_n. \tag{73}$$

It has been shown above that in this month divergence of L_o is common, and that it is greater during the day than at night. Hence $L_o(R)$ should change more rapidly than $L_o(T_s)$ with R_n, thus explaining the difference in β^* values. Later in the season convergence dominates, and similar arguments lead to the conclusion that β^* obtained using $L_o(R)$ should be lower than that using $L_o(T_s)$.

Some idea of the importance of the other components of the energy balance can be inferred from the data of August 28 - 30th. The 28th and 30th were approximately cloudless, while some cloud occurred in the middle of the 29th. This can be seen from the net radiation variations for the three days (Figure 28). The surface temperature range for the 29th, however, was considerably higher than that for the other days. Diurnal variations of air temperature and humidity were approximately the same for each day, and the lake was calm throughout the period. The major difference between the days was in the wind speed, which was over 4.5 m sec^{-1} on the 28th and 30th, but less than 2.5 m sec^{-1} on the 29th. This may have led to a considerable reduction of heat exchange between the surface and the air on the 29th. Consequently most of the energy would be used for surface heating. $\beta^*(T_s)$ values clearly show the greater surface heating on the 29th (Table 21).

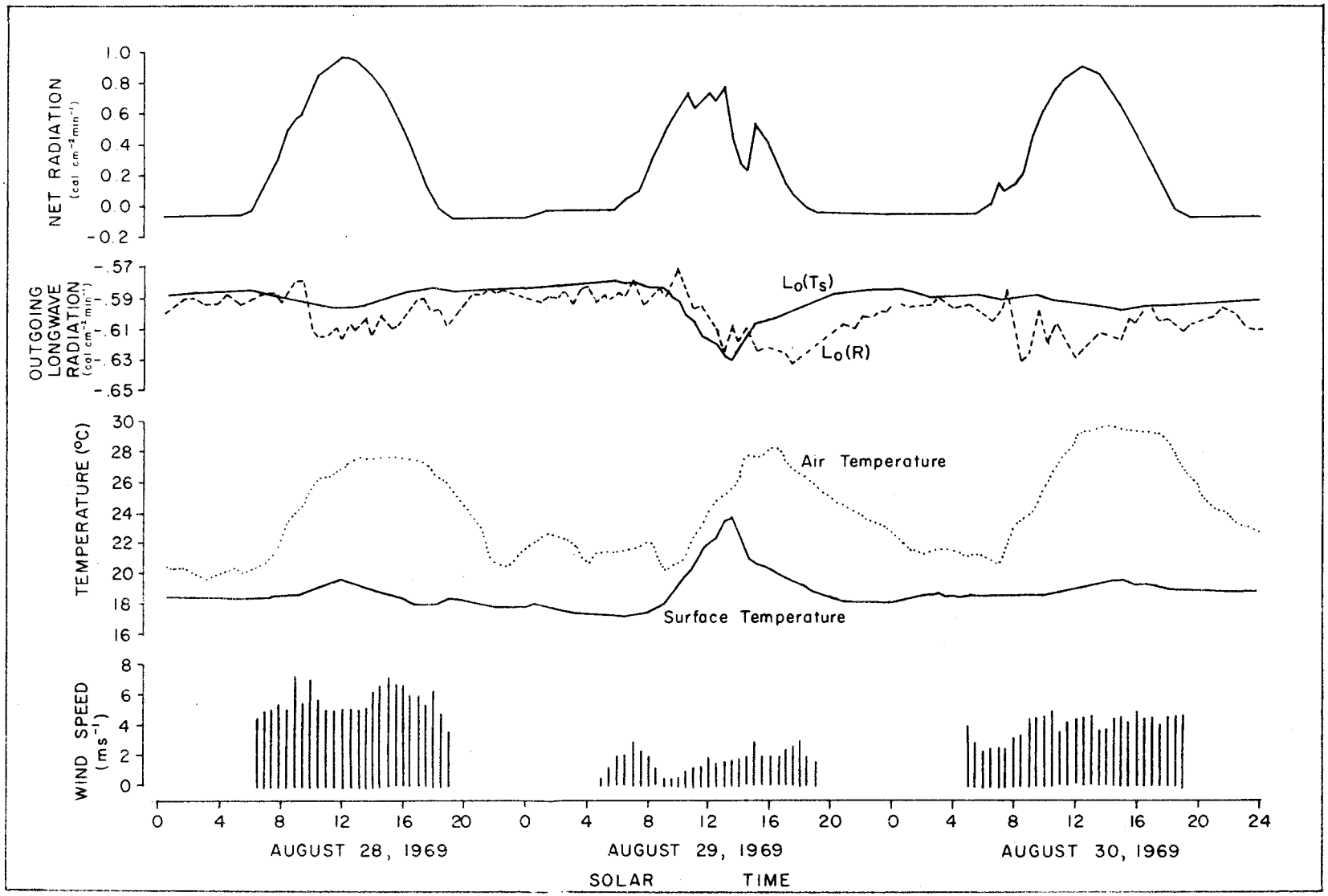

FIGURE 28 NET RADIATION, OUTGOING LONGWAVE RADIATION, AIR AND SURFACE TEMPERATURES AND WIND SPEED FOR AUGUST 28–30, 1969.

TABLE 21: β^*VALUES FOR AUGUST 28th - 30th

	28-8	29-8	30-8
$\beta^*(R)$	.022	-.011	.019
$\beta^*(T_s)$	.009	.032	.002

However, the value of $\beta^*(R)$ for 29th August is the lowest of all three days, and indicates an opposite interpretation. This apparent anomaly can be tentatively explained in terms of the divergence of the outgoing longwave flux. Since for the 28th and 30th divergence is present and $T_a > T_s$, $L_o(R)$ must be partly controlled by the temperature close to the measurement level, in addition to the flux from the surface. However, since wind speeds are high, it can be postulated that there is rapid exchange between the two measurement levels, so that the diurnal courses of T_s and T_a are similar. On the 29th, however, heat exchange will be less rapid, and there is a marked lag in the T_a maximum behind the T_s maximum (Figure 28). Hence $L_o(R)$, responding to T_a changes, does not reach a maximum until 1700 hours. Consequently, it is out of phase with R_n, and $\beta^*(R)$ on this day is negative.

Unfortunately on no other day when surface temperature records were available was there both a calm lake and low wind speeds. Hence it was not possible to test this hypothesis. However, it seems likely that if β^* is determined from measurements some distance above the surface, it may not represent conditions at the surface.

The data of Figure 28 demonstrate the importance of the non-radiative components of the surface energy balance in β^* determination. Hence surface heating cannot be specified from consideration of net radiation alone. However, β^* is useful mainly as a parameter defining theoretical surface temperature changes as a result of R_n changes, which may be termed the true radiative heating rate. Table 20 suggests that this value varies with season, ranging from about 0.008 in summer to 0.001 in winter. This variation must be attributed partly to variations in the other components of the energy balance. Superimposed on the seasonal change are short-term changes induced by the other components of the balance. As a result, a wide range of β^* values was found (Figure 27). Although the present data do not allow an analysis of factors causing departures from the radiative heating rate, Figure 27 shows that the non-radiative components can modify the radiative heating rate by several hundred percent. This is especially marked late in the season, when radiative heating rates approach zero.

CHAPTER 7

METHODS OF ESTIMATING NET RADIATION

Two methods of estimating net radiation are discussed in this chapter. The first uses the measurements of Q_n and R_n to obtain regression equations for predicting R_n when Q_n is known. The second compares the net radiation data at the lake site to data from a nearby land site to provide conversion factors for the determination of R_n over water from measurements over land. Finally a comparison is made of the accuracies of prediction of R_n by these two methods and by other methods which require measurements of Q_n and estimates of the longwave fluxes.

A. RELATIONSHIP BETWEEN NET RADIATION AND NET SHORTWAVE RADIATION

Various values for the constants in equations 33 and 34 were obtained by linear regression. Empirical evidence indicates that the regression coefficient varies significantly with time, and Idso et al (1969) showed that the coefficient obtained for daylight total data was significantly lower than that from the same data analysed on an hourly

basis. Since the Lake Ontario data represent a relatively long time series (for such data), values of the regression coefficient can be evaluated for different time periods, and the reasons for variations examined. Half-hourly values for the dawn-to-dusk period were pooled for regressions for each day, each month, and for all the data. Also, values integrated over the dawn-to-dusk period were used to obtain a bulk regression equation for daylight totals.

1. Daily Relationships

Only days with complete R_n, Q_i and Q_n records were used. The correlation coefficient between R_n and Q_i, and R_n and Q_n, exceeded 0.95 on most days. If Q_n is replaced by $(1-\alpha)Q_i$, and α is considered constant, then equation 36 becomes

$$\partial R_n / \partial Q_i = (1-\alpha)b' = b. \qquad (74)$$

For a plane water surface, α increases with zenith angle and cannot be considered a fixed value. In normal conditions Q_i increases as zenith angle decreases, so that there is a relationship between Q_i and α. Consequently the R_n:Q_i relationship is non-linear, and equation 33 is not strictly correct. Since α commonly varies between 0.05 and 0.15 for water, b varies between 0.95 and 0.85 if L_n is constant. As a

result of this relationship b'>b in all cases. Over land surfaces equations 33 and 34 are equally satisfactory since there is little albedo variation with zenith angle. However, over water equation 34 is preferable. Greater attention will be given to this form in the following sections.

(a) Regression Coefficient

The regression coefficient b' is related to λ_n by

$$b' = \lambda_n + 1. \tag{75}$$

Hence the frequency distributions of b' are the same as those of λ_n, and the appropriate b' values are shown in Figure 23. The explanation of λ_n variation given in Chapter 6 has equal validity for b'.

b' values lie between 0.8 and 1.2, with all values >1.0 occuring after September 1st. The relatively stable values in July and August have been explained in terms of surface heating and diurnal cloud amount variation. Many previous workers over land surfaces have ensured, or assumed, constant L_i by considering cloudless days only, so that surface heating would be dominant. Their results, although variable, indicate b' values ranging from around 0.7 for a bare soil surface (Monteith and Sceicz 1961, Berger-Landfeldt 1964) to over 0.9 for agricultural crops (Fritschen 1967), suggesting a general increase

in b' as water content increased. This is to be expected, since, if $\lambda_i=0$, b' depends on λ_o. The high heat capacity and solar radiation transmission properties of water indicate that surface heating should be slow as compared to that of land. Hence a value close to 1.0 would be expected. However, in the present data the influence of the cloud factor appears to be very important, and leads to lower values, around 0.87 for July and 0.95 in August. It appears likely that, with the relatively small changes in L_o that are common for a water surface, the diurnal cloud amount variation will frequently control b' values.

(b) Regression Constant

Although no definite physical meaning has been attributed to the regression constant a' by previous workers, it is often considered to represent R_n when Q_n goes to zero. Hence a' approximates to L_n at the ends of the daylight period, $L_{n(d)}$. a' and $L_{n(d)}$ are unlikely to be identical since a' must be obtained by extrapolation. In addition, since a' is a statistical parameter, it is actually a measure of the average difference between R_n and $b'Q_n$ through the daylight period.

The difference between $L_{n(d)}$ and a' shows a marked trend with season (Figure 29). The frequency distribution is similar to that for b' (Figure 23). Since a' must be obtained from the data by

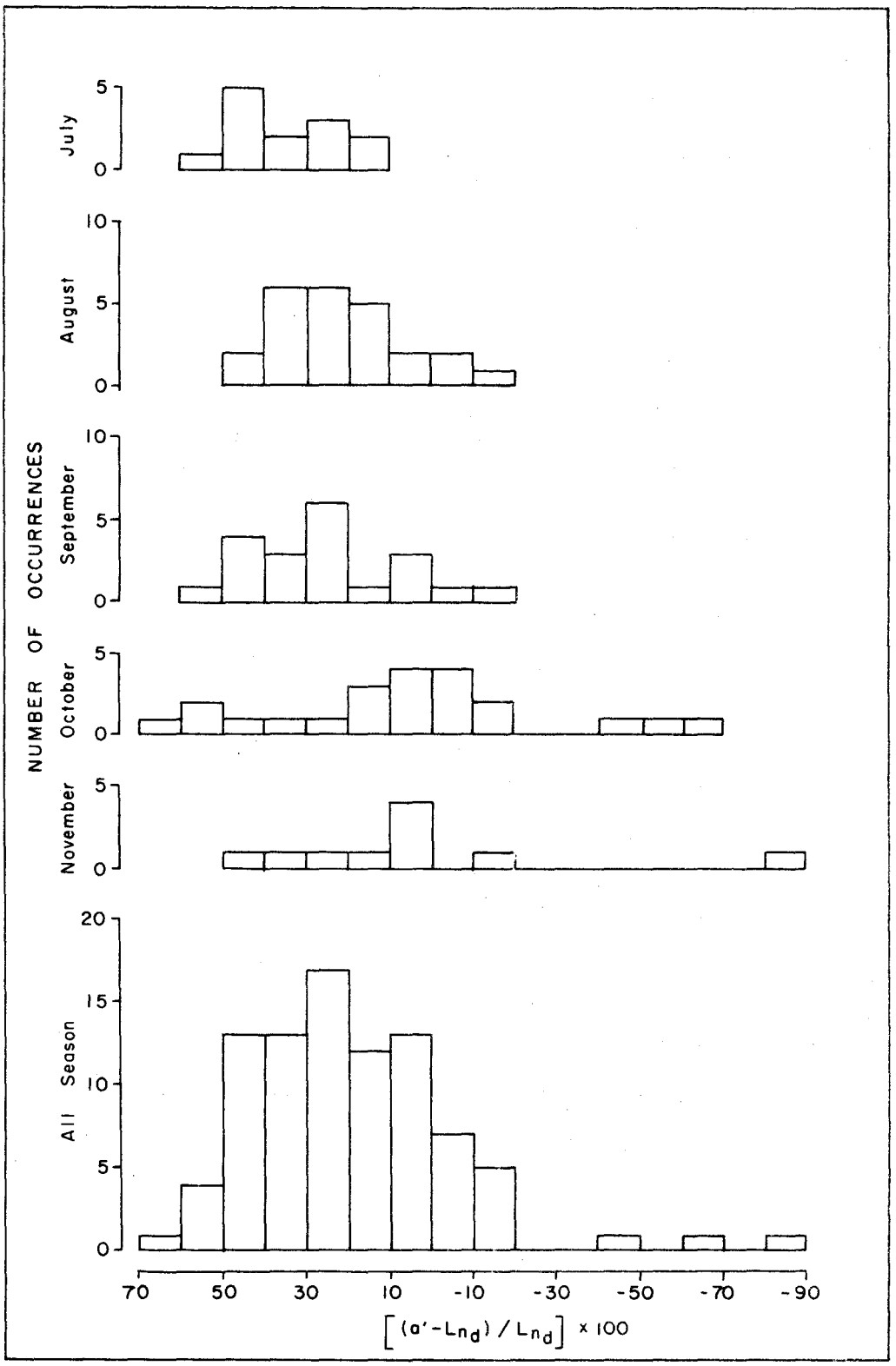

FIGURE 29 FREQUENCY DISTRIBUTION OF PERCENTAGE DIFFERENCE BETWEEN a' AND L_{nd} FOR EACH MONTH

extrapolation, it must be assumed that the rate of change of L_n is the same at the ends of the day as throughout the daylight period. However, surface heating is smaller, and hence L_n changes less rapid, at the ends of the day than during the daylight period. Consequently this will lead to an under- or over-estimate of $L_{n(d)}$, depending on the manner of the diurnal variation of L_n. This variation also determines b', and hence there is a relation between b' and $L_{n(d)}$-a', with

$$L_{n(d)} > a' \quad \text{for } b'>1,$$
$$L_{n(d)} = a' \quad \text{for } b'=1,$$
$$L_{n(d)} < a' \quad \text{for } b'<1.$$

Hence the $L_{n(d)}$ - a' differences have a similar distribution to that of b'.

Although the percentage differences between $L_{n(d)}$ and a' are often large, both have small absolute values, so that absolute differences are small. While the value of a', therefore, approaches that of $L_{n(d)}$, they will be identical only in conditions when b'=1, since with this situation L_n is constant throughout the daylight period and is likely to remain so as the day ends. When $b' \neq 1$, however, the difference will depend not only on the value of b', but also on the variation in L_n close to the ends of the daylight period.

2. Monthly Relationships

All half-hourly data for each month were grouped to give general relationships between R_n and Q_n (Table 22), to determine whether the slope value is constant with time period of record. Most of the comments concerning the daily relationships are equally relevant here. Correlation coefficients are high for each month.

TABLE 22. R_n v Q_n REGRESSIONS FOR EACH MONTH USING HALF-HOURLY DATA

	July	August	September	October	November
Intercept	-.039	-.034	-.053	-.058	-.029
Slope	.868	.917	.959	.911	.885
Correlation Coefficient	.99	.99	.99	.97	.96
Standard Error (cal $cm^{-2}min^{-1}$)	.039	.042	.048	.056	.048
No. of Obs.	679	796	704	649	247

There is a seasonal change in the b' value. For the July to September period, it behaves as expected, with b' increasing as the L_n range decreases (Figure 30). Since L_n is approximately diurnally constant in October and November, b' should approach 1.0. This is not the case. However, a comparison of the monthly regression slopes and the mean value

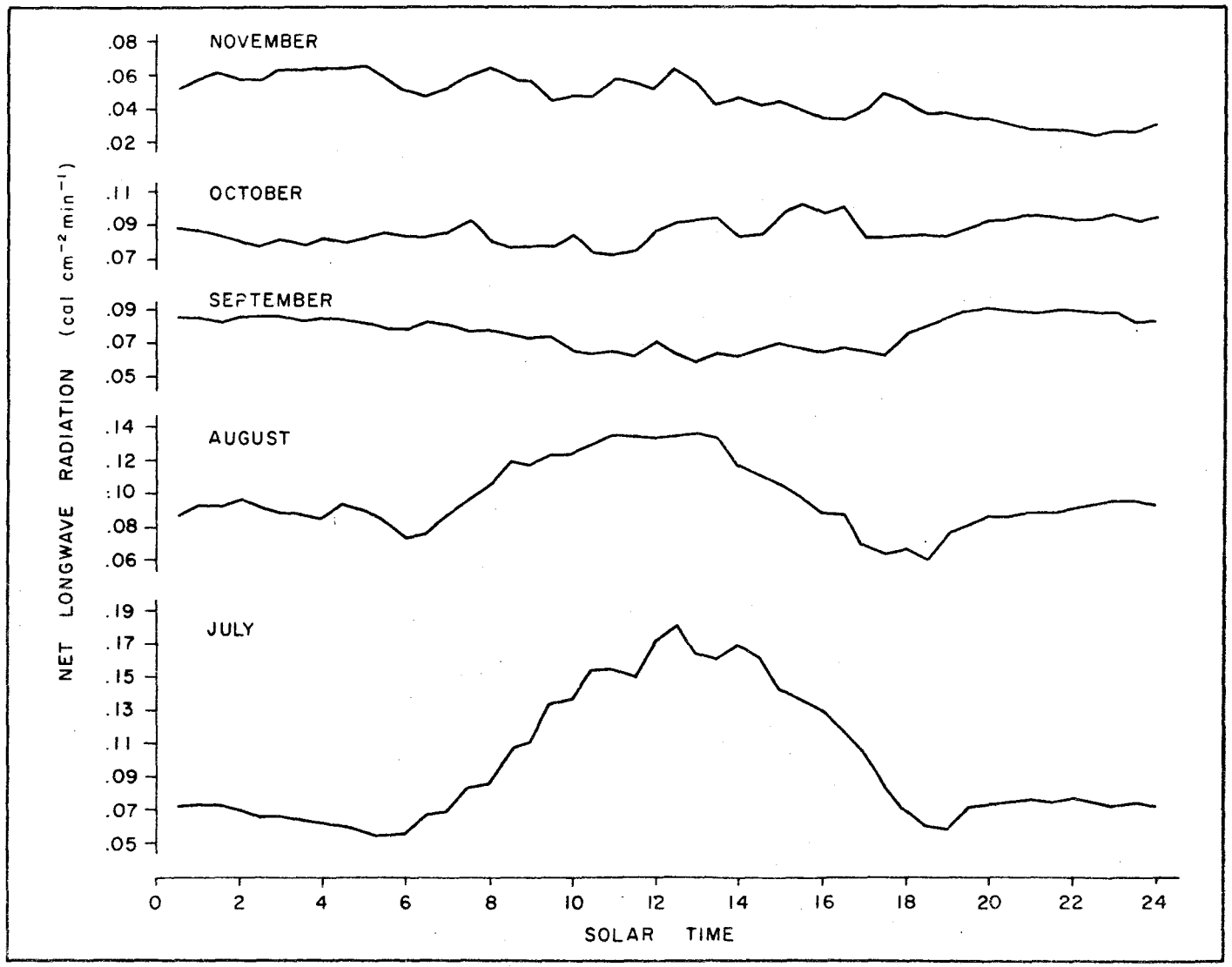

FIGURE 30 MONTHLY AVERAGE DIURNAL VARIATION OF NET LONGWAVE RADIATION

obtained from the daily relationship (Table 23), shows that lower values occur for the former for each month.

TABLE 23. b' OBTAINED BY MONTHLY REGRESSION AND MEAN OF DAILY REGRESSIONS

	July	August	September	October	November
$\overline{b}'$ - daily regression mean	.873	.936	.969	.967	.945
b'm - monthly regression	.868	.917	.959	.911	.885
$\overline{b}'$-b'm	.005	.019	.010	.056	.060

This may account for the fact that the October and November values are less than expected. While daily values can be explained mainly in terms of the diurnal L_n cycle, the monthly variation in L_n must also be included for a complete explanation of monthly relationships. Throughout each month L_n increased (became less negative) (Figure 30) and at the same time Q_n decreased. Since b' depends on λ_n, the value of b' is decreased from the value obtained by use of the diurnal cycle only. Consequently b' cannot be used with any certainty outside the time period for which it was originally obtained.

Since the difference between $L_{n(d)}$ and a' is partly controlled by the b' value, the influence of seasonal changes in L_n are also reflected in the a' values obtained. Hence the a' value

obtained as the mean of the daily regressions is lower than those derived in the monthly regressions (Table 24). Also the mean of the daily values gives a better estimate of $L_{n(d)}$.

TABLE 24. a' OBTAINED BY MONTHLY REGRESSION AND MEAN OF DAILY REGRESSION

	July	August	September	October	November
a'-daily regression mean	-.044	-.067	-.060	-.085	-.042
a' -monthly regression	-.039	-.054	-.053	-.058	-.029
$L_{n(d)}$-monthly mean	-.069	-.086	-.077	-.089	-.051

3. Overall Relationship

The regression equation for all half-hourly data is

$$R_n = .902\ Q_n - .046; \qquad r=.99, \quad S=.05\,. \qquad (76)$$

The only other published results for a water surface are given by Stanhill et al (1966) for a small fish pond. They obtained

$$R_n = 1.02\ Q_n - .12; \qquad r=.98. \qquad (77)$$

Their b' value is larger than that from the present data and exceeds unity. It implies a minimum of L_n near midday, and hence, if L_i is

constant, a midday T_s minimum. For the calm, shallow water of the fish pond greater surface heating is to be expected than for a lake, and hence their value should be lower than the present one. If, however, the surface temperature is reduced around midday by evaporative cooling, the discrepancy can be explained. In addition, Stanhill et al present data for two separate months, with b'=1.0 in February and b'=1.09 in May, which lead to the reasonable conclusion that evaporation is at a maximum in the summer.

Since the basic regression equation of R_n upon Q_n, equation 34, is not restricted in time, the b' value for a single surface should be approximately constant, whatever time period is used. However, Table 25 indicates that b' decreased as time period increased. Also, as a result of the b' variations, a' increased as the time period increased (Table 25). Reasons for this variation have been given above. Hence it is not valid to compare b' or a' for different surfaces if the time period used to obtain the values is different.

The mean value of b' for all terrestrial surfaces, obtained from published data, is about 0.88. Clearly, therefore, b' is lower for land than for water. There are two reasons for this. First, surface heating of land is greater than of water, since land has a lower heat capacity, and also allows lesser depth penetration of solar

radiation. Secondly, there is less surface cooling, associated with lower evaporation rates, from a land surface than from a water surface. Further, a slope value approaching unity implies almost constant L_n. Since b' values in the present work are closer to 1.0 than most values for land, it appears that the influence of longwave radiation fluxes on net radiation is generally less marked over water than over land.

TABLE 25. VARIATION OF a' AND b' WITH TIME PERIOD OF REGRESSION

	Mean Daily	Mean Monthly +	All Season
a'	-.064	-.050	-.046
b'	.942	.915	.902

+ - weighted for number of days data in month

4. Relationship for Daylight Total Data

Several workers have obtained regressions of R_n upon Q_i or Q_n for daylight total data, but there has been some controversy over the correct value of the coefficient of such regressions. Davies (1967) obtained a coefficient of 0.617, which was considerably lower than values given by Shaw (1956), Sholte-Ubing (1959) and Chang (1961). Fritschen (1967) suggested that the reason for differences was the lack of data for low solar radiation totals, and Idso et al (1969) demonstrated

that the inclusion of such data led to higher slope values. Hence they recommended that only data with a wide range of values be used to determine regression equations. The Q_n measurements in this study were fairly uniformly spread from 50 to 700 cal cm^{-2} day^{-1} (Figure 31). Consequently, the conclusions of Fritschen (1967) and Idso et al (1969) could be tested using data for a single surface and single measurement technique.

The results of the regression of daylight total R_n upon daylight total Q_n for the whole season and for each month are shown in Table 26. The monthly regressions all have slopes less than the full season value. This is the reverse of the trend found using half-hourly data. Idso et al (1969) explain such daylight total trends in terms of the length of daylight. They note that near dawn and dusk R_n is negative, and the amount of negative R_n is approximately constant irrespective of daylength. Consequently for long days this portion is relatively insignificant, but its importance increases as daylength decreases. They therefore maintain that short days will have less net radiation than the amount predicted by extrapolation of results from data obtained for long days. Hence an equation obtained using data for days of variable length should have a steeper slope than one for days of constant length.

This analysis implies that the slope increases as daylength decreases, but the present data does not support this conclusion. The monthly regression lines, plotted between the extreme values for

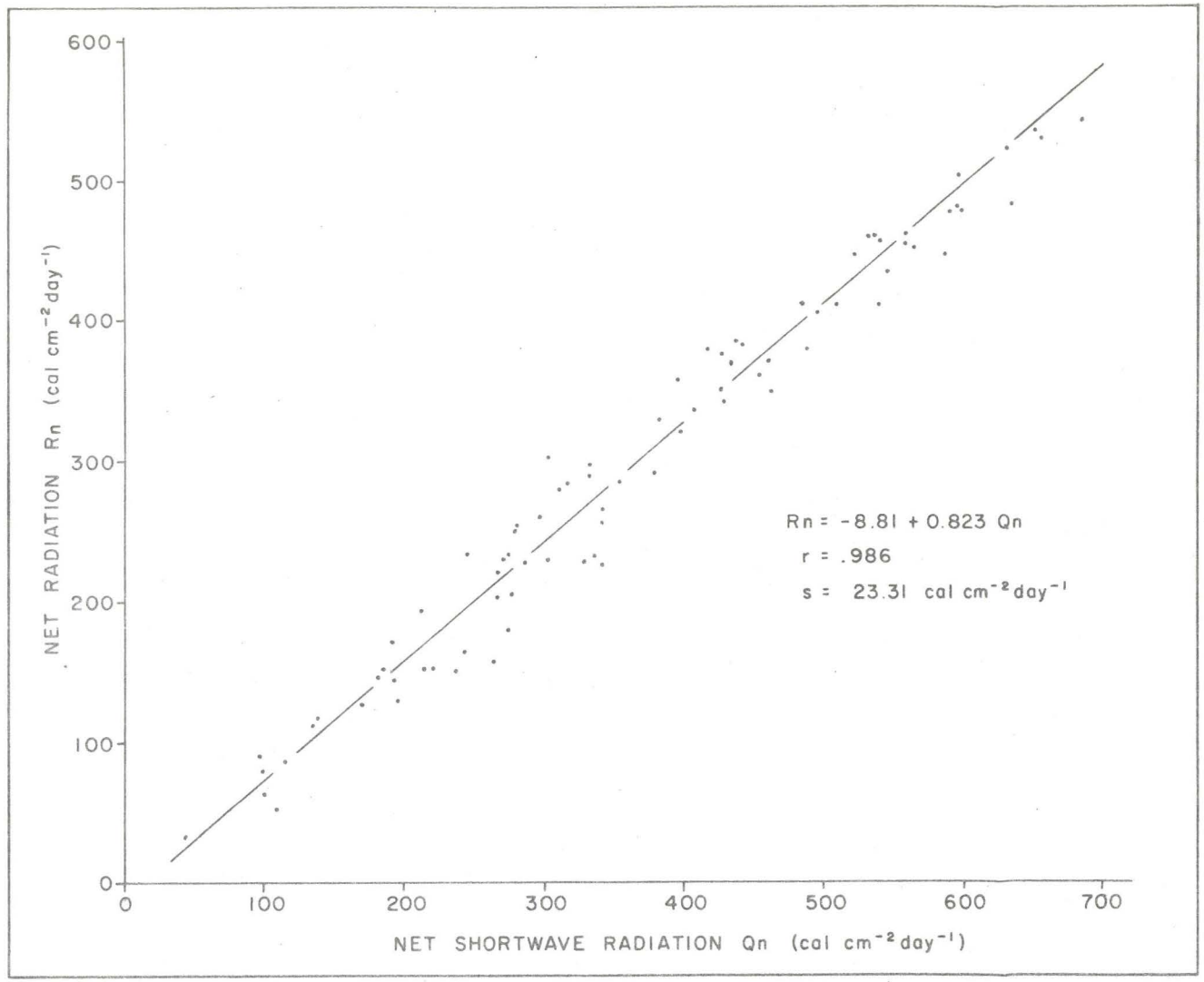

FIGURE 31 RELATION BETWEEN DAYLIGHT TOTALS OF NET RADIATION AND NET SHORTWAVE RADIATION

each month in Figure 32, have slopes that appear to depend on the range of values used, irrespective of daylength. An alternative explanation to that of Idso et al (1969) can be proposed. First it must be assumed that the amount of negative net radiation accumulated is approximately constant for any day. For high R_n daylight totals, the amount of negative R_n is insignificant, but for low values it will have great significance. Hence, for a small range of R_n totals, of whatever absolute amounts, the effect of negative R_n is constant. If a large range is present the variation in the relative effects of negative R_n leads to an apparently lower R_n at low values and greater R_n at high values, hence steepening the slope. While high and low totals may be associated with long and short days, daylength per se is not a sufficient explanation of the slope differences.

TABLE 26. R_n v Q_n REGRESSIONS FOR EACH MONTH USING DAYLIGHT TOTAL DATA

	July	August	September	October	November	All Season
Intercept	4.12	72.47	16.96	29.62	-4.59	-8.81
Slope	.79	.68	.78	.61	.75	.82
Correlation Coefficient	.99	.95	.95	.86	.90	.99
Standard error	17.97	14.44	23.11	22.95	22.83	23.31
No. of Obs.	14	24	20	22	10	90

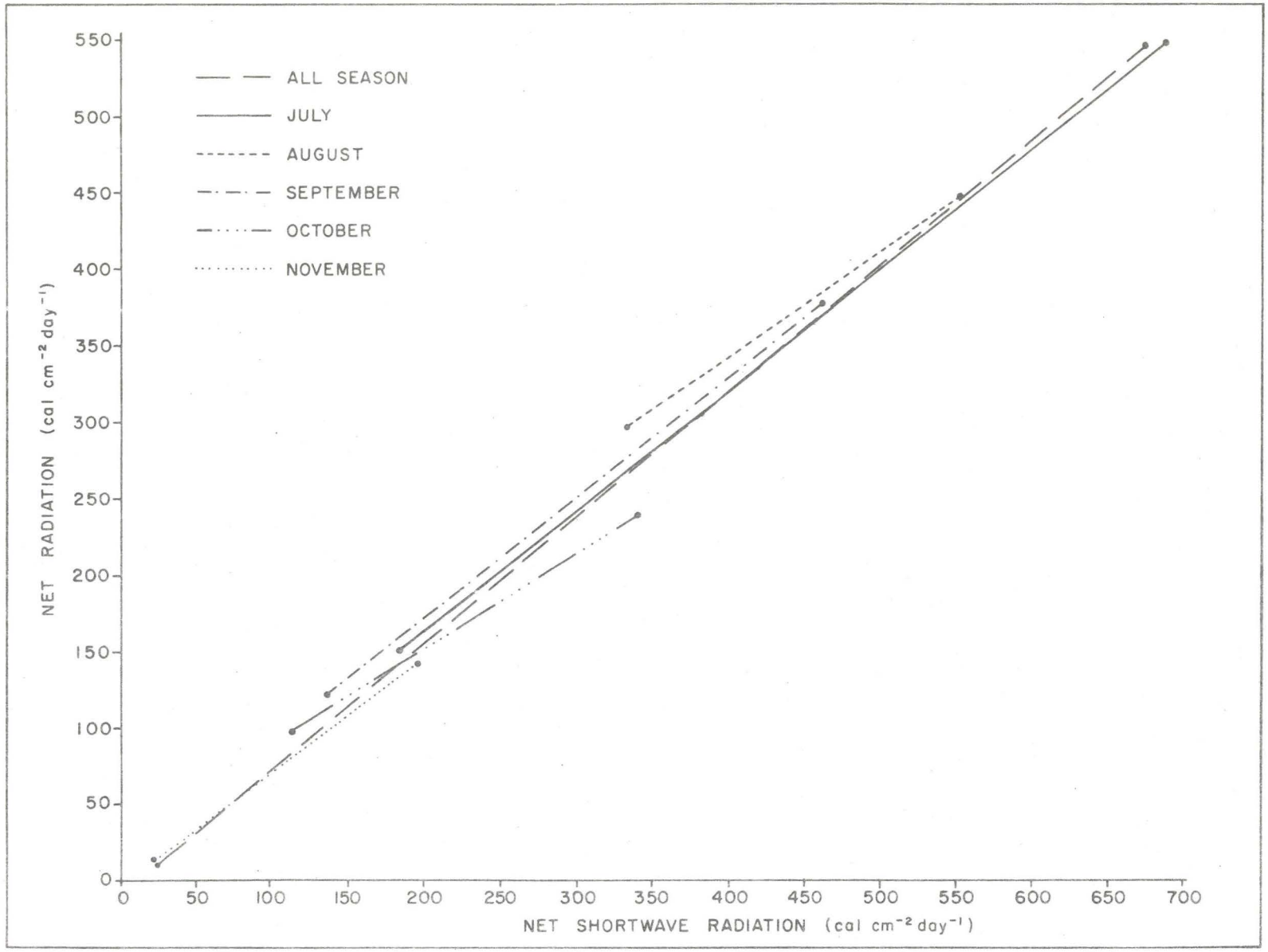

FIGURE 32 REGRESSION LINES FOR MONTHLY REGRESSIONS OF DAYLIGHT TOTAL NET RADIATION UPON NET SHORTWAVE RADIATION

The analysis given here, however, explains differences in both the present data and that of Idso et al (1969). The position of the regression lines of Figure 32 relative to each other depends on the average total daylight L_n in each month, variation in which leads to a shift in position relative to the R_n axis in Figure 32. Although these regression lines must be the most representative of the data for a given month, the 'all season' line is a good approximation to all of them, and hence can be applied for estimates at any time during the season. This conclusion, however, follows because data for a wide range of daylight totals are used. If only a restricted range is available, such as the August data, R_n is considerably overestimated at low Q_n values.

The slope of the all season daylight total data regression (0.82) is considerably less than that from the pooled half-hourly data (0.90), although the mathematical analysis of Idso et al (1969) indicates that the two should be in close agreement. For daylight total data the increasing slope with increasing data range has been demonstrated. Hence, if the range were further increased to a point where the negative term was of great significance, a slope greater than 0.82 would result. For pooled half-hourly data, such conditions are included. The two types of regression have different absolute ranges. However, the pooled half-hourly data range approaches closer to the absolute maximum range theoretically possible than does the daylight total data. Hence pooled half-hourly data has a higher slope value than daylight total data.

B. COMPARISON OF LAKE ONTARIO AND TORONTO NET RADIATION VALUES

Net radiation is measured routinely over grass at the Toronto Meteorological Research Station, about 60 km from the Lake Ontario site. Published data from Toronto for the period of the Lake Ontario measurements (Department of Transport 1969) were used for comparison with the lake data.

The result of the comparison for daily total fluxes is shown in Figure 33. Good correlation is to be expected between the two measurement sets since R_n is strongly dependent on Q_i. Differences in Q_i between the two sites should be small if the influence of cloud is not great. Seasonal changes of Q_i will be similar for both sites. The departure from the 1 : 1 relationship indicated by the regression between the two sets is largely explained by albedo differences between the surfaces. If grass albedo is assumed to be 0.25, and the daily average albedo for water is 0.06 (Nunez 1971), then

$$R_n \text{ (Toronto)} = L_n + .75Q_i, \quad R_n \text{ (Lake)} = L_n + .94\ Q_i, \tag{78}$$

where R_n (Lake) and R_n (Toronto) are net radiation at the lake site and Toronto respectively. If L_n and Q_i are assumed equal at both sites,

$$R_n \text{ (Lake)} - R_n \text{(Toronto)} = .19\ Q_i. \tag{79}$$

Regression of R_n upon Q_i for daylight total data for the whole season (Table 26) indicates that R_n(Lake) $\simeq 0.82Q_n$. Hence, using equation 74, R_n (Lake) $\simeq 0.78Q_i$, and

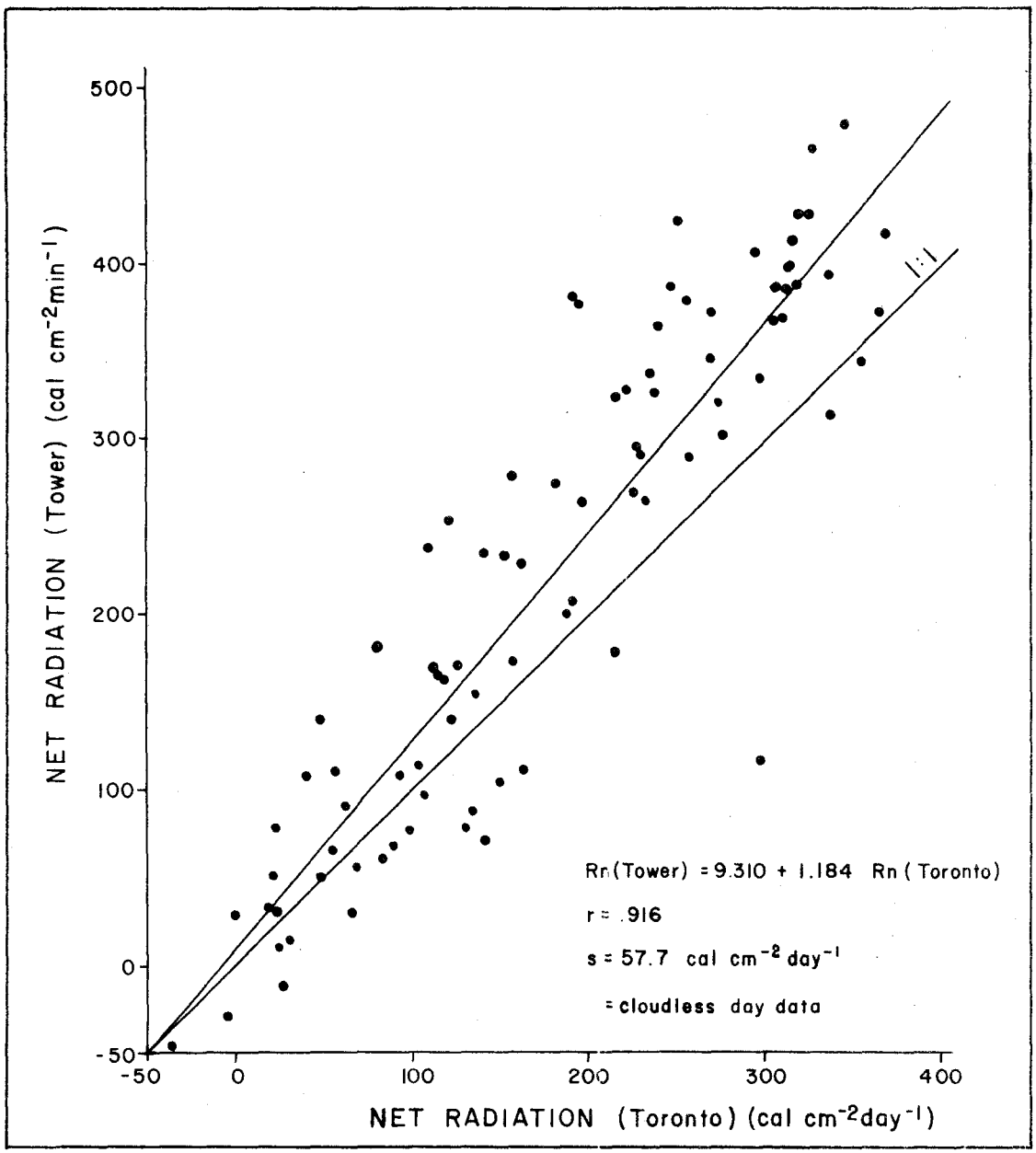

FIGURE 33 RELATION BETWEEN NET RADIATION AT TORONTO AND TOWER

$$R_n(\text{Lake}) = 1.18\ R_n(\text{Toronto}). \qquad (80)$$

The coefficient of equation 80 is close to that given in Figure 33, and demonstrates that the difference in surface albedo between the two sites largely accounts for the R_n difference indicated by the regression equation.

The scatter of points in Figure 33 is probably due to differences in local cloud cover. The two completely cloudless days during the season have values that fall close to the regression line.

Regression between the two R_n measurement sets for pooled hourly total data for the season (Table 27) gave a slope value similar to that of the regression of daily total data.

TABLE 27 : REGRESSION OF R_n(Lake) UPON R_n(Toronto) FOR ALL SEASON HOURLY TOTAL FLUX DATA

	All Data	Daylight Only	Night Only
Intercept	0.12	2.13	-1.86
Slope	1.23	1.19	0.88
Correlation Coefficient	.94	.90	.61
Standard error	6.58	8.73	2.36
Number of observations	2869	1465	1267

Using only daylight data, the slope is again greater than unity and shows the influence of albedo on the relationship. At night, when albedo can have no effect, the slope value should be close to 1.0. However, if L_i is assumed constant over time and between the two surfaces,

$$dR_n(\text{Toronto})/dL_o(\text{Toronto}) = dR_n(\text{Lake})/dL_o(\text{Lake}) = 1. \quad (81)$$

Hence, rearranging and integrating,

$$R_n(\text{Lake}) = [dL_o(\text{Lake})/dL_o(\text{Toronto})]R_n(\text{Toronto}) + \text{constant}. \quad (82)$$

The slope for the nocturnal data therefore gives some indication of differences in rates of change of surface temperature of the two sites, and Table 27 shows that generally the changes are slower for water than for land. The correlation coefficient of the nighttime relationship is lower than for the daylight, but it is still significant above the 1 percent level. The lower coefficient occurs probably because a constant L_i cannot be assumed for more than a few hours, and changes in L_o which are unconnected with R_n are possible.

The slope values for the monthly regressions of the nighttime data have a seasonal trend (Table 28). Early in the season, when Q_i intensity is high, the land surface warms more quickly than the water, while in the last two months the two rates of temperature change are approximately the same. All intercept values indicate that R_n(Lake) is lower than R_n(Toronto). If equal L_i at the two sites is assumed, the

difference must be a function of the temperature difference between water and land. The data indicate maximum temperature differences in September, and almost equal temperatures in November.

TABLE 28. MONTHLY REGRESSION OF R_n (Lake) UPON R_n (Toronto) FOR HOURLY VALUES: NOCTURNAL DATA ONLY

	July	August	September	October	November
Intercept	-2.26	-1.85	-3.14	-2.60	-0.27
Slope	.56	.87	.61	.98	.98

C. COMPARISON OF METHODS OF ESTIMATING NET RADIATION

Techniques of R_n estimation will be examined and the errors associated with them assessed. Table 2 indicates that net radiation can be determined to within $\pm$ 10 percent by direct measurement.

If no measurements of any kind at a desired location can be made, estimation based on the results from a nearby site is possible. The comparison of Toronto and Lake Ontario data indicates that, with an albedo correction for surface differences between the two sites, R_n can be estimated to within about $\pm$ 20 percent. If surface temperature differences are also considered, the estimates may be somewhat better. The distance between the sites is probably unimportant provided Q_i and

L_i are approximately the same. Consequently care must be taken to ensure that the experimental and control sites have similar cloud regimes.

Other estimation methods depend on the ability to measure Q_n at the desired location. R_n can then be determined either by empirical determination of L_n or by use of the regression relationship between Q_n and R_n.

L_n can be estimated using the empirical methods discussed in Chapter 5 to within about 10 percent in cloudless conditions. Hence, since L_n is usually a small portion of R_n, and Q_n can be measured to within 8 percent (Table 2), results by this method are almost as good as direct measurement. However, in cloud conditions the L_n estimation methods have a poor performance, and errors in L_n are likely to be large.

The regression relation between Q_n and R_n can be used in all cloud conditions. The major drawback to this method lies in assigning reasonable values for the regression constant and coefficient. The values must depend both on the time period of interest and on whether hourly or daylight total data are available. The data in Tables 25 and 26 may be taken as representative for a lake surface. However, the long period data were collected when L_n was increasing with time. Hence if spring and summer is the period of interest, L_n will be decreasing and the variation of values with time period will be in the opposite

direction to those of Table 25. Assuming that reasonable values can be assigned, however, the regression method leads, with an assumed Q_n measurement error of 8 percent, to R_n determinations to within $\pm$ 18 percent.

Hence, even with Q_n measurements, the error in R_n estimate can be almost twice as much as that from direct measurement when clouds are present. Since some form of instrument platform must be installed for the Q_n sensors, it would appear advantageous to measure R_n directly at the same site. If measurement is impossible, the easiest method, which has an error comparable to that using Q_n measurements alone, is to estimate R_n from measurements at a nearby accessible site.

CHAPTER 8

CONCLUSIONS

The components of the radiation balance can be resolved from measurements of R_n, Q_i, Q_o, and T_i with commercially available sensors. The maximum error in L_o when it is determined as a residual from such measurements is ±15 percent. However, for a water surface it can be determined to within about 1 percent from the Stefan-Boltzmann law if surface emissivity and temperature are known. Surface emissivity for water was found to be close to 0.975, irrespective of water composition. If a surface contaminating film, such as oil, is present the emissivity may decrease by a few percent. Surface temperature can be determined with good accuracy using floating sensors or with a remote temperature sensor. Both methods generally yielded results within ±1 C of the true temperature. Hence, if a knowledge of radiation balance components is required for a water surface, it is recommended that R_n, Q_i, Q_o and T_s should be measured. L_i and L_o can then be obtained by calculation. This approach may prove difficult for a land surface, since T_s cannot be measured precisely, and the surface emissivity will not be constant.

Although the radiometric determination of L_o has a maximum error of ±15 percent for individual observations, the long-term average value should be considerably more accurate. The two methods of L_o determination were used to compute the divergence of outgoing longwave radiation between the surface and radiometer level on a seasonal basis. In summer divergence dominated. Average values were about 0.004 cal $cm^{-2}min^{-1}m^{-1}$ during daylight and 0.002 cal $cm^{-2}min^{-1}m^{-1}$ at night, corresponding to a change in flux of about 1 and 0.5 percent per metre respectively. Later in the season convergence was common, being larger than 0.001 cal $cm^{-2}min^{-1}m^{-1}$ during the day, and considerably less than this at night. For surface flux values a floating sensor system is recommended since measurements some distance above the surface will not be representative of the surface. Since divergence is common on a seasonal basis, it is likely to influence significantly the heating rate of the air layer close to the surface. Careful short-term measurements, similar to those carried out by Funk (1960) over land, are needed to determine the frequency and magnitude of divergence over a water surface.

With a constant emissivity the outgoing longwave flux is controlled by surface temperature alone. Changes in L_o depend on surface heating which is partly determined by net radiation. A heating coefficient relating L_o to R_n was examined. Its value

varied between 0.008 in summer and 0.001 in fall. These values are dependent on the level above the surface at which L_o is measured, because of flux divergence in the air layer between the surface and the sensor height. True values require that L_o be measured at the surface. The few values of this heating coefficient that have been obtained over land are considerably higher, thereby indicating a more rapid change of T_s with R_n. Several workers over land have determined surface heating by relating L_n to R_n in conditions where L_i is nearly constant. This approach was not possible over water for much of the season, since L_o variations were small and L_n variations were frequently controlled by small changes in L_i, which were unrelated to the surface. In addition to radiative heating, surface temperature changes can be induced by other components of the surface energy balance, namely sensible and latent heat exchange with the overlying air, vertical exchange with deeper layers and horizontal advection of energy. Such component-induced changes can exceed those caused by radiative heating by several hundred percent. It is clear that water surface heating cannot adequately be explained in terms of radiative changes alone. The departures from the radiative heating rate indicate the magnitude of the non-radiative influences. While wind speed influence on surface heating has been demonstrated, the influence of the various energy balance components cannot be separated with the present data.

Incoming longwave radiation cannot be regarded as constant in cloudless conditions, since short-term variations of up to 20 percent were recorded. L_i also varied with cloud amount. High cloud appeared to have little influence on L_i, but an increase in both medium and low cloud amounts increased the flux. Variations in both clear-sky radiation and cloud distributions, however, made it difficult to specify cloud influence on L_i. Hence a study of L_i when cloud distributions, heights and base temperatures are known is required to determine the role of clouds in producing L_i variations.

The performance of chart methods for estimating L_i was poor, probably because the radiosonde data from low levels were more representative of land than water. Empirical formulae, however, performed well. The Swinbank (1963) formula proved the most convenient to use, since it required only screen temperature measurements. In cloudless conditions L_i can be estimated by this formula to within ±10 percent. When cloud was present a correction using the Bolz (1949) coefficients led to estimates within about ±15 percent for the whole season, but gave wider variability for individual days.

Variations in net radiation are controlled mainly by variations in net shortwave radiation during the daylight hours.

In summer both L_i and L_o had marked diurnal cycles and produced diurnal changes in L_n which were opposite to those of Q_n. Consequently variations in R_n were about 10 percent less than those produced by Q_n changes alone. Later in the season, when diurnal changes in L_o were small and L_i had little diurnal pattern, the influence of L_n on R_n was variable and generally small. R_n variations for a water surface appear to be reduced less by changes in L_n than those for land, where the diurnal L_o cycle is more marked.

Estimates of net radiation at remote locations over water can be made to within about ±20 percent by using measurements from a nearby land site with corrections for differences in albedo and surface temperature between the sites. The distance between sites is probably unimportant provided that the cloud regime is similar at both sites. If Q_n can be measured or estimated at the site, R_n can be estimated either by use of a regression relations between R_n and Q_n, or by measurement of T_s and estimation of L_i. The regression equation gives estimates to within ±18 percent, but is limited to daylight data. Further, the slope of this relation, whether for half-hourly or daylight total data, depends on L_n variations and varies both from day to day and with the length of record used to determine the relationship. A representative slope will be obtained only if the range of values used in the regression approaches

the maximum possible. The accuracy of this method, however, is not affected by the presence of cloud. Measurement of T_s and determination of L_i by the Swinbank formula yields estimates of R_n in cloudless conditions with an accuracy comparable to those of direct measurement (±10 percent). Accuracy decreases when clouds are present, especially if short-term values are required. Therefore, while no single method of estimating R_n can be used in all conditions, R_n can generally be estimated, with careful selection of the method appropriate to the conditions and time period of interest, to within ±20 percent. A considerably more accurate estimate is possible in cloudless conditions.

APPENDIX

LIST OF SYMBOLS

A_s	Constant in 2nd atmospheric radiation equation of Swinbank
A_λ	Spectrophotometer response for standard surface (arbitrary units)
a	Constant of regression of R_n upon Q_i
a'	Constant of regression of R_n upon Q_n
a_a	Constant in atmospheric radiation equation of Ångström
a_b	Constant in atmospheric radiation equation of Brunt
a_e	Constant in atmospheric radiation equation of Elsasser
a_j	Constant in atmospheric radiation equation of Idso and Jackson
a_s	Constant in 1st atmospheric radiation equation of Swinbank
B_s	Constant in 2nd atmospheric radiation equation of Swinbank
B_λ	Spectrophotometer response for sample surface (arbitrary units)
b	Coefficient of regression of R_n upon Q_i
b'	Coefficient of regression of R_n upon Q_n
b_a	Constant in atmospheric radiation equation of Ångström
b_b	Constant in atmospheric radiation equation of Brunt

b_e Constant in atmospheric radiation equation of Elsasser

b_j Constant in atmospheric radiation equation of Idso and Jackson

b_s Constant in 1st atmospheric radiation equation of Swinbank

c Bulk cloud coefficient in equation of Gal'perin

c_2 Constant in Planck function

c_3 Constant in Planck function

c_H Coefficient for high cloud

c_L Coefficient for low cloud

c_M Coefficient for medium cloud

E Latent heat exchange between surface and air (cal $cm^{-2}min^{-1}$)

e Vapour pressure (mb)

F_1 Radiative flux in all directions and for all wavelengths (cal $cm^{-2}min^{-1}$)

$F_\lambda(T)$ Monochromatic black-body flux from a body at temperature T (cal $cm^{-2}min^{-1}$)

$F'_\lambda(T)$ Monochromatic flux from a real body at temperature T (cal $cm^{-2}min^{-1}$)

G Heat exchange between surface and deeper layers (cal $cm^{-2}min^{-1}$)

H Sensible heat exchange between surface and air (cal $cm^{-2}min^{-1}$)

K Spectrophotometer response constant

k Cloud coefficient in equation of Bolz

k_* Constant relating radiometer output to radiative flux

L_i Incoming longwave radiation (cal $cm^{-2}min^{-1}$)

$L_{i(c)}$ Incoming longwave radiation in cloudless conditions (cal $cm^{-2}min^{-1}$)

$L_{i(n)}$ Incoming longwave radiation in cloudy conditions (cal $cm^{-2}min^{-1}$)

$L_{i(t)}$ Incoming longwave radiation with complete cloud cover (cal $cm^{-2}min^{-1}$)

L_n Net longwave radiation (cal $cm^{-2}min^{-1}$)

$L_{n(c)}$ Net longwave radiation in cloudless conditions (cal $cm^{-2}min^{-1}$)

$L_{n(d)}$ Net longwave radiation at dawn and dusk (cal $cm^{-2}min^{-1}$)

L_{ns} Net longwave radiation at the surface (cal $cm^{-2}min^{-1}$)

L_o Outgoing longwave radiation (cal $cm^{-2}min^{-1}$)

$L_o(R)$ Outgoing longwave radiation determined by radiometer (cal $cm^{-2}min^{-1}$)

$L_o(T_s)$ Outgoing longwave radiation determined from surface temperature (cal $cm^{-2}min^{-1}$)

n Cloud amount (tenths)

n_H Amount of high cloud (tenths)

n_L Amount of low cloud (tenths)

n_M Amount of medium cloud (tenths)

$\overline{p_i}$ Average pressure of i th atmospheric layer (mb)

p_o Surface atmospheric pressure (mb)

Q_i Incoming shortwave radiation (cal $cm^{-2}min^{-1}$)

Q_n Net shortwave radiation (cal $cm^{-2}min^{-1}$)

Q_o Outgoing shortwave radiation (cal $cm^{-2}min^{-1}$)

$\overline{q_i}$ Mean specific humidity of i atmospheric layer (g kg^{-1})

R_n	Net radiation (cal $cm^{-2}min^{-1}$)
r	Correlation coefficient
S	Standard error of estimate (various units)
$S_{\lambda(c)}$	Monochromatic reflectivity of standard surface
$S_{\lambda(s)}$	Monochromatic reflectivity of sample surface
T_a	Air temperature (^oC)
T_c	Radiometer cavity temperature (^oK)
T_i	Total (shortwave + longwave) incoming radiation (cal $cm^{-2}min^{-1}$)
T_i^1	Output of radiometer measuring T_i (mV)
T_n	Temperature of cone for emissivity measurement (^oC)
T_r	Radiative temperature of a surface (^oC)
T_s	Surface temperature (^oC)
$T_{s(b)}$	Surface temperature measured by infra-red thermometer (^oC)
$T_{s(m)}$	Surface temperature measured by multiple sensor float (^oC)
$T_{s(r)}$	Surface temperature calculated from outgoing longwave flux (^oC)
$T_{s(s)}$	Surface temperature measured by single sensor float (^oC)
T_u	Radiative temperature of the atmosphere (^oC)
u	Corrected optical depth of j atmospheric layers (cm)
u_i	Corrected optical depth of i th atmospheric layer (cm)
u_t	Total corrected optical depth of atmosphere (cm)
V	Radiometer output voltage (mV)
α	Surface albedo
β	Rate of change of L_n with R_n

β^*	Rate of change of L_o with R_n - the radiative heating coefficient
$\beta^*(R)$	Radiative heating coefficient determined from radiometric measurements
$\beta^*(T_s)$	Radiative heating coefficient determined from surface temperature measurements
γ	Constant in atmospheric radiation equation of Ångström
ΔF	Subsurface horizontal heat flux (cal $cm^{-2}min^{-1}$)
Δp_i	Pressure difference between top and bottom of i th atmospheric layer (mb)
ΔT	Difference between surface and air temperature (^oC)
ΔT_*	Temperature difference between two radiometer surfaces (^oC)
ε	Surface emissivity
ε_a	Apparent emissivity of a cone
ε_c	Effective emissivity through apex of a cone
ε_f	Effective emissivity of the atmosphere
ε_λ	Spectral emissivity
$\varepsilon_\lambda(u)$	Emissivity coefficient for atmospheric radiation exchange
λ	Wavelength (microns)
λ_i	Rate of change of L_i with Q_n
λ_n	Rate of change of L_n with Q_n
λ_o	Rate of change of L_o with Q_n
σ	Stefan-Boltzmann constant
σ_s	Standard deviation (various units)
ϕ_λ	Spectral sensitivity of a sensor (percent)
ω	Solid angle of sight of a sensor (steradians)

REFERENCES

Abraham, F.F. 1960 Determination of long wave atmospheric radiation. J. Meteorol., 17, 291-295.

Allen, J.R. 1971 Measurements of cloud emissivity in the 8-13μ waveband. J. Appl. Meteorol., 10, 260-265.

Anderson, E.R. 1954 Energy-budget studies. In: Water Loss Investigations: Lake Hefner Studies, Technical Report. U.S.G.S. Prof. Paper, 269, pp. 71-119. Washington D.C.

Ångstrom, A. 1916 Über die Gegenstrahlung der Atmosphäre. Meteorol. Z., 33, 529-538.

Bell, E.E. 1957 An atlas of reflectivities of some common types of materials. Interim Eng. Rept., Contract AF33(616)-3312. Ohio State Univ., Columbus, Ohio. 15pp.

Berger-Landfeldt, U. 1964 Über der Strahlungshaushalt verschiedener Pflanzenbestande. Bericht. Deuts. Bot. Ges., 77, 27-48.

Bolz, H.M. 1949 Die Abhangigkeit der infraroten Gegenstrahlung von der Bewolkung. Zeit. f. Meteorol., 3, 201-203.

Brooks, F.A. 1952 Atmospheric radiation and its reflection from the ground. J. Meteorol., 9, 41-52.

Brunt, D. 1932 Notes on radiation in the atmosphere. Quart. J. Roy. Meteorol. Soc., 58, 389-420.

Buettner, K.J.K. and C.D. Kern. 1965 The determination of infrared emissivities of terrestrial surfaces. J. Geophys. Res., 70, 1329-1337.

Chandrasekhar, S. 1950 Radiative Transfer, Oxford, Univ. Press, 393pp.

Chang, Jen-Hu. 1961 Microclimate of sugar cane. Hawaiian Planters Record, 56, 195-225.

Davies, J.A. 1967 A note on the relationship between net radiation and solar radiation. Quart. J. Roy. Meteorol. Soc., 93, 109-115.

Davies, J.A. and P.H. Buttimor. 1969 Reflection coefficients, heating coefficients and net radiation at Simcoe, Southern Ontario. Ag. Meteorol., 6, 373-386.

Davies, J.A., P.J. Robinson and M. Nunez. 1970 Grimsby tower radiation data. 2nd Rept., Contract HO 81276, Gov. of Canada, Dept. Energy, Mines and Resources, Canada Centre for Inland Waters, Great Lakes Division, Burlington, Ontario.

Davies, J.A., P.J. Robinson, and M. Nunez. 1971 Field determinations of surface emissivity and temperature for Lake Ontario. J. Appl. Meteorol., 10, 811-819.

Deacon, E.L. 1950 Radiative heat transfer in the air near the ground. Aust. J. Sci. Res., A, 3, 274-283.

Deacon, E.L. 1970 The derivation of Swinbank's long wave radiation formula. Quart. J. Roy. Meteorol. Soc., 96, 313-319.

Department of Transport. 1962 Manupp - Manual of upper air observations, Meteorol. Branch, Toronto, Ontario.

Department of Transport. 1969 Monthly Radiation Summary, July- November 1969, Meteorol. Branch, Toronto, Ontario.

Ekern, P.C. 1965 The fraction of sunlight retained as net radiation in Hawaii. J. Geophys. Res., 70, 785-793.

Elsasser, W.M. 1942 Heat transfer by infrared radiation in the atmosphere. Harvard Meteorol. Studies., 6, 106 pp.

Elsasser, W.M. and M.F. Culbertson. 1960 Atmospheric radiation tables. Meteorol. Mono., 4, 23.

Fritschen, L.J. 1967 Net and solar radiation relations over irrigated field crops. Ag. Meteorol., 4, 55-62.

Fuchs, M. and C.B. Tanner. 1968 Surface temperature measurements of bare soil. J. Appl. Meteorol., 7, 303-305.

Funk, J.P. 1959 Improved polyethelene-shielded net radiometers. J. Sci. Instr., 36, 267-270.

Funk, J.P. 1960 Measured radiative flux divergence near the ground at night. Quart. J. Roy. Meteorol. Soc., 86, 382-389.

Funk, J.P. 1961 A note on the longwave calibration of convectively shielded net radiometers. Arch. Meteorol., Geophys., Bioklim., B, 11, 70-74.

Funk, J.P. 1962 A net radiometer designed for optimum sensitivity and a ribbon thermopile used in a miniaturised version. J. Geophys. Res., 67, 2753-2760.

Gal'perin, B.M. 1949 The radiation balance at the lower Volga during the warm season. Trudy GGO, 80, 18.

Gates, D.M. 1965 Radiant energy, its receipt and disposal. Meteorol. Mono., 6,28, 1-24.

Gay, L.W. 1971 The regression of net radiation upon solar radiation. Arch. Meteorol., Geophys., Bioklim., B, 19, 1-14.

Gier, J.T. and R.V. Dunkle. 1951 Total hemispherical radiometers. Trans. Amer. Inst. Elec. Eng., 70, 339-343.

Godson, W.L. 1953 The evaluation of infrared radiative fluxes due to atmospheric water vapour. Quart. J. Roy. Meteorol. Soc., 79, 341-367.

Goody, R.M. 1964 Atmospheric Radiation I: Theoretical Basis. Oxford, Univ. Press., 436pp.

Hettner, G. 1918 Uber das Ultrarote Absorptionsspektrum des Wasserdampfes. Ann. der Phys., 55, 476-496.

Idso, S.B. 1968 An analysis of the heating coefficient concept. J. Appl. Meteorol., 7, 716-717.

Idso, S.B. and R.D. Jackson. 1969 Thermal radiation from the atmosphere. J. Geophys. Res., 74, 5397-5403.

Idso, S.B. D.G. Baker, and B.L. Blad. 1969 Relations of radiation fluxes over natural surfaces. Quart. J. Roy. Meteorol. Soc., 95, 244-257.

Kimball, H.H. and H.E. Hobbs. 1923 A new form of thermoelectric recording pyrheliometer. J. Opt. Soc. Amer. and Rev. Sci. Instr., 7, 707-718.

Kislovskii, L.D. 1959 Optical characteristics of water and ice in the infrared and radiowave regions of the spectrum. Optics and Spectroscopy, 7, 201-206.

Kondrat'yev, K. Ya. 1965 Radiative heat exchange in the atmosphere. Oxford, Pergamon. 411pp.

Lettau, H.H. 1951 Theory of surface-temperature and heat-transfer oscillations near a level ground surface. Trans. Amer. Geophys. U., 32, 189-200.

List R.J. 1966 Smithsonian Meteorological Tables, Smithsonian Inst. Misc. Coll., 114.

Lorenz, D. 1966 The effect of long wave reflectivity on natural surfaces on surface temperature measurements. J. Appl. Meteorol., 5, 421-430.

McSwain, B. and J. Bernstein. 1960 Specular reflectance of water in the 1.5 to 15-micron region as a function of wavelength and incidence angle. Navwets Rept., 7162, Quart. Rept. Oct.- Dec.

Malevskiy-Malevich, S.P. 1963 The measurement of temperature of the water surface. Soviet Hydrology, 4, 326-330.

Marlatt, W.E. 1967 Remote and in situ temperature measurements of land and water surfaces. J. Appl. Meteorol., 6, 272-279.

Möller, F. 1951 Long wave radiation. In: T.F. Malone (ed), Compendium of Meteorology. Boston, Mass., Amer. Meteorol. Soc., pp 34-49.

Möller, F. 1954 Ein Kurzverfahlen zur Bestimmung der langwellige Ausstrahlung dicker Atmosphärenschichten. Arch. Meteorol., Wien, A, 7.

Monteith, J.L. 1959 Solarimeter for field use. J. Sci. Instr., 36, 341-346.

Monteith, J.L. and G. Sceicz. 1961 The radiation balance of bare soil and vegetation. Quart. J. Roy. Meteorol. Soc., 87, 159-170.

Morgan, D.L. W.O. Pruitt, and F.J. Lourence. 1971 Estimation of atmospheric radiation. J. Appl. Meteorol., 10, 463-468.

Nunez, M. 1971 Solar radiation and albedo at a tower site over Lake Ontario. 3 rd Rept., Contract HO 81276, Gov. of Canada, Dept. of Energy, Mines and Resources, Canada Centre for Inland Waters, Great Lakes Division, Burlington, Ontario.

Paltridge, C.W. 1970 Day-time long-wave radiation from the sky. Quart. J. Roy. Meteorol. Soc., 96, 645-653.

Phillips, H. 1940 Bad Homburg v.d.H., zur Theorie der Warmestrahlung in Bodennahe. Beit. z. Geophysik, 56, 3.

Reuter, H. 1950 Calculation of minimum temperatures and the prediction of ground frost. Circ. 1768, Tech. Paper 70, Department of Transport, Meteorol. Branch, Toronto, Ontario.

Robinson, G.D. 1950 Notes on the measurement and estimation of atmospheric radiation - 2. Quart. J. Roy. Meteorol. Soc., 76, 37-51.

Robinson, N. 1966 Solar Radiation. London, Elsevier. 347pp.

Scholte-Ubing, D.W. 1959 Overstraling de warmtebalons en de verdamping van gras. Mededel. Landbouwhoogeschool, Wageningen, 59, 1-93.

Sellers, W.D. 1965 Physical Climatology, Chicago, Univ. Chicago 272pp.

Shaw, R. 1956 Comparison of solar radiation and net radiation. Bull. Amer. Meteorol. Soc., 37, 205-206.

Shekter, F.N. 1950 Calculation of thermal radiation fluxes in the atmosphere. Trudy GGO, 84, 22.

Sloan, R, J.H. Shaw and D. Williams. 1955 Infrared emission spectrum of the atmosphere. J. Opt. Soc. Amer., 45, 455-460.

Sparrow, E.M. and V.K. Jonsson. 1963 Radiant emission characteristics of diffuse conical cavities. J. Opt. Soc. Amer., 53, 816-821.

Stanhill, G., G.J. Hofstede and J.D. Kalma. 1966 Radiation balance of natural and agricultural vegetation. Quart. J. Roy. Meteorol. Soc., 92, 128-140.

Suomi, V.E. M. Franssila and N.F. Islitzer. 1954 An improved net-radiation instrument. J. Meteorol., 11, 276-282.

Swinbank, W.C. 1963 Long wave radiation from clear skies. Quart. J. Roy. Meteorol. Soc., 89, 339-348.

Swinbank, W.C. 1964 Discussion of 'Long wave radiation from clear skies'. Quart. J. Roy. Meteorol. Soc., 90, 488-493.

Tanner, C.B. 1963 Basic instrumentation and measurements for plant environment and micrometeorology. Univ. Wisc., Dept. Soil Sci., Soils Bull., 6.

Yamamoto, G. 1952 On a radiation chart. Tohoku Univ., Sci. Rept., Ser. 5, Geophysics, 4, 9-23.

Zdunkowski, W.G. and I. Choronenko. 1969 Incomplete blackness of clouds in the infrared spectrum. Beit. z. Phys. Atmos., 206-224.